The Pennsylvania State University

The Graduate School

Department of Energy & Mineral Engineering

DEVELOPMENT OF AN ARTIFICIAL EXPERT SYSTEM FOR ESTIMATING THE RATE OF GROWTH OF GAS CONE

A Thesis in

Energy and Mineral Engineering

by

Shashank Sharma

Submitted in Partial Fulfillment
of the Requirements
for the Degree of

Master of Science

August 2011

The thesis of Shashank Sharma was reviewed and approved* by the following:

Turgay Ertekin
Professor of Petroleum and Natural Gas Engineering
George E. Trimble Chair in Earth and Mineral Sciences
Thesis Advisor

Zuleima Karpyn
Assistant professor of Petroleum and Natural Gas Engineering

Li Li
Assistant professor of Petroleum and Natural Gas Engineering

Larry Grayson
Professor of Energy and Mineral Engineering

*Signatures are on file in the Graduate School

ABSTRACT

Oil bearing zones are often accompanied by a gas cap which may enhance oil recovery by gas cap drive mechanism. As the well starts producing, the pressure around the wellbore depletes rapidly. This allows gas to migrate from the gas cap toward the perforation. The gas oil contact is lowered significantly around the wellbore and forms an inverted bell shape called gas cone.

Gas coning is an undesirable phenomenon as it reduces well productivity, efficiency of gas drive mechanism and overall field recovery. Various factors such as production rate, vertical and horizontal permeability and fluid densities affect the extent and rate of formation of gas coning.

An artificial neural network was structured and trained to take these parameters as input and estimate the extent of the gas cone formation in the reservoir. Artificial neural networks (ANN) have the capability to provide solutions which are not easily analyzed by other computing methods.

Feed forward back propagation type of networks with two hidden layers was designed to estimate gas saturation values up to 160 feet from the reservoir. The gas saturation values generated by the neural network will help the user to investigate the impact of reservoir properties and well operations on the gas cone formation.

TABLE OF CONTENTS

LIST OF FIGURES

LIST OF TABLES

ACKNOWLEDGEMENTS

I would like to express my sincere gratitude to my thesis advisor Dr. Turgay Ertekin for providing me with continuous support for my Master's of Science thesis project. It was my honor to have him as my thesis advisor. I truly appreciate his contributions and suggestions given at every stage of my research. He was always accessible and helped me deal with each hurdle patiently.

I am grateful to Dr. Li Li and Dr. Zuleima T. Karpyn for showing their interest in serving as committee members and for making themselves available at short notice.

I would also like to thank doctoral students Yogesh Bansal and Amir Mohammad Nejad for their constant support and the department of Energy and Mineral Engineering for the financial support.

This thesis would have been impossible without support from my mother Madhu Sharma and my father Dr. Rakesh Sharma and I am highly indebted to them.

Finally, I would like to thank all my friends for their emotional support at different times.

Chapter 1

INTRODUCTION

Oil Reservoirs often have gas-oil contact with gas cap overlying oil bearing zone. Gas coning can be a serious problem in such cases. As the well starts producing, the pressure around the wellbore depletes rapidly and the gas starts to migrate downward toward the wellbore. Since the pressure drop is larger nearer the wellbore, the dip in the gas oil contact is larger near the wellbore region forming an inverted cone like shape. Several reservoir rock and fluid properties with implemented production strategies can affect gas cone formation. Some of them are vertical permeability, lateral permeability, production rate, difference in densities and porosity.

Eventually gas breakthrough occurs and gas starts to flow into the wellbore. As a result, the gas-oil ratio increases significantly. This can severely reduce the recovery factor of the reservoir and also increase handling and separation costs at the surface. Gas coning can be avoided by producing the well below a critical rate however this may render production operations uneconomical after a certain period of time. The other option would be to re-perforate at a lower depth however this gives smaller contact with the reservoir and a larger drawdown would be required to compensate for it further enhancing gas coning problem.

The relationship between reservoir properties, operating conditions and gas cone extent is complex and often a simulator is required to predict the severity of the problem.

Simulators are often used to predict reservoir behavior under various operating conditions, however, the use of a numerical simulator can be laborious and may require a trained engineer to utilize it. Artificial neural networks provide another practical alternative and are widely used in various engineering disciplines. They are modeled over biological neural networks and come handy when the relationship between inputs and outputs is nonlinear and complex. The networks developed in this study were trained to estimate the gas cone extent at the end of each year for the first five years of production. This gives an accurate idea how fast the cone is developing both in vertical and horizontal directions. The neural network takes into account several influential factors such as permeability, production rate and porosity and estimates the gas saturation values around the wellbore in the upper layers of the reservoir where gas coning problem is most severe. These parameters can be changed and the effect of these parameters can be immediately seen on gas cone formation. The engineer can then decide optimum production rate for any given reservoir and also understand how reservoir properties and production rate influence the formation of gas cone.

Chapter 2

LITERATURE REVIEW

Most of the papers published on gas coning use analytical methods for predicting the critical flow rate and breakthrough time but only a few of them discuss the impact of reservoir properties on the gas cone formation rate. In this section some of these analytical methods are presented.

2.1 Gas coning

Few of the main factors affecting gas coning phenomena are difference in densities of gas and oil, viscosity differences, formation permeability, pressure drawdown and flow rate. Since the coning tendency is inversely proportional to the density difference, gas has relatively lower tendency to cone compared to water. Gas is lighter than water and the density difference between gas and oil is greater than density difference between oil and water and hence gravity segregation is more significant in case of gas coning than water coning (D.G. Hatzignatiou 1994). Due to gravity segregation, it takes longer for the gas cone formation.

A vertical well creates a greater pressure gradient near the wellbore and hence is more susceptible to coning problems. In gas-coning system, the downward force due to pressure gradient near the wellbore is high and cannot be equalized by the density

difference between oil and gas and in such cases the gas starts to migrate toward the perforations until it starts leaking into the wellbore(R. Recham 2001).

Coning can be avoided if the well is produced at a certain minimum production rate. This production rate is called critical flow rate. If the production rate exceeds critical production rate, coning problems are inevitable.

Simulation methods are useful to predict critical rates in reservoirs with complex heterogeneities and boundaries but they are manpower intensive and require a good degree of expertise. There are many analytical methods available to compute the critical production rate, however, the assumptions made are often limiting. Moreover these analytical solutions can only compute the critical oil production rate and break-through time and there is no correlation to predict impact of reservoir parameters and well production rate on the extent of gas cone.

Several correlations exist to predict gas breakthrough time and critical production rate. Three of these correlations are considered in this thesis project.

2.1.1 Meyer-Garder

Meyer and Garder (Meyer 1954) developed a flow rate equation for homogenous and isotropic reservoirs with following well penetration and fluid parameters:

1. Oil and gas density difference
2. Depth from the original gas-oil contact to the top of the perforations
3. The oil column thickness

$$Q_{oc} = 0.246 * 10^{-4} \left[\frac{\rho_o - \rho_g}{ln\frac{r_e}{r_w}}\right] [\left(\frac{k_o}{\mu_o * B_o}\right) [h^2 - (h - D_t)^2]$$

where,

Q_{oc}: critical oil flow rate in a gas-oil system

ρ_o : density of oil in lb/ft3

ρ_g: density of gas in lb/ft3

k_o: effective oil permeability, md

r_e: external drainage radius in feet

r_w: wellbore radius in feet

B_o: formation volume factor

h: oil column thickness in feet

D_t: distance from the gas-oil contact to the top of the perforation in feet

h_p: $h - D_t$ in feet

The correlation shows that the critical oil production rate is directly proportional to the difference between oil and gas densities, effective oil permeability and inversely proportional to the viscosity of oil. The flow rate equation developed is only applicable for isotropic reservoir and thus vertical permeability is excluded from consideration.

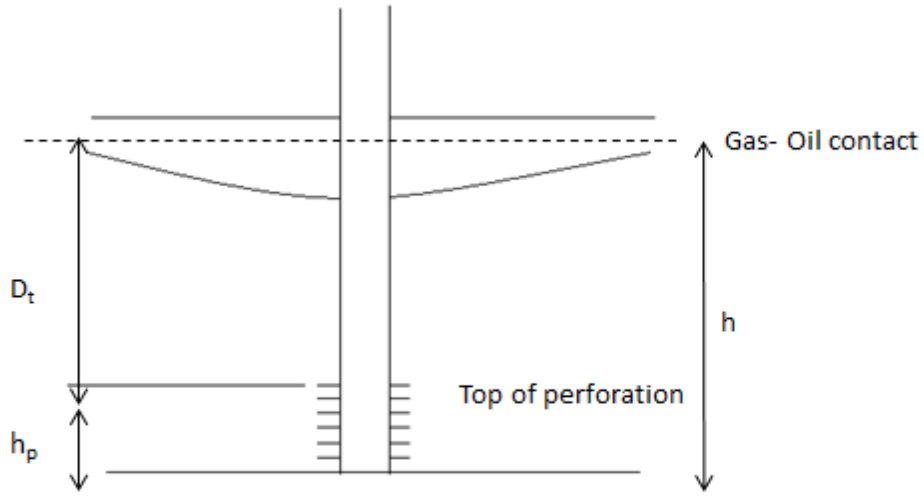

Figure **2-1**: Lowering of gas-oil contact near the wellbore.

2.1.2 Chierici-Ciucci

Chierici and Ciucci (Chierici G.L 1964) developed a potentiometric model and predicted critical oil rate in vertical wells. They generated dimensionless graphs to take into consideration the permeability anisotropy. The charts can be used for the following purposes

a. Critical oil rate can be determined once the reservoir properties, fluid properties, location and perforated interval length are described.
b. Location of the perforation interval can be determined if reservoir properties and fluids characteristics are given.

Dimensionless parameters were defined that can be determined from a graphical correlation to compute the critical oil rate.

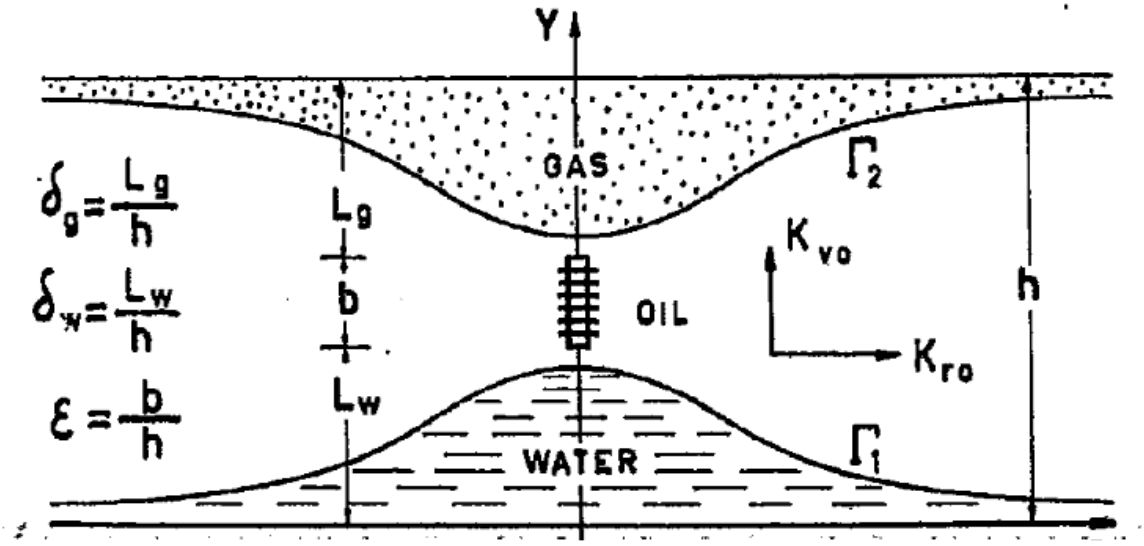

Figure **2-2**: Gas cone formation and the definitions used(Chierici G.L 1964).

One of the dimensionless parameter introduced was the effective dimensionless radius, r_{DE} and is mathematically defined as follows:

$$r_{DE} = \frac{r_e}{h}\sqrt{\left(\frac{k_v}{k_{ro}}\right)}$$

and it is valid for the range given below

$$5 \leq r_{DE} \leq 80$$

The authors then described dimensionless perforated length ε. It is mathematically defined as follows

$$\varepsilon = \frac{b}{h}$$

this graphical correlation is only valid for the given range

$$0 \leq \varepsilon \leq 0.75$$

The dimensionless gas cone ratio as defined by the following relationship

$$\delta_g = L_g/h$$

with

$$0.070 \leq \delta_g \leq 0.9$$

$$Q_{og} = 0.492 * 10^{-4} \left[\frac{h^2(\rho_o - \rho_g)}{B_o * \mu_o}\right](k_{ro}k_h)\psi_g(r_{DE}, \varepsilon, \delta_g)$$

where,

Q_{og}: critical oil flow rate in gas-oil system STB/ day

ρ_o: oil density in lb/ft3

ρ_g: gas density in lb/ft3

k_{ro}: horizontal permeability in md

k_h : vertical permeability in md

ψ_g: gas dimensionless function

B_o: oil formation volume factor

μ_o: viscosity of oil

Chierici and Ciucci developed graphs to compute gas dimensionless function ψ_g from the dimensionless parameters calculated which is used to compute the critical rate. The set of curves are only applicable for homogenous reservoirs. Figure 2-3 shows one of the working graphs used to predict critical oil flow rate. The dimensionless gas function is computed for r_{DE} = 30 and for various values of dimensionless perforated length.

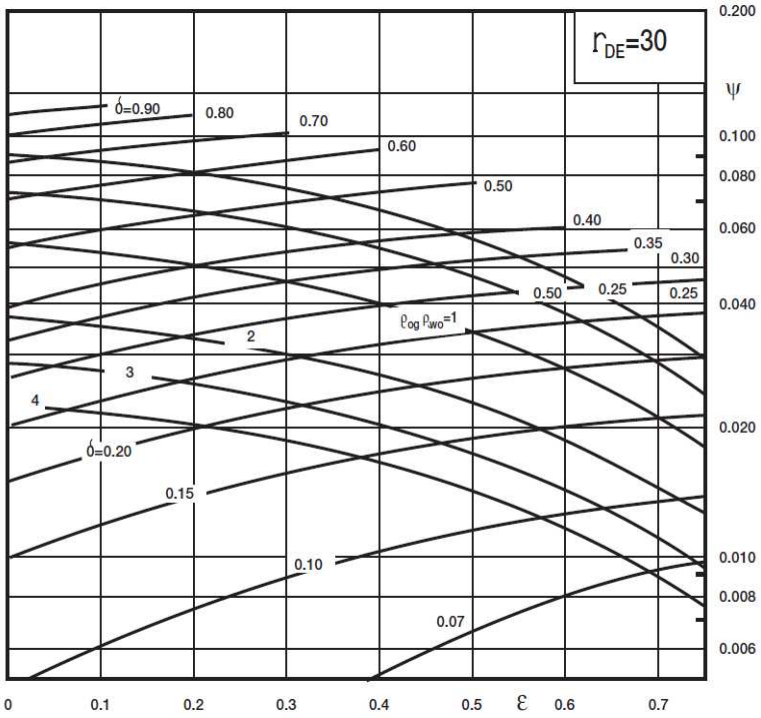

Figure **2-1**: One of the working plots developed for prediction of the critical production rate (Chierici G.L 1964).

2.1.3 Chaney Et. al

Chaney et. al (Chaney P.E. 1956) developed graphs to determine the critical oil flow rate. The authors used a potentiometric study and extended the model developed by Muskat and Wyckoff in 1935. The rates obtained (Q_{curve}) from the curves are then corrected for reservoir rock and fluid properties.

The critical oil flow rate in case of gas-oil system can be described by the following equation:

$$Q_{oc}= \ 0.2672 * 10^{-4} \left[\frac{ko*(_o - _g)}{(\mu_o * B_o)}\right] * Q_{curve}$$

where,

Q_{oc}: critical oil flow rate in gas-oil system STB/ day

ρ_o: oil density in lb/ft3

ρ_g: gas density in lb/ft3

k_o: permeability in md

B_o: oil formation volume factor

μ_o: viscosity of oil

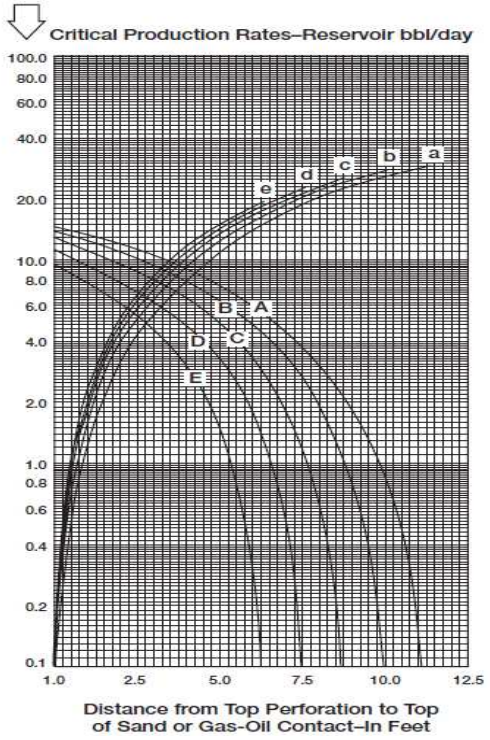

Figure **2-4**: One of the plots developed by Chaney et. al. to compute critical rates (Chaney P.E. 1956).

2.2 Artificial Neural Networks

In contrast to conventional Von-Neumann computers, neural networks often are used to find complex and previously unknown relationships between input and output parameters. The model of artificial neural networks was taken from the structure of biological neural network and their way of learning and solving complex problems. These models consist of many non-linear computational elements that operate in parallel and arranged in patterns similar to biological neural networks. Each of these Computational elements is connected via weights and these weights are typically changed to improve performance of the neural network. The construction and working of ANN is fundamentally different from conventional Von-Neumann computers. In Von-Neumann computers, the transmission delay of the transistors limits the speed of computation. Neural networks on the other hand, perform computations at much higher speed due to their parallel nature. Neural networks have adaptive and non-linear nature which allows them to adapt to changing data, learn characteristics of input data and also perform functional approximations which are otherwise almost impossible to achieve using optimal linear techniques.

Two basic steps are involved when using ANNs to find solutions.

1. The problem is formulated so as to minimize feedback ANN energy function.
2. Approximate solutions are obtained after several iterations by solving the corresponding mean field equations (Cartsen Peterson 1997).

2.2.1 Basic structure

In case of biological neural networks, neurons gather signals from others through very thin structures called dendrites. The information is sent out in form of spikes of electrical activity using thin long strands called axon, these axons then splits into thousands of branches. Each branch ends with synapse and these synapses converts activity from axon which then excites or inhibits other connected neurons. Neurons fire electrical activity down the axon when it receives excitatory input higher than inhibitory input. Influence of one neuron on the other is changed by changing the effectiveness of these synapses and this is how learning takes place.

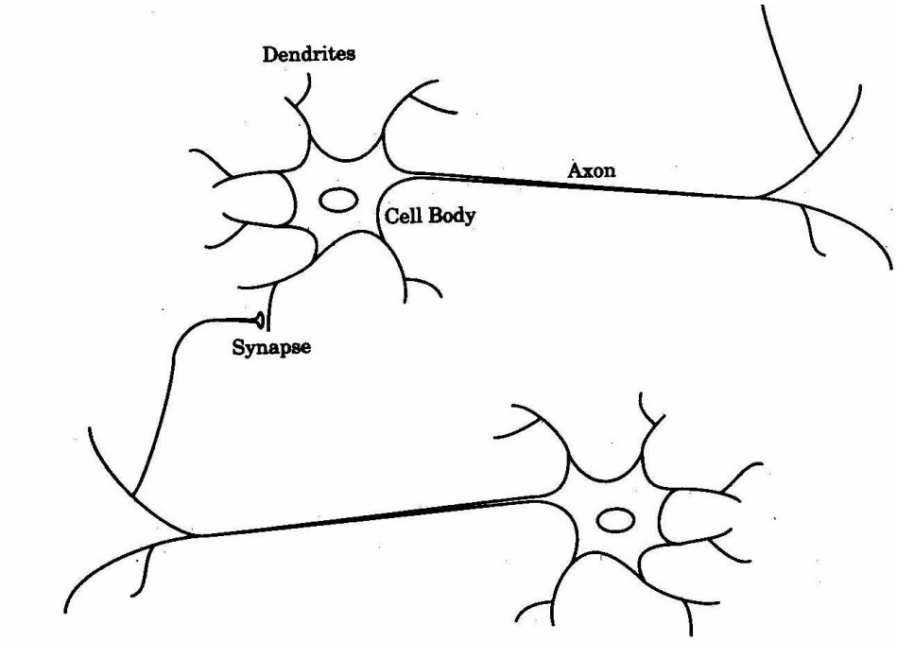

Figure **2-5**: A typical biological nerve cell and network.

2.2.2 Artificial neurons

Artificial neurons are constructed in similar ways. Inputs signals $x_1,x_2,x_3...x_n$ are merged to form an activation variable a (Gurney 2010). Each of the inputs is assigned certain weight. The inputs are multiplied by their associated weights and their sum gives activation variable *a*. Mathematically, the activation variable *a* can be described by the following equation:

$$a = \sum_i wi * xi$$

The inputs may have positive or negative weights. The output is limited to narrow range which usually varies either between -1 and 1 or between 0 and 1. This is done using a squashing function and this transformation also introduces certain non-linearity which becomes crucial for better performance (Gurney 2010). The following figure shows tan sigmoid function.

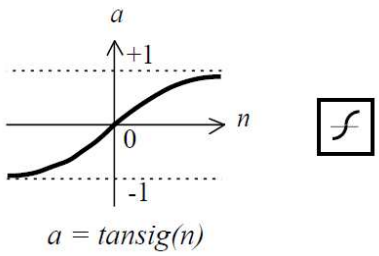

Figure **2-6**: Graph of tan sigmoid function.

The following equation gives tan sigmoid function:

$$y = \frac{exp(a) - exp(-a)}{exp(a) + exp(-a)}$$

The output *y* takes mid-value at the origin. The node is most sensitive at this mid-point and the output changes drastically near this point.

2.2.3 Feed-forward networks

In case of feed-forward network, the information flows only in one direction i.e. from the input layer toward the output layer. It may consist of several hidden layers and each hidden layer may consist of several neurons. Since the flow of information is unidirectional, there are no loops involved. The inputs may be arranged in any order and their purpose is to receive information and distribute it to the set of neurons in the first layer. These inputs are arranged in one dimensional matrices and are called as vectors. Except for the input and output layers, all the other layers are called hidden layers since it isvery difficult to check the results in this region.

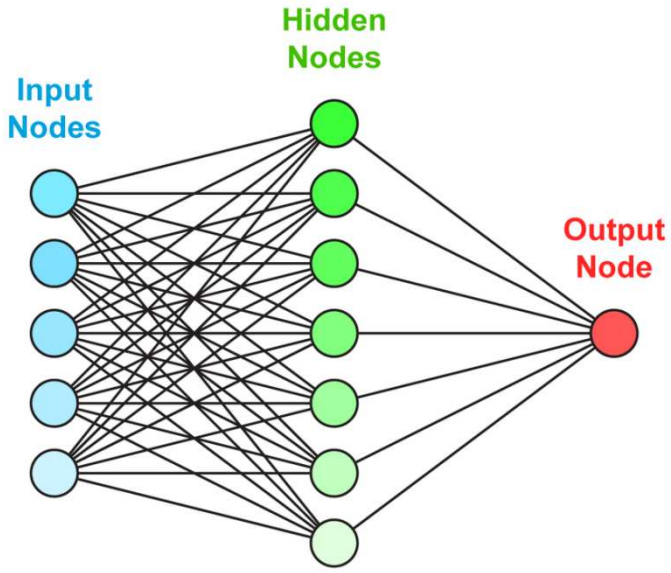

Figure **2-7**: Example of feed-forward type of network.

2.2.4 Training of feed-forward networks

The training of these networks is done by supplying a set of inputs. The output from the network is then compared with the actual target. In case there is significant difference between the network output and the actual desired output then the weights are changed to bring the network output closer to the target. This type of training is called supervised training. To check for the performance, difference between network's output and target is taken and squared, this is to make sure that the difference is always positive. The error is defined as:

$$ep = (yp - tp)^2$$

and the overall error E to be the sum of the ep over all members of the training set (Gurney 2010). Mathematically this can be defined as follows:

$$E = \sum_p (yp - tp)^2$$

The idea is then to minimize E by making suitable adjustments in the network weights (Gurney 2010). Initial weights are usually kept equal for all inputs and are changed gradually. Training progresses by making suitable adjustments to these weights and bring the network's output closer to the targets. Training stops when the error goes below the tolerance level.

Chapter 3

STATEMENT OF THE PROBLEM

Gas coning has been given significant consideration over the span of few decades. As mentioned earlier, gas coning creates many problems for the operating companies. Although many papers have been written over the years describing analytical solutions to predict critical oil rate and break-through time, only a few discuss the impact of several reservoir and well production parameters on gas coning. Simulators can help answer some of these questions however it can prove to be cumbersome to exploit the power of simulators. Artificial neural networks can offer alternative approaches to reservoir simulations. They are easy to use and require no prior knowledge to operate them unlike traditional simulators.

This research project investigates how reservoir properties such as porosity, permeability, production rate and other factors influence gas cone formation. Artificial neural networks (ANN) were trained and developed to predict how aggressively the cone forms under given reservoir properties and well production rate.

In our analysis only the upper half of the oil bearing zone was considered where the gas coning problem is most significant. ANNs were developed to generate data for the top 5 layers and for the first 5 years of production. This gives a good estimate of how fast the cone is propagating in vertical and horizontal directions. The results from ANN were then compared with a commercial black oil simulator.

Chapter 4

RESERVOIR MODEL

Often, numerical reservoir simulations are used to predict the production behavior of any given reservoir. Reservoir properties such as permeability, porosity and vertical permeability contrast are already known and are used as inputs for the simulator. These reservoir properties generally do not change much with time. Other inputs for the simulators are surface production rate, bottom hole flowing pressure and well completion and these are decided by the engineers. These simulation runs predict several parameters such as production decline, gas and oil saturation and reservoir pressure with respect to time. Based on the output from simulation runs, the engineers have to decide best operating conditions to maximize oil recovery from the field.

When there is gas-oil or water-oil contact present in the reservoir, gas-coning and water-coning can be a significant problem. It may become necessary to produce oil below a certain critical production rate so as to avoid these coning problems however these are rates that may render well production uneconomical. Artificial neural networks were trained to track the growth of gas cone in upper layers of the reservoir where gas coning is most significant. Several simulation results were generated using a commercial simulator to train the artificial neural network effectively. The reservoir considered is homogenous and anisotropic in nature.

4.1 Fluid types and initial reservoir conditions

A black oil formulation was considered to model oil bearing zone. The reservoir temperature was excluded from consideration as it has relatively small or no impact on gas coning formation. The gas oil contact also was kept constant without significant loss of accuracy. The initial reservoir pressure was varied from 3000 psia to 7000 psia for different simulation runs.

4.2 Well pattern and gridding pattern

The well is centrally located in a cylindrically shaped reservoir of external radius of 5000 feet. The radial coordinate system is considered in all the simulation runs and the well fully penetrates the oil bearing zone. The reservoir is divided into a total of twenty layers in the vertical direction. The oil bearing zone and the gas cap both are divided into ten layers each. The induction of a large number of layers helps in increasing the accuracy of the simulation runs in the vertical direction. Figure 4-1 shows the division of gas cap and oil bearing zone into different layers and Figure 4-2 shows the placement of blocks on the logarithmic scale.

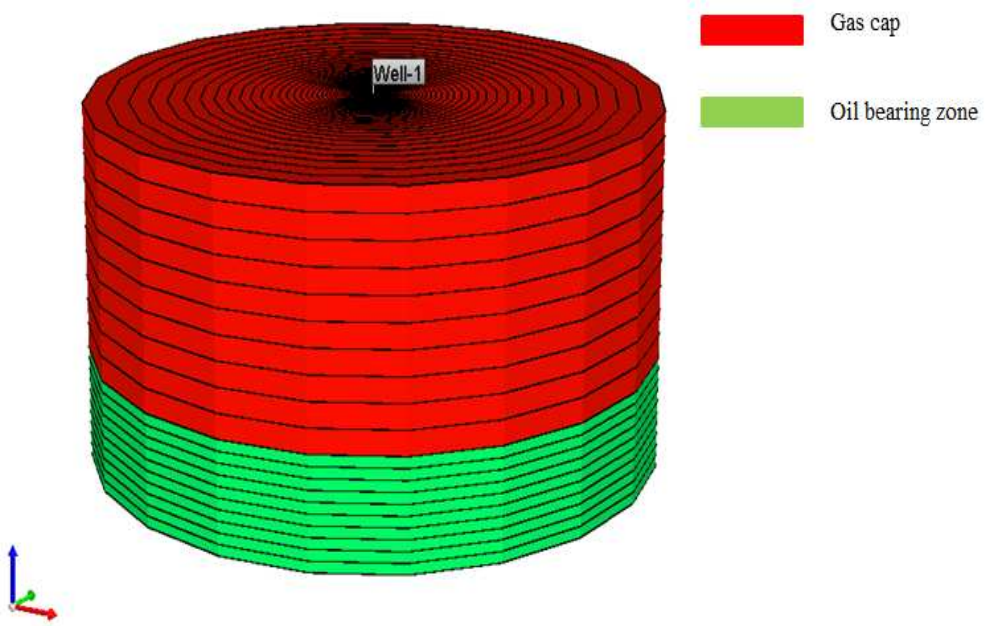

Figure **4-1**: Division of oil bearing zone and gas cap into 20 layers.

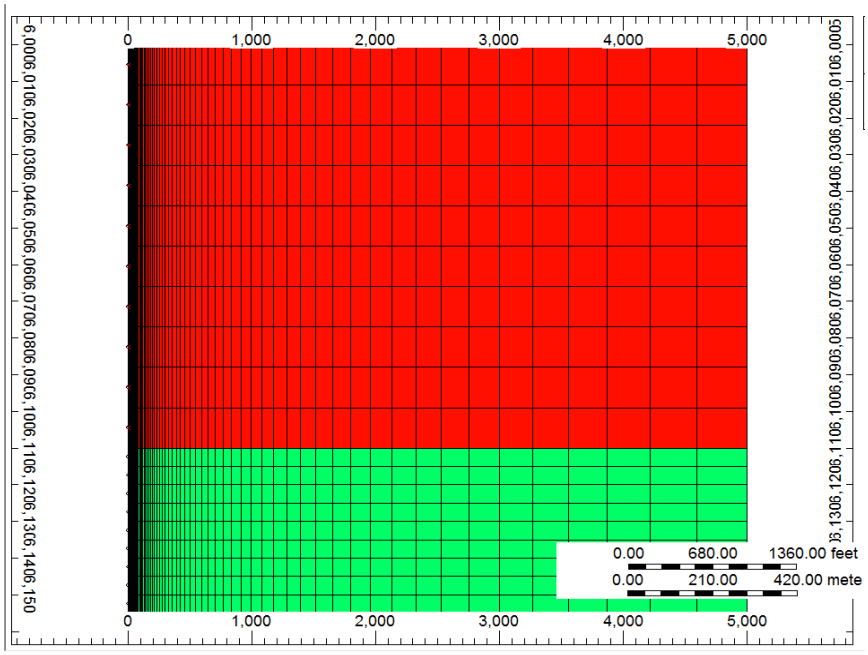

Figure **4-2**: Placement of blocks on the logarithmic scale in the radial direction.

The reservoir is divided into a total of 100 blocks in the radial direction and a logarithmic block spacing is considered. The logarithmic spacing allows having more number of blocks closer to the wellbore which is essential to improve accuracy around the wellbore.

4.3 Relative permeability

Relative permeability curve was generated using correlations provided by the simulator. The connate, critical, irreducible and residual fluid saturations values have been kept at 0. This allows the gas saturation fraction in the gas cap to be maintained at 1 for all the runs and remains constant for all the five years of production. The relative permeability of oil at connate water and gas, relative permeability of water at irreducible oil and relative permeability of gas at connate liquid all have been kept as 1. The following equation is an analytical representation used to estimate relative permeability values by the black oil simulator:

$$k_{rog} = k_{rogcg} * \frac{\left(s_l - s_{org} - s_{wcon}\right)^{n_{og}}}{\left(1 - s_{gcon} - s_{org} - s_{wcon}\right)^{n_g}}$$

$$k_{rg} = k_{rgcl} * \frac{\left(s_g - s_{gcrit}\right)^{n_g}}{\left(1 - s_{gcrit} - s_{oirg} - s_{wcon}\right)^{n_g}}$$

Where,

k_{rog} : relative oil permeability

k_{rocgc}: relative oil permeability at connate liquid

k_{rgcl} : relative gas permeability at connate liquid

k_{rogcg} : relative gas permeability at connate gas

k_{rg} : relative gas permeability

s_g: gas saturation

s_{gcrit}: critical gas endpoint saturation

s_{oirg}: irreducible oil for gas-liquid table

s_{wcon}: connate water endpoint saturation

$n_{g:}$: exponent for calculating gas permeability

n_{og}: exponent for calculating gas relative permeability

s_{gcon}: connate gas end point saturation

The exponent used to compute these relative permeability values have been kept as 2 which is typical of conventional oil reservoirs.

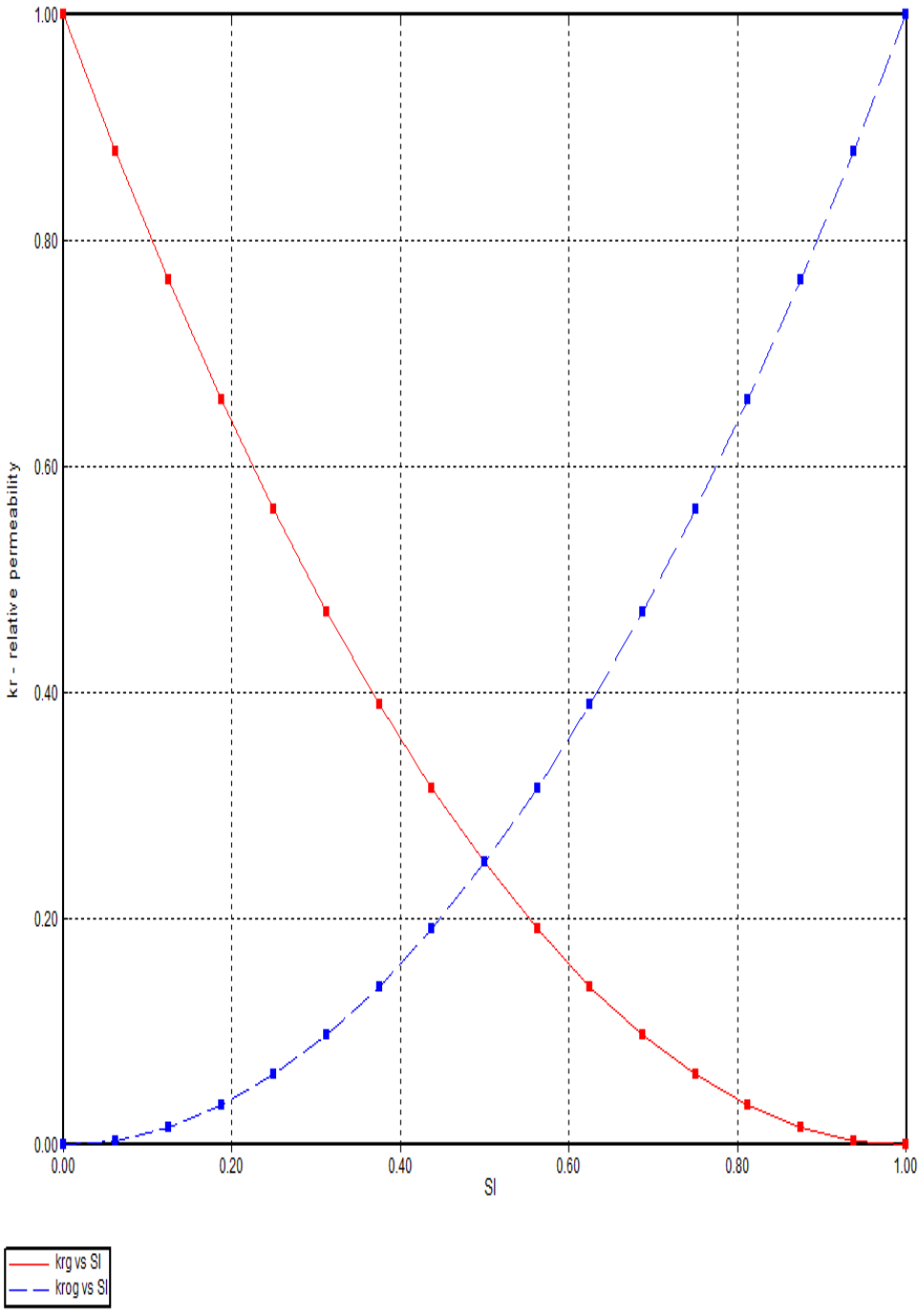

Figure **4-3**: The relative permeability curve versus saturation of liquid s_l.

Table **4-1**: Relative permeability values generated using the correlations.

Sr. No.	S_l	k_{rg}	k_{rog}
1	0	1	0
2	0.0625	0.878906	0.003906
3	0.125	0.765625	0.015625
4	0.1875	0.660156	0.035156
5	0.25	0.5625	0.0625
6	0.3125	0.472656	0.097656
7	0.375	0.390625	0.140625
8	0.4375	0.316406	0.191406
9	0.5	0.25	0.25
10	0.5625	0.191406	0.316406
11	0.625	0.140625	0.390625
12	0.6875	0.097656	0.472656
13	0.75	0.0625	0.5625
14	0.8125	0.035156	0.660156
15	0.875	0.015625	0.765625
16	0.9375	0.003906	0.878906
17	1	0.00000	1

Chapter 5

DEVELOPMENT OF THE ANN BASED TOOL

The gas cone formation rate can be monitored by estimation of the gas saturation values in the oil column at the end of each year once the well is put on production. Artificial neural networks were trained to estimate the gas saturation values in the oil bearing zone. This chapter includes selection of inputs and outputs, and training and performance evaluation of neural networks.

5.1 Inputs and outputs

The area of interest has been divided into 10 layers and has been represented by 100 blocks in the radial section. One of the ways of estimating gas saturation values can be done by considering the area of interest column by column starting with regions near the wellbore and then moving toward the outer boundary in the radial direction. The other alternative would be to consider the oil bearing region layer by layer. For this thesis project the problem was solved by considering the area of interest layer by layer. Layer no.1 is closest to the gas-oil contact whereas layer no.10 is furthest away from the gas-oil contact. A total of nine important parameters are identified which affect the gas cone formation rate and these are considered as inputs for the networks. Reservoir temperature was excluded from consideration as it made little or no significant impact on the results. Table 5-1 shows the inputs used and the range specified for these inputs. The neural networks trained accept the values of these parameters as input and generates an output of 60 vectors which gives the gas saturation fraction up to 160 feet from the wellbore in the

area of interest. The gas cone formation starts near the gas oil contact and is more severe in the upper region of the oil bearing zone and hence only the upper half of the oil column was considered as the area of interest. Since the vertical permeability is usually a fraction of the horizontal permeability the gas cone grows much faster in the horizontal direction than in the vertical direction and hence the area of interest was extended up to 160 feet in the lateral direction. The artificial neural networks trained generate gas saturation values for first the 5 layers and for the first 5 years of production of the well.

Table **5-1**: The ranges of reservoir properties and well production rate considered in the study.

Sr. No.	Input	Min	Max
1.	Horizontal permeability (md)	10	200
2.	Vertical permeability contrast (fraction)	0.01	1
3.	Porosity (fraction)	0.1	0.3
4.	Production rate (bbls/ day)	500	2000
5.	Oil density (API)	48	53
6.	Gas gravity (fraction)	0.7	1.1
7.	Reservoir Pressure (psi)	3000	7000
8.	Gas cap height (feet)	5	200
9.	Oil bearing zone thickness (feet)	5	200

5.2 Training of artificial neural networks

The data required for training the neural networks was obtained from 177 different cases generated using a commercial black oil simulator. The samples were divided randomly for training, testing and validation and of these 177 training samples

107 samples were used for training, 35 samples were used for testing and 35 samples were used for validation. A total of 25 neural networks were trained which predicts gas saturation fraction for the top 5 layers of oil bearing zone and for the first 5 years of production. The number of neurons and layers required for each network depends on the size of the input, size of the output and the number of samples considered for training. Initially, only one hidden layer with 10 neurons was considered for training purposes and the type of network considered was feed-forward, back-propagation type network. The number of neurons and hidden layers were increased gradually to improve the accuracy of the results. Two algorithms were considered to train these networks, namely, Levenberg-Marquardt algorithm and scaled conjugate gradient algorithm. It is noticed that Levenberg-Marquardt algorithm generates better results as compared to scaled conjugate gradient algorithm for the first 3 layers, however, Levenberg-Marquardt algorithm took longer to train these networks and took much more memory on the computer. The scaled conjugate gradient algorithm was considered for the lower layers in the oil bearing zone where the Levenberg-Marquardt algorithm was producing larger errors. For improving the accuracy of the networks, mean square error (MSE) was considered and it gave satisfactory results. Other methods such as mean square error regularization (MSEREG) were also considered but they did not significantly improve the performance of the first network. The first layer was modeled with two hidden layers. The first hidden layer required 30 neurons and the second hidden layer required 40 neurons to generate satisfactory results. Figure 5-1 shows the structure of the network used. The performance of the network deteriorated upon an increment of number of neurons in the hidden layers. The same neural network structure was then used to

generate gas saturation values for the remaining layers however the bottom two layers gave significant amount of error when the same network was used to predict results as that of the first three layers. The networks for the bottom two layers had to be designed differently. The first hidden layer contains 35 neurons and second hidden layer contains 40 neurons. The performance of these networks did not improve upon increment of the number of neurons in the hidden layers. In spite of using a different structure of neural networks, the error observed in the bottom two layers were still considerably larger than the ones from the first three layers. The amount of error increases as one proceeds from the 1^{st} layer to the 5^{th} layer. This observation can be explained as follows. ANN solves the problem by non-linear interpolation and tries to fit a curve for the output and if part of the output has constant values then ANN will find it difficult to fit a curve for these flat profiles and this result in large errors. In a large number of sample runs used for training these networks, the gas cone could not penetrate all the way till the 5^{th} layer. In such cases, the gas saturation value in these layers was found to be very close to zero and remained constant throughout the layer and hence generated flat profiles in the output. It was noticed that neural networks experienced some extensive difficulty predicting these flat profiles. This explains why the amount of error increases from the 1^{st} layer to the 5^{th} layer. A similar problem was noticed in the lateral direction as well. In a significant number of cases, the gas cone extent remained close to the wellbore and gas saturation fraction was zero for the remaining region in the layers. Hence the error increases as one moves further and further away from the wellbore. Each network generates a few outliers and these values are not indicative of the reservoir behavior. The possible cause could be due to the fact that the size of the output generated is comparatively larger than the size

of the input and the system is slightly underbalanced. These outliers usually occur at locations away from the wellbore and hence can be ignored easily. The mean square error due to these outliers increased significantly however the overall trend of the gas saturation fraction predicted is still reasonable. The error in the first two layers is around 10% but the error increases in the bottom two layers and can be as high as up to 30%. The 6th layer and layers lower than that gave still higher amount of error and thus were excluded from consideration. Three transfer functions are available and these are "tansig", "logsig" and "purelin" and the transfer function selected for all the networks and all the layers was "tansig" transfer function.

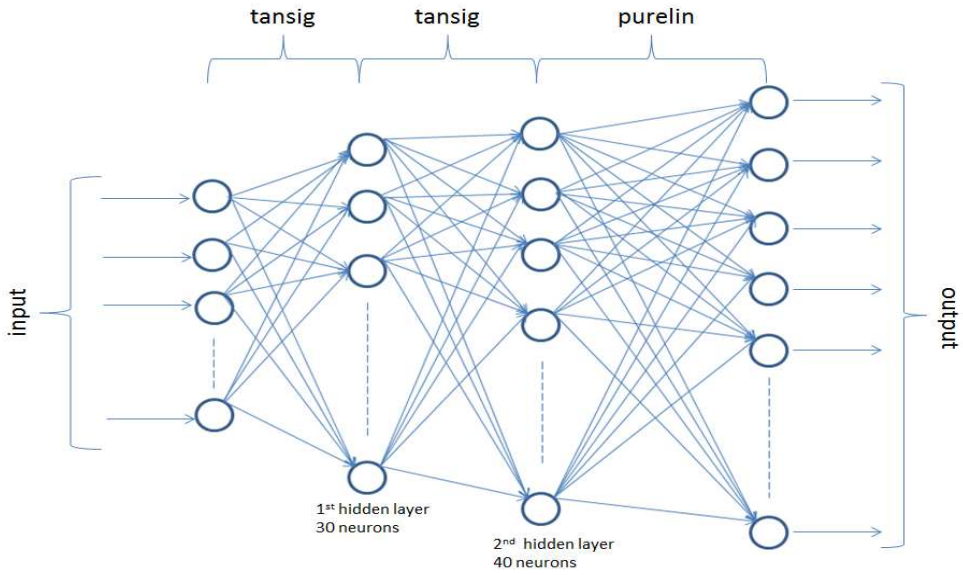

Figure **5-1**: Structure of artificial neural network used.

5.3 Performance evaluation of artificial neural networks

Three different case studies are presented in this section and the results generated using ANN are compared with the numerical models. In the first case study, the properties of reservoir and production rate are chosen such that the expected gas cone formation rate would be lower. In the second case, the horizontal and vertical permeability and the oil production rate are slightly increased and hence the expected gas cone growth rate would be slightly higher. Finally in the third case study, the horizontal and vertical permeability and oil production rate are significantly increased and the expected gas cone growth rate should be significantly higher. The vertical permeability is expressed as a fraction of the horizontal permeability and varies between 0.01 and 1. A radial cross-section of the reservoir is used for analysis of the results. The plot shows gas saturation fraction at various locations in the reservoir as predicted by numerical model and the expert system. Higher gas saturation regions are indicated by darker shades of red whereas regions having lower gas saturation values are indicated by darker shades of green. A color bar is also shown along with each plot indicating gas saturation values. These numerical models were generated using a commercial black oil simulator. Figure 5-2 shows the comparison of the three numerical models used for performance analysis of the networks.

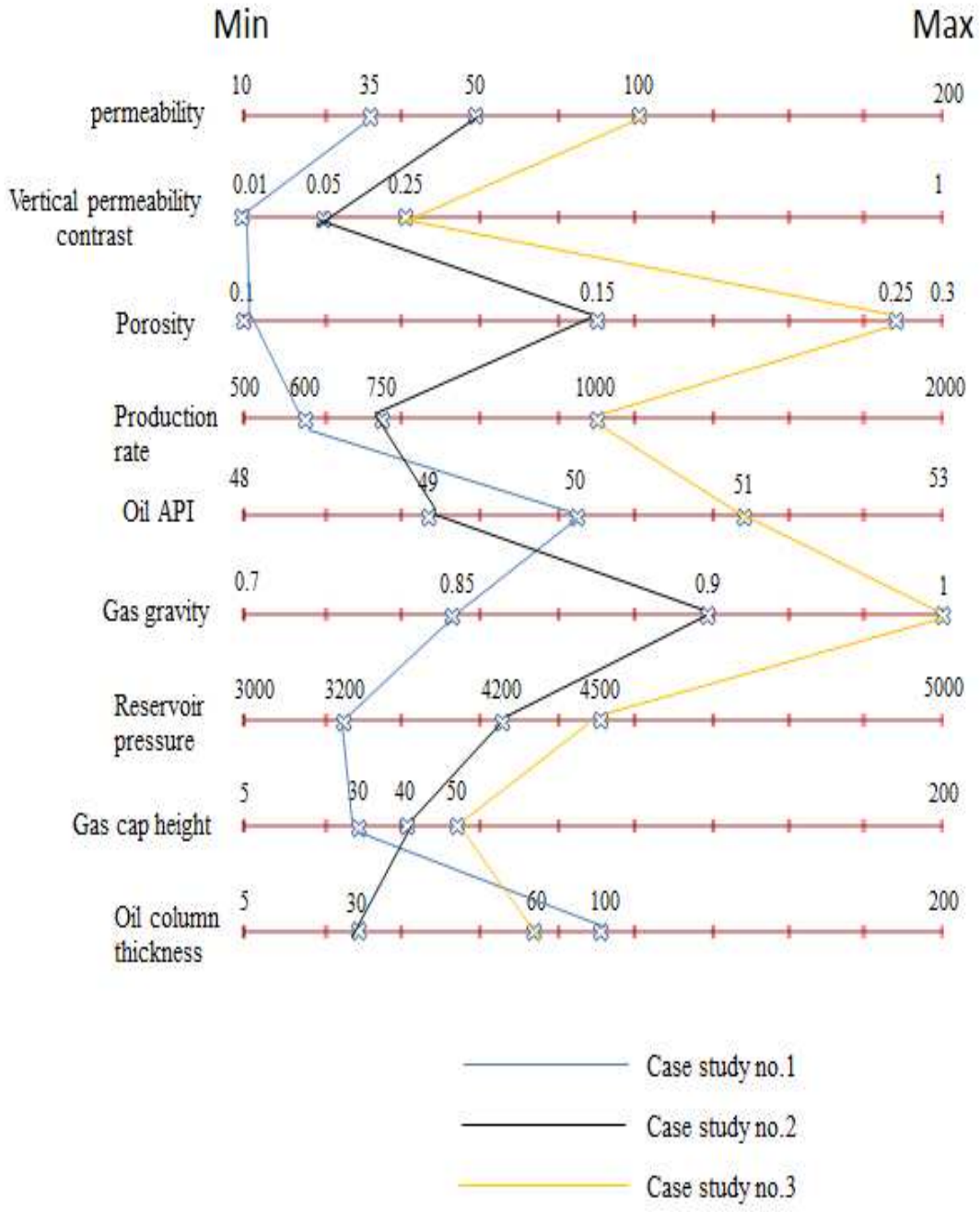

Figure **5-2**: Comparison of reservoir rock and fluid properties and production rate for three different case studies presented.

5.3.1Results and discussion for case study no.1

Table 5-2 shows the input values used for case study no.1 used to test neural networks. Since the vertical and lateral permeability values are low in this case, the gas cone formation rate is expected to be much slower in the vertical and horizontal directions. The results are compared using gas saturation color map. The gas saturation fraction varies between 1 and 0 in the oil bearing zone. The wellbore is placed on *y*-axis and the *x*-axis shows the block addresses from the wellbore.

Table **5-2**: Input used for case study no. 1 to test the neural networks.

Sr. No.	Input	Value
1.	Horizontal permeability (md)	35
2.	Vertical permeability anisotropy (fraction)	0.01
3.	Porosity (fraction)	0.1
4.	Production rate (bbls/ day)	600
5.	Oil density (API)	50
6.	Gas gravity (fraction)	0.85
7.	Reservoir Pressure (psi)	3200
8.	Gas cap height (feet)	30
9.	Oil bearing zone thickness (feet)	100

Figure 5-3 shows the gas saturation values predicted in the area of interest by the numerical model after the end of first year of production. The production rate, vertical

and lateral permeability are low in this case and as a result the rate of gas cone formation is also low. The convex shape of the curve shows that the gas saturation value decreases as the distance from the wellbore increases. The 1st layer of the oil bearing zone shows that the gas saturation is close to 0.5 while it is close to 0.2 in the 2nd layer. For the remaining region, the gas saturation is close to 0. Figure 5-4 shows the gas saturation values as predicted by the expert system. There are certain outliers in each layer however the gas saturation fraction predicted is still reasonably accurate. Figure 5-5 shows the comparison of results predicted by the numerical model and ANN and the regression value obtained is close to 85%, *y*-axis shows the result predicted by the numerical model and the *x*-axis shows the result predicted by the expert system. The error is significantly higher in the lower layers and this reduces the regression correlation coefficient considerably. Figure 5-6 shows the error between the numerical model and the expert system. The numerical model shows that the gas saturation fraction is close to zero in the lower layers however the gas saturation values predicted by the expert system are slightly higher in these layers. The error plot confirms this result and shows that there is significantly high amount of error in the lower layers. The error plot also shows that the error is higher near the boundaries of the area of interest. In spite of the outliers, the result obtained for the first three layers has only 10% error.

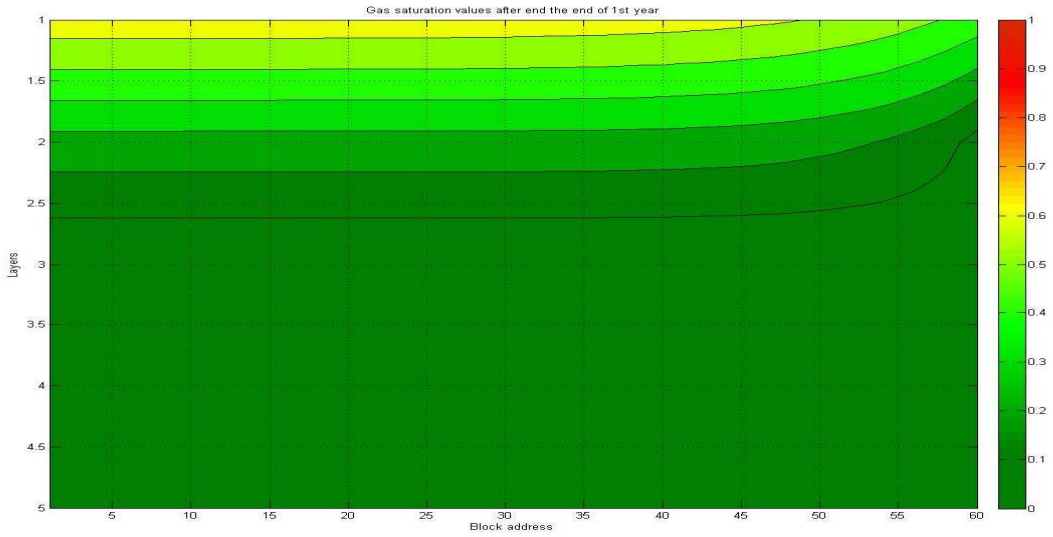

Figure **5-3**: Gas saturation values predicted by the numerical model at the end of 1st year for case study no.1.

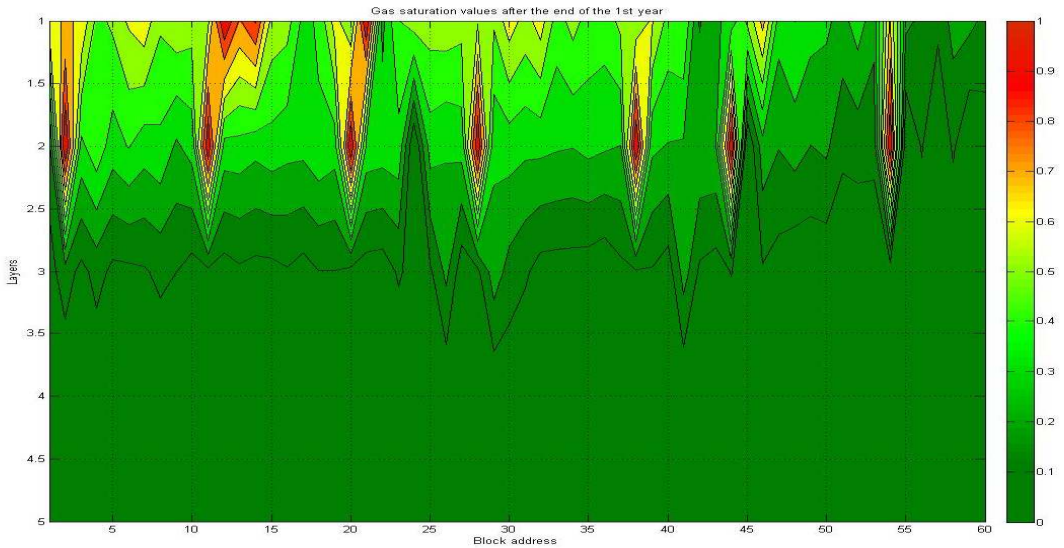

Figure **5-4**: Gas saturation values predicted by the expert system at the end of 1st year for case study no.1.

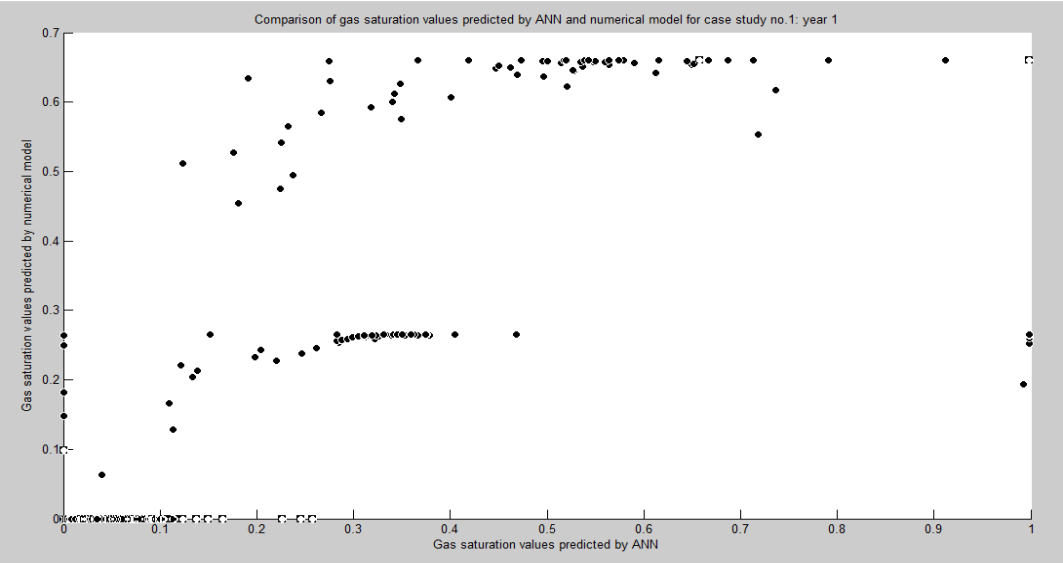

Figure **5-5**: Comparison of gas saturation values predicted by the expert system and the numerical model after the end of 1st year for case study no.1.

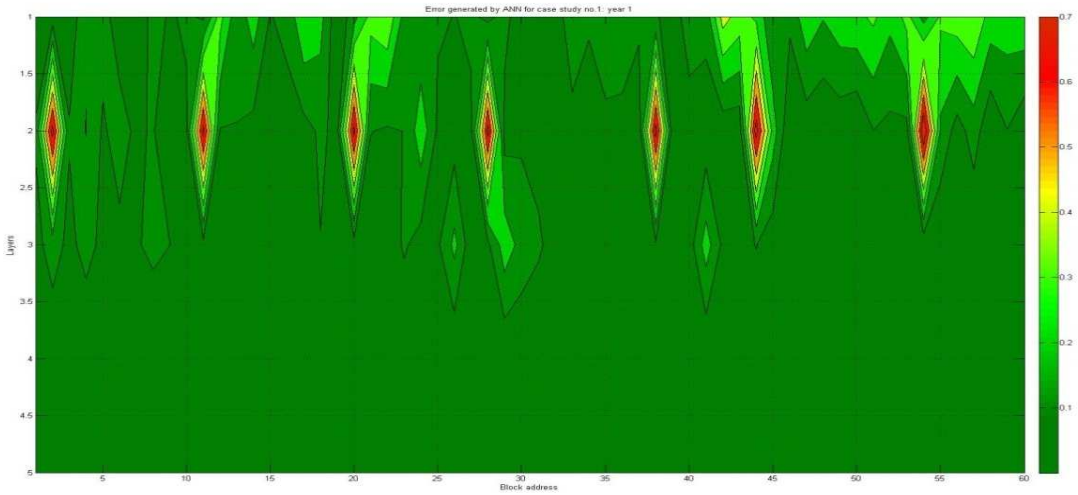

Figure **5-6**: Error plot for case study no.1 at the end of 1st year.

Figure 5-7 shows the gas saturation values predicted by the numerical model after the end of the 2nd year. The gas cone formation rate observed is low due to low vertical reservoir permeability and low production rate. The average gas saturation values predicted by the numerical model in the 1st layer and the 2nd layer are still close to 0.6 and 0.2 respectively. The gas cone curve is much flatter and is due to the fact that the vertical permeability of the reservoir is much smaller compared to the horizontal permeability of the reservoir. For rest of the region the gas saturation is almost 0. Figure 5-8 shows the gas saturation values predicted by the expert system. Again, in this case, there are certain outliers in each layer though most of them are located near the boundaries of the area of interest. Figure 5-9 shows the comparison of gas saturation values predicted by the numerical model and the expert system. The *x*-axis shows the results generated using the expert system and the*y*-axis shows the result generated using the numerical model. From the figure, it is seen that for very small gas saturation values predicted by the numerical model, the expert system predicts much higher values and is almost close to 0.1. A similar problem is noticed for gas saturation values close to 0.4. The expert system generates values between 0.35 and 0.45. The regression correlation coefficient however obtained in this case is much better and is close to 90%. This plot also shows certain outliers. The error increases toward the outer boundaries and in the lower layers of the area of interest. Figure 5-10 shows the error produced by the expert system. The error is about 0.1 in almost the entire region but is slightly more in the lower layers and region closer to the boundaries of the area of interest.

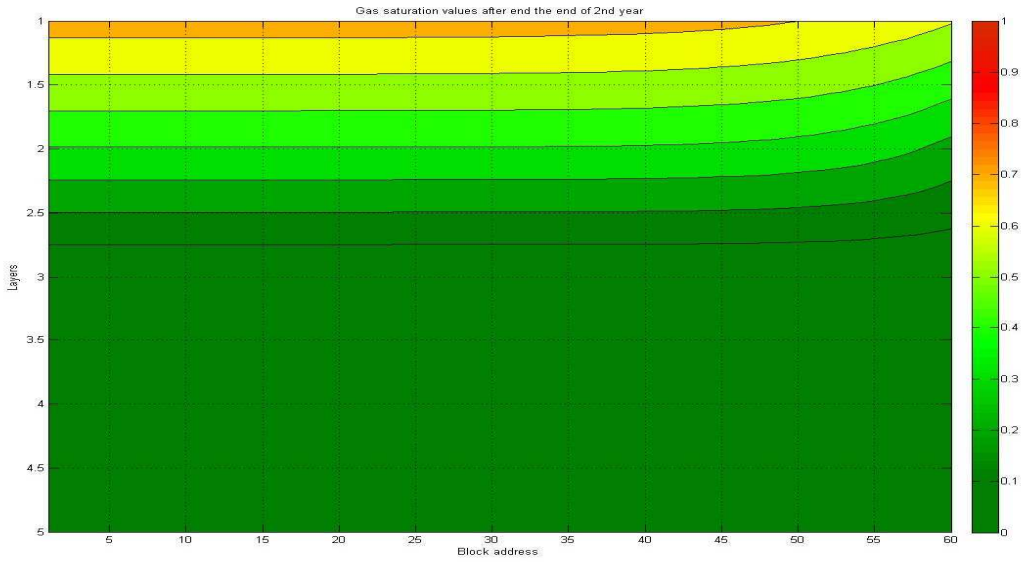

Figure **5-7**: Gas saturation values predicted by the numerical model at the end of 2nd year for case study no.1.

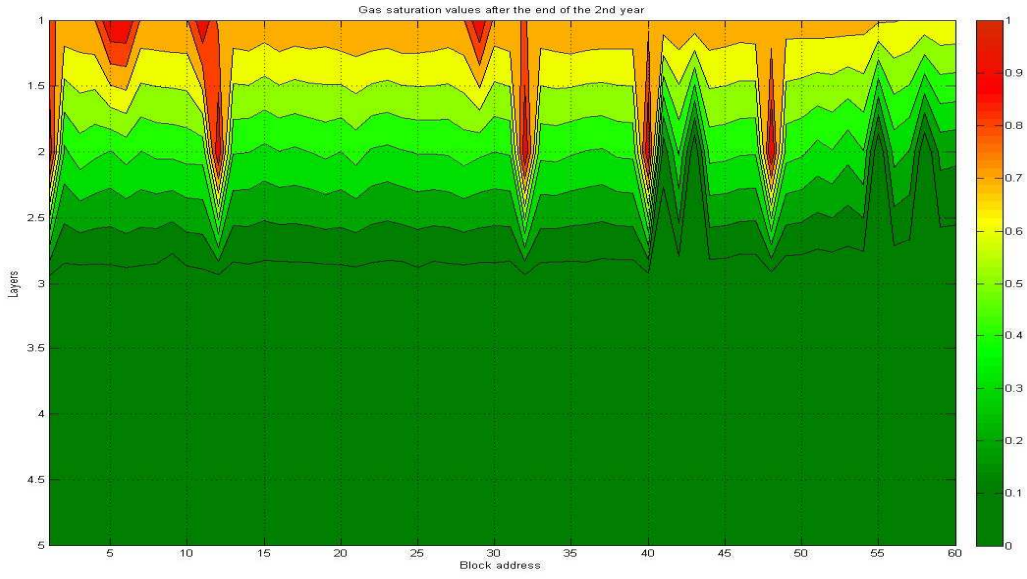

Figure **5-8**: Gas saturation values predicted by the expert system at the end of 2nd year for case study no.1.

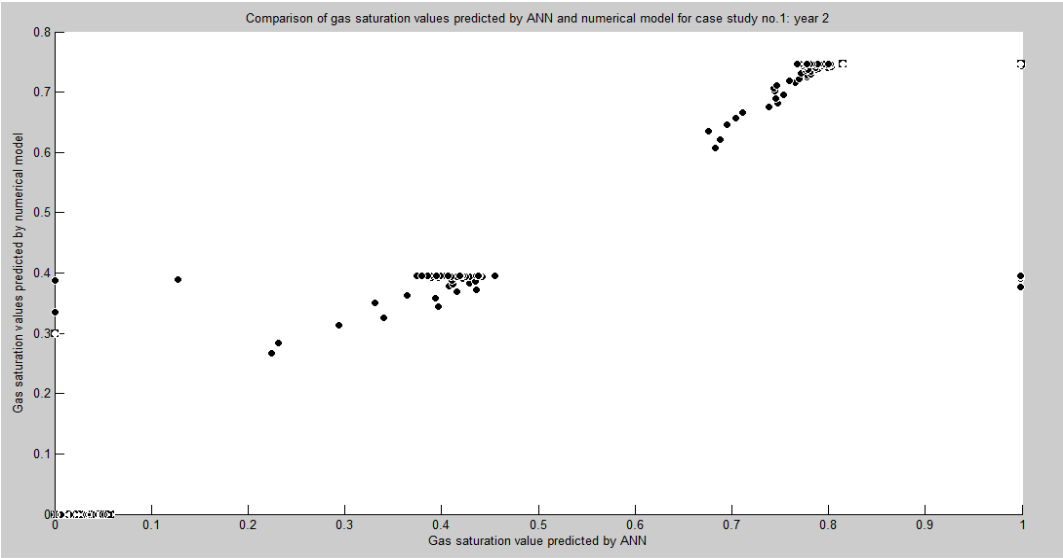

Figure **5-9**: Comparison of gas saturation values predicted by the expert system and the numerical model after the end of 2nd year for case study no.1.

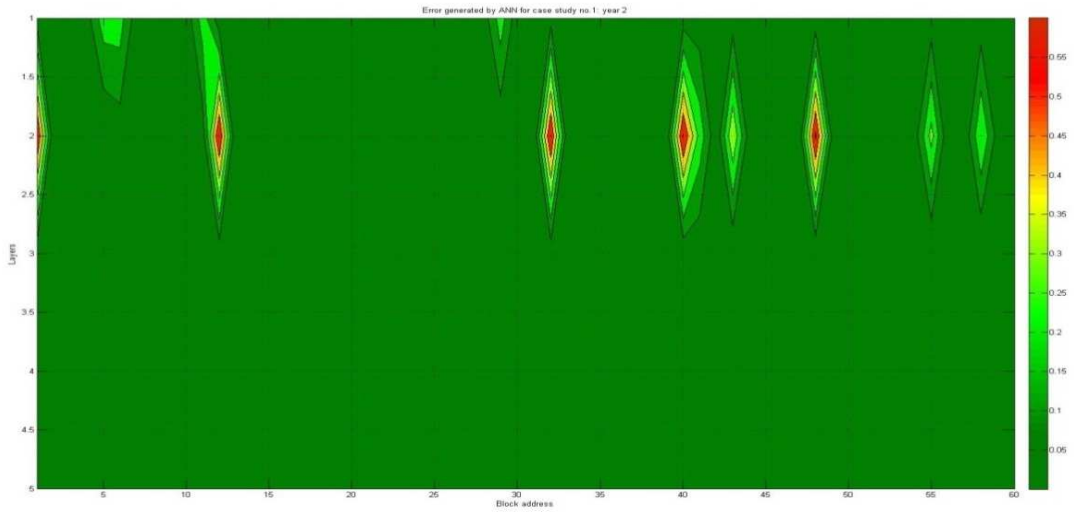

Figure **5-10**: Error plot for case study no.1 at the end of 2nd year.

Figure 5-12 suggests that the gas saturation values predicted by the artificial expert system are consistent with the numerical model. Result generated using the numerical model is shown in Figure 5-11 confirms that the gas cone encroachment rate is still low and barely extends till the 3rd layer. The average gas saturation fraction in the 1st layer has slightly increases to 0.7 and in the 2nd layer it is close to 0.3 and for the rest of the region, it is still close to 0. It is observed that the gas cone encroachment rate is much faster in the lateral direction than in the vertical direction. This is due to the fact that the lateral permeability is much higher compared to the vertical permeability. The oil column considered for this case study is much thicker and hence the gas cone extends only for a fraction of the reservoir. Figure 5-12 shows the gas saturation values generated using the expert system. There are certain outliers in each layer but most of these are located closer to the boundaries of the domain of interest. The gas saturation fraction values predicted by the expert system are in reasonable agreement with the numerical model. Figure 5-13 shows the comparison of gas saturation values predicted by the expert system and the numerical model and the regression value obtained is close to 90%. The plot shows that the expert system produces higher error for lower gas saturation values. Figure 5-14 shows the error produced by the expert system in the area of interest. The plot shows that percentage error in the first three layers is much lower than compared to the percentage error in the bottom two layers. The plot also confirms that the error is slightly larger toward the boundaries of the domain of interest.

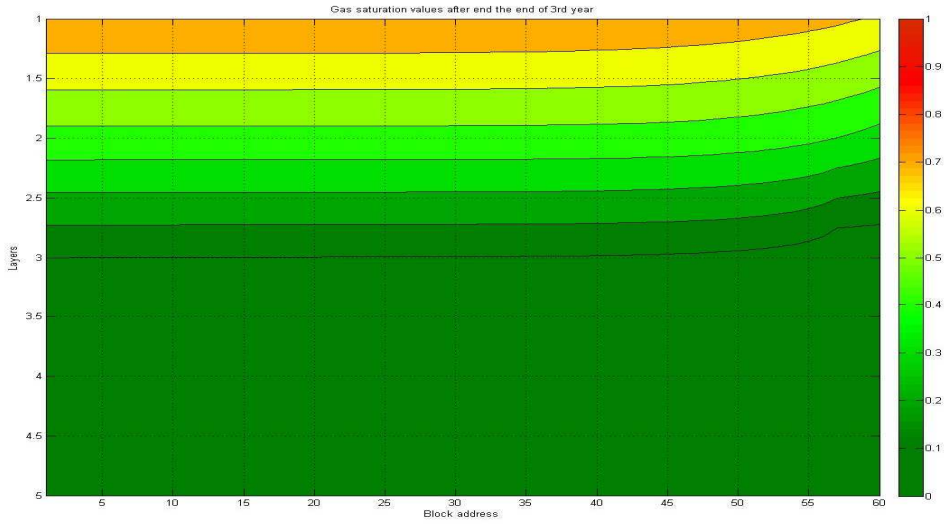

Figure **5-11**: Gas saturation values predicted by the numerical model at the end of 3rd year for case study no.1.

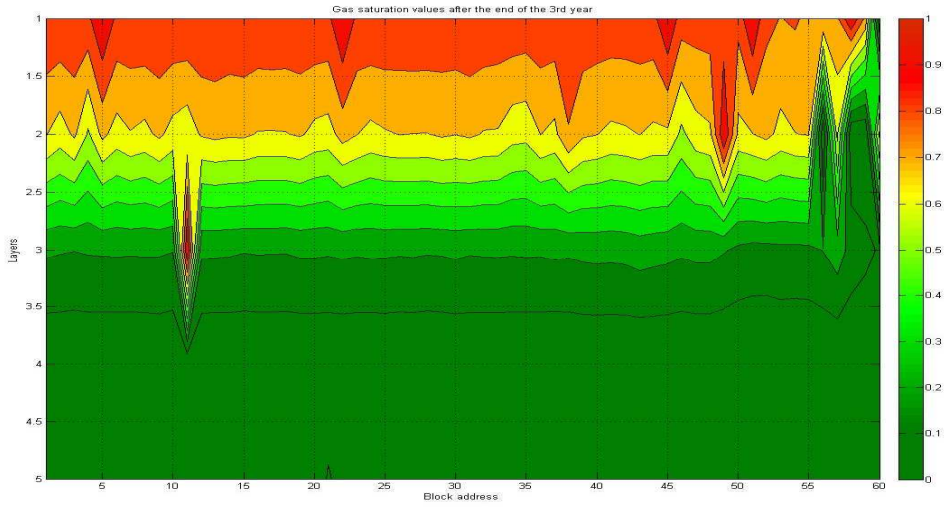

Figure **5-12**: Gas saturation values predicted by the expert system at the end of 3rd year for case study no.1.

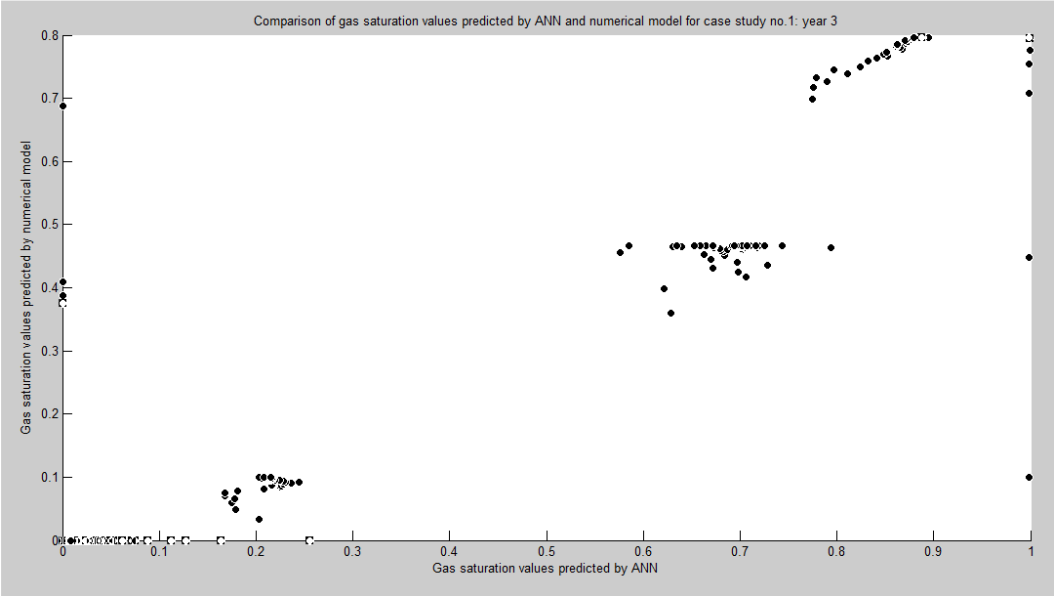

Figure **5-13**: Comparison of gas saturation values predicted by the expert system and the numerical model after the end of 3rd year for case study no.1.

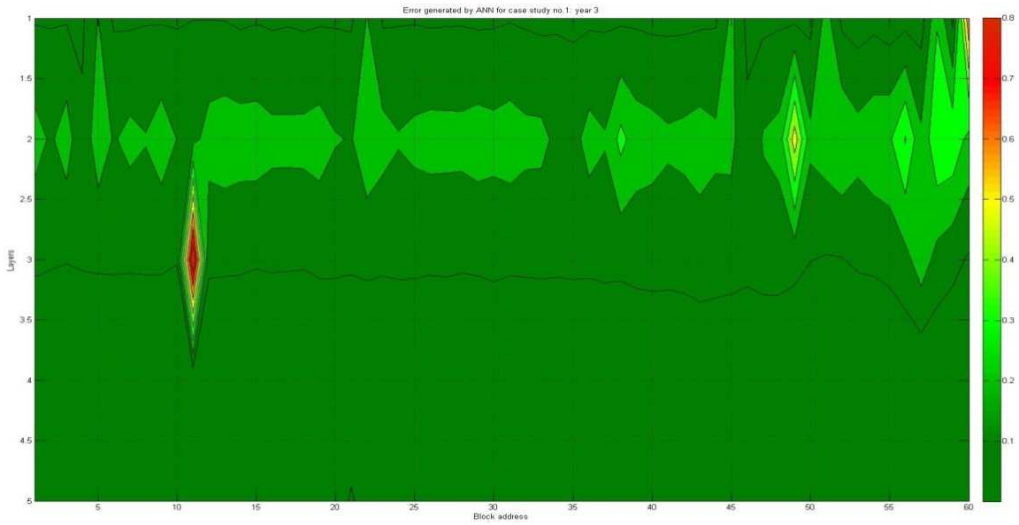

Figure **5-14**: Error plot for case study no.1 at the end of 3rd year.

Figure 5-15 shows the gas saturation values predicted by the numerical model after the end of 4th year of production. The average gas saturation value predicted for the 1st layer is close to 0.8 and for the second layer it is 0.4 and for the rest of the region it is almost 0. Figure 5-16 shows the gas saturation values predicted by the expert system and it is in reasonable agreement with the numerical model. The gas saturation values predicted in the 2nd and the 3rd layer are slightly overestimated however the error is less than 10% in this region. Figure 5-18 shows the error produced by the expert system and the plot confirms that the percentage of error is much higher toward the boundaries of the area of interest. The error is also high for the 4th and the 5th layer. Figure 5-17 shows the comparison of gas saturation values predicted by the expert system and the numerical model. The plot shows that for lower gas saturation values, the expert system produces larger error.

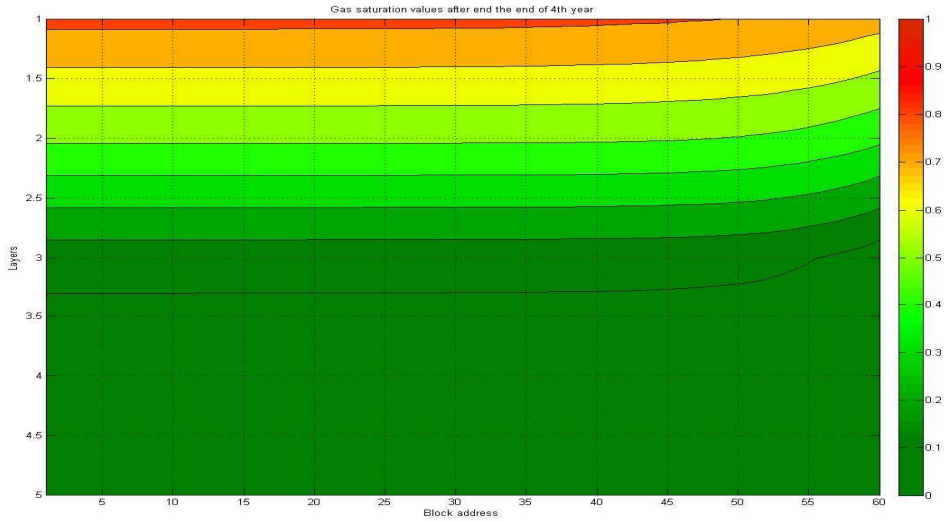

Figure **5-15**: Gas saturation values predicted by the numerical model at the end of 4th year for case study no.1.

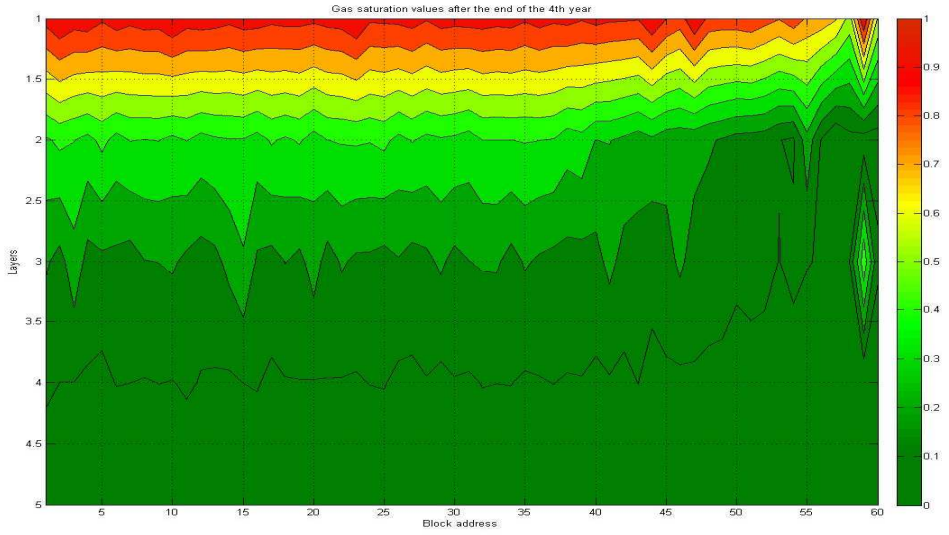

Figure **5-16**: Gas saturation values predicted by the expert system at the end of 4th year for case study no.1.

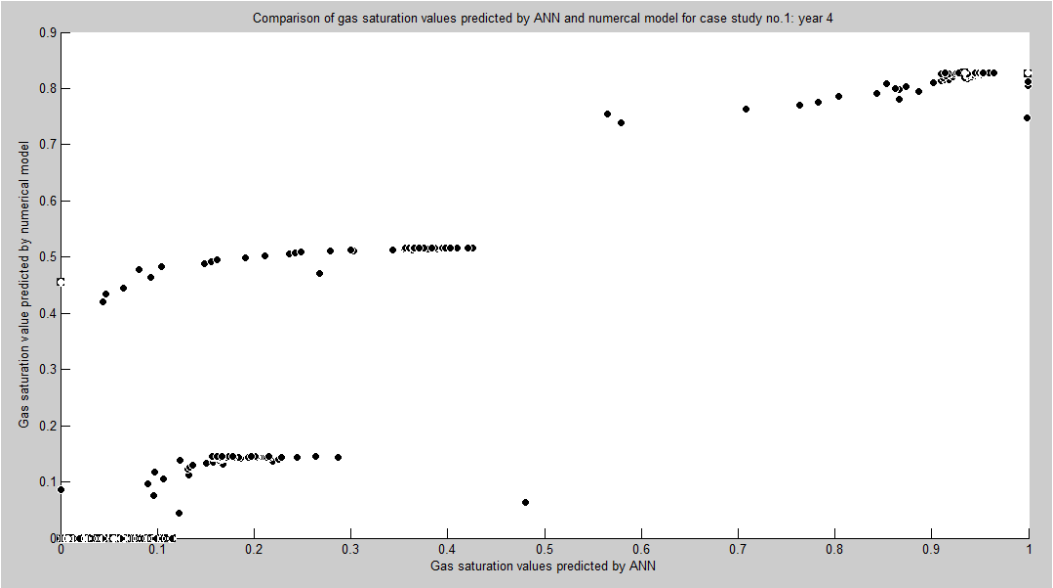

Figure **5-17**: Comparison of gas saturation values predicted by the expert system and the numerical model for the end of 4thyear for case study no.1.

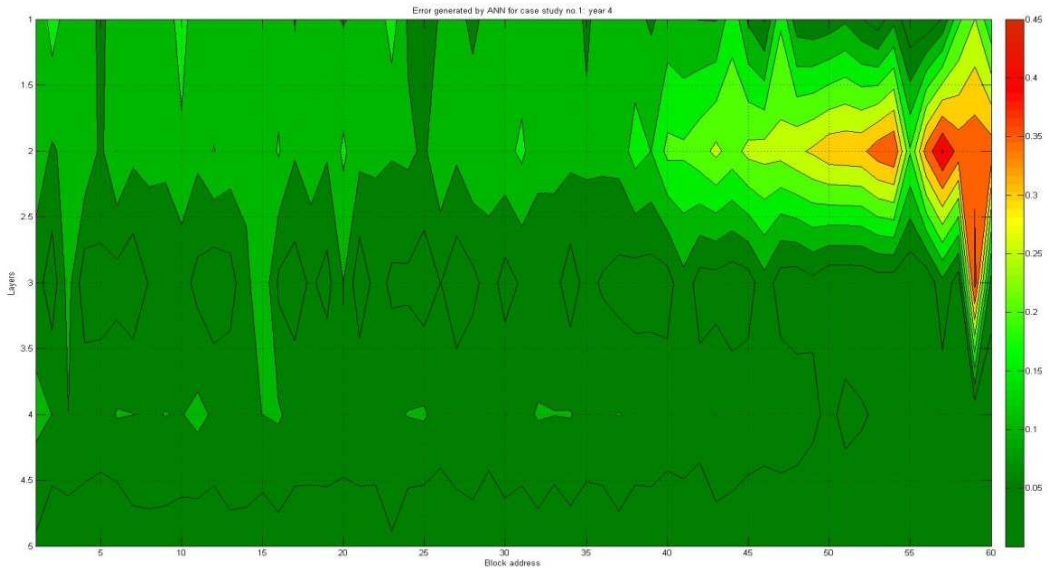

Figure **5-18**: Error plot for case study no.1 at the end of 4thyear.

Figure 5-20 shows the result generated using the artificial expert system. The number of outliers is significantly larger in the 4th and 5th layer and hence the error produced is much higher in these layers than the remaining top three layers. The gas saturation values predicted by the expert system in the 1st and the 2nd layer are slightly overestimated and the difference is of the order of 0.1 to 0.15 as shown in the Figure 5-22. Figure 5-19 shows the gas saturation values predicted by the numerical model after the end of 5th year of production. The average gas saturation value in the 1st layer has increased to 0.8 and is close to 0.4 in the 2nd layer. The gas saturation value in the 3rd layer is close to 0.1 and for the remaining layers it is 0. The plot confirms low gas cone formation rate both in the vertical and in the horizontal directions. A comparison of result generated using the numerical model and the expert system is shown in Figure 5-21. The plot shows that for lower gas saturation values, the error produced is much larger by the expert system. These lower gas saturation values are usually present in 4th and the 5th layer. The regression correlation coefficient value obtained due to these factors is much lower.

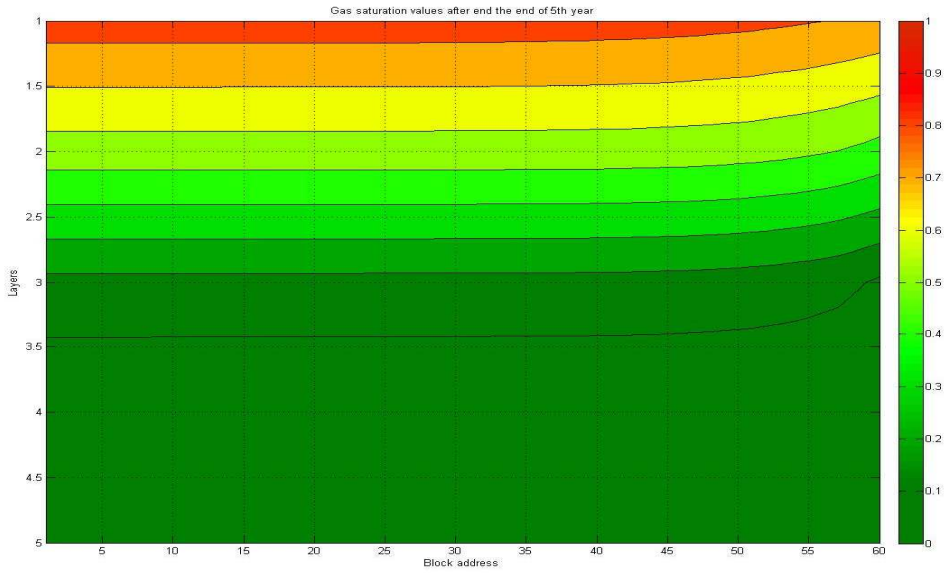

Figure **5-19**: Gas saturation values predicted by the numerical model at the end of 5th year for case study no.1.

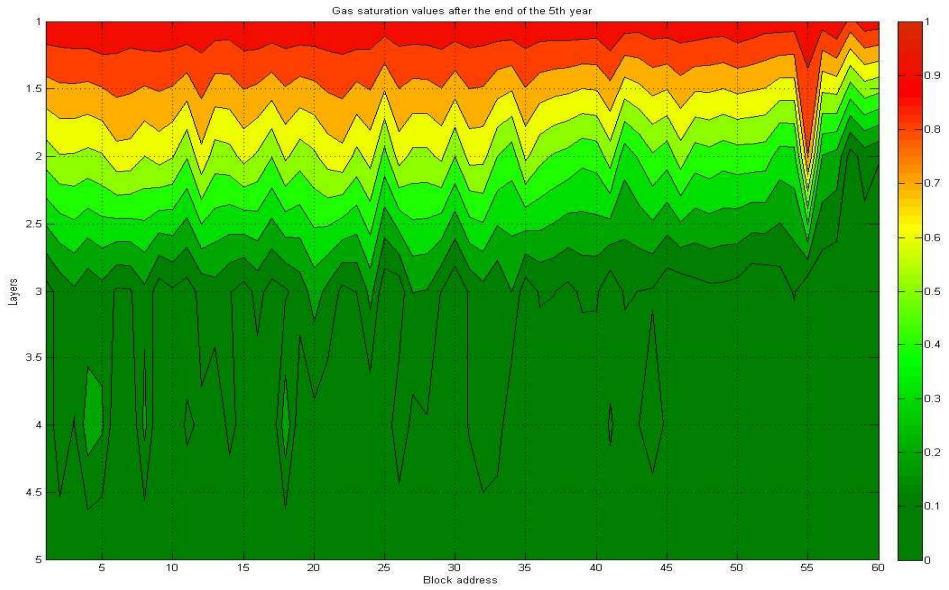

Figure **5-20**: Gas saturation values predicted by the expert system at the end of 5th year for case study no.1.

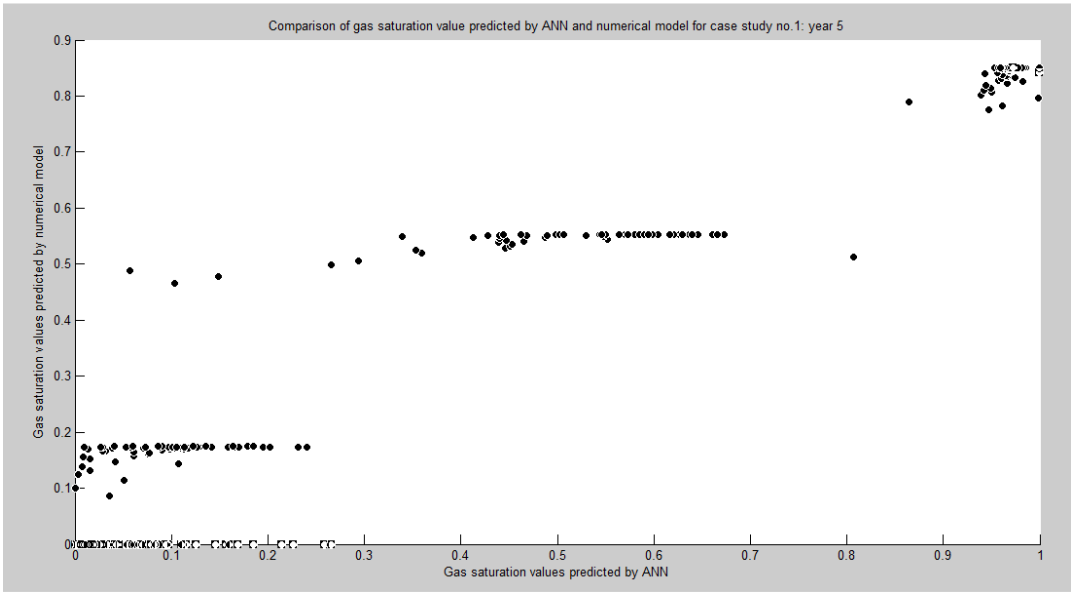

Figure **5-21**: Comparison of gas saturation values predicted by the expert system and the numerical model after the end of 5th year for case study no.1.

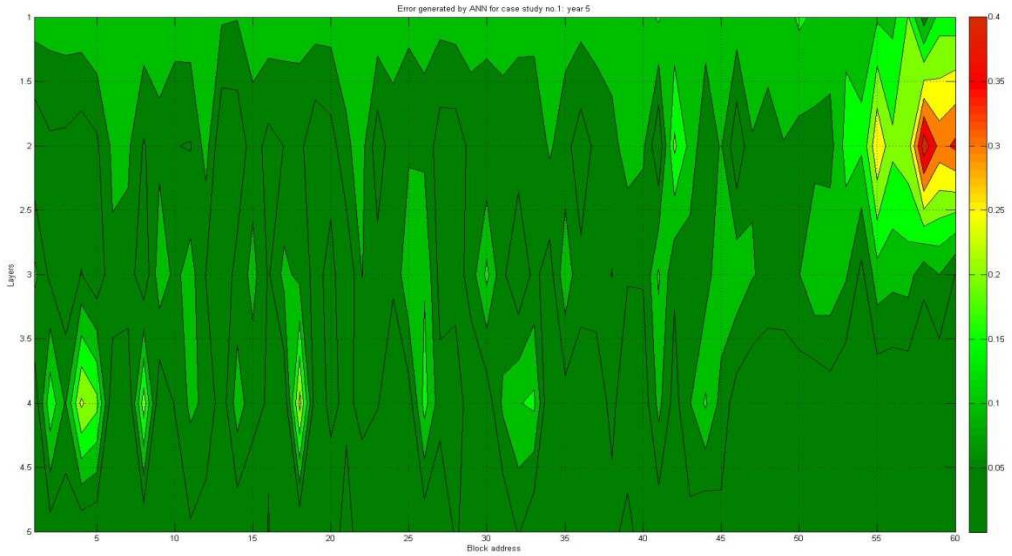

Figure **5-22**: Error plot for case study no.1 at the end of 5th year.

5.3.2 Results and discussion for case study no.2

Table 5-4 shows the input values used for case study no.2 used to test the neural networks. The reservoir permeability in the horizontal direction has been increased to 50 md while the vertical permeability contrast is increased to 0.05. The production rate is also increased to 750 bbls/ day which is much higher than the critical production rate for this reservoir. The oil bearing zone has a smaller thickness of 30 feet. Due to these factors, the expected gas cone formation rate will be higher than compared to case study no.1. The expected curvature of gas cone curve will also be slightly larger than the previous case study. The results are represented using gas saturation color map. The gas saturation fraction varies between 1 and 0 in the oil bearing zone. The wellbore is placed on *y*-axis and the *x*-axis shows the block addresses from the wellbore.

Table **5-3**: Input used for case study no. 2 to test the neural networks.

Sr. No.	Input	Value
1.	Horizontal permeability (md)	50
2.	Vertical permeability anisotropy (fraction)	0.05
3.	Porosity (fraction)	0.15
4.	Production rate (bbls/ day)	750
5.	Oil density (API)	49
6.	Gas gravity (fraction)	0.9
7.	Reservoir Pressure (in psi)	4200
8.	Gas cap height (in feet)	40
9.	Oil bearing zone thickness (in feet)	30

Figure 5-23 shows the gas saturation values predicted by the numerical model for case study no.2 after the end of 1st year. The vertical and horizontal permeability chosen are slightly higher for this case study and as a result the gas cone formation rate is more rapid. As expected, the gas coning problem is much more severe in this case. The oil column considered has a thickness of only 30 feet hence the gas cone extends till the 5th layer in this case. The curvature of the gas cone curve is also higher and this is due to the

fact that the vertical permeability is slightly higher than compared to the case study no.1. Figure 5-24 shows the gas saturation values predicted by the expert system. The average gas saturation value predicted by the numerical model in the 1st layer is close to 0.9 whereas the expert system predicts about 0.8. If we compare the gas saturation values predicted by the numerical model and the expert system, we can observe that the expert system predicts the result with a high degree of accuracy. Figure 5-25 shows the comparison of the gas saturation values predicted by the expert system and the numerical model, the regression correlation coefficient obtained in this case is higher than 90%. The regression line is skewed with a slope higher than unity which indicates that the expert system slightly underestimated the gas saturation values. The error plot as shown in Figure 5-26 confirms the same observation and the same plot also suggests that the error produced by the expert system is slightly higher for the region away from the wellbore. The error is also higher in the 4th and the 5th layer as compared to the first three layers. Each layer contains a few outliers but the gas saturation values predicted by the expert system are still in reasonable agreement with the numerical model.

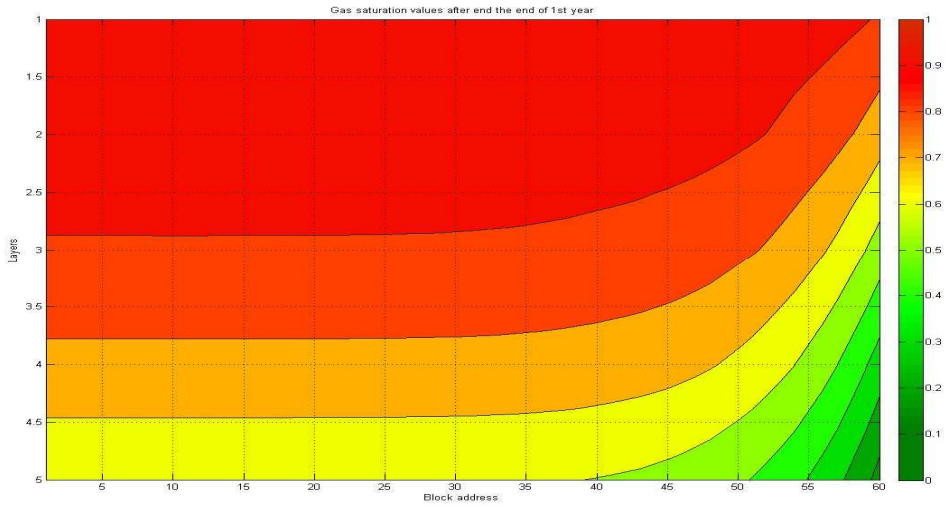

Figure **5-23**: Gas saturation values predicted by the numerical model at the end of 1st year for case study no.2.

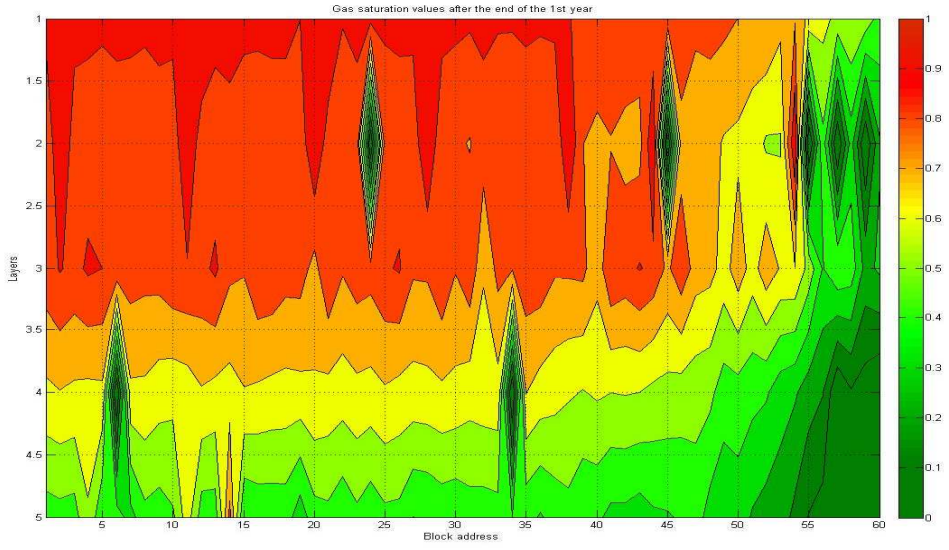

Figure **5-24**: Gas saturation values predicted by the expert system at the end of 1st year for case study no.2.

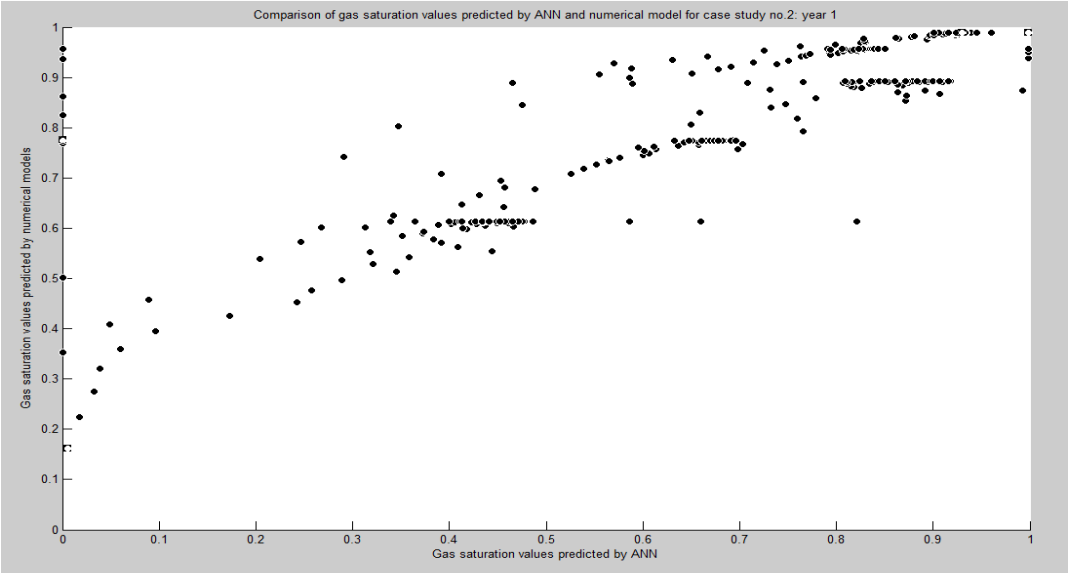

Figure **5-25**: Comparison of gas saturation values predicted by the expert system and the numerical model after the end of 1st year for case study no.2.

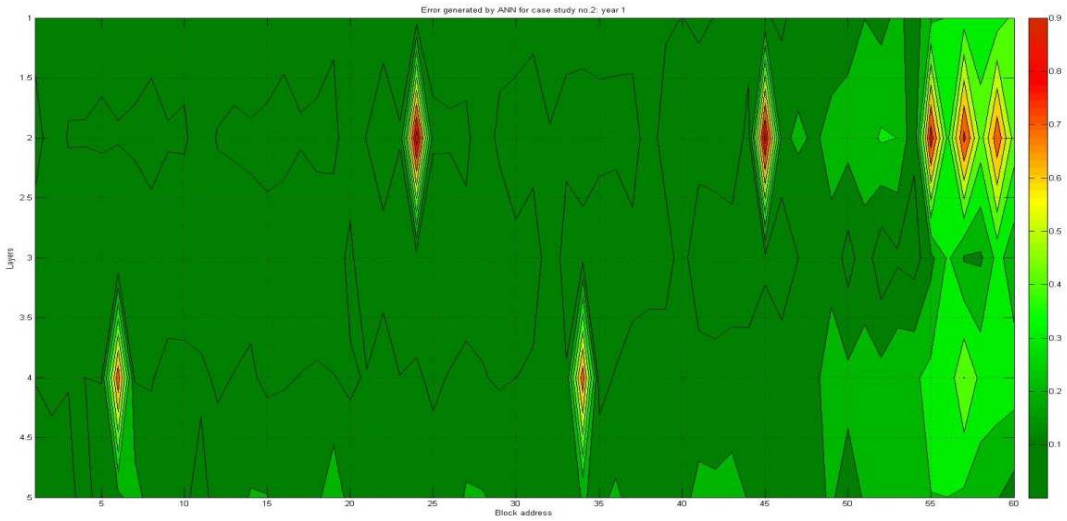

Figure **5-26**: Error plot for case study no.2 at the end of 1st year.

Result predicted by the numerical model is shown in Figure 5-27. The gas cone extent has significantly increased both in the vertical and in the horizontal directions after the end of 2nd year as expected. Figure 5-28 shows the gas saturation values predicted using the expert system. The gas saturation curve as predicted by the expert system is distorted due to presence of outliers however the result generated using the expert system still matches well with the result generated using the numerical model. The average gas saturation value for the first 3 layers is close to 0.9 however the expert system predicts a slightly lower value of about 0.8. This can also be confirmed by the plot shown in Figure 5-29. Ideally, the regression line should be a straight line with slope equal to unity and passing through the origin however in this case the slope is slightly higher indicating that the expert system slightly underestimated the gas saturation values. Most of the outliers present in each layer are located closer to the boundaries of the domain of interest and thus can be excluded from the consideration. Figure 5-29 shows the comparison of results generated using ANN and the numerical model. The regression correlation coefficient in this case is close to 90% in spite of the presence of outliers. Figure 5-30 shows the error produced by the ANN and shows that error is in the range of 0 to 0.15 for region closer to the wellbore. The error is significantly higher near the boundary of the domain of interest.

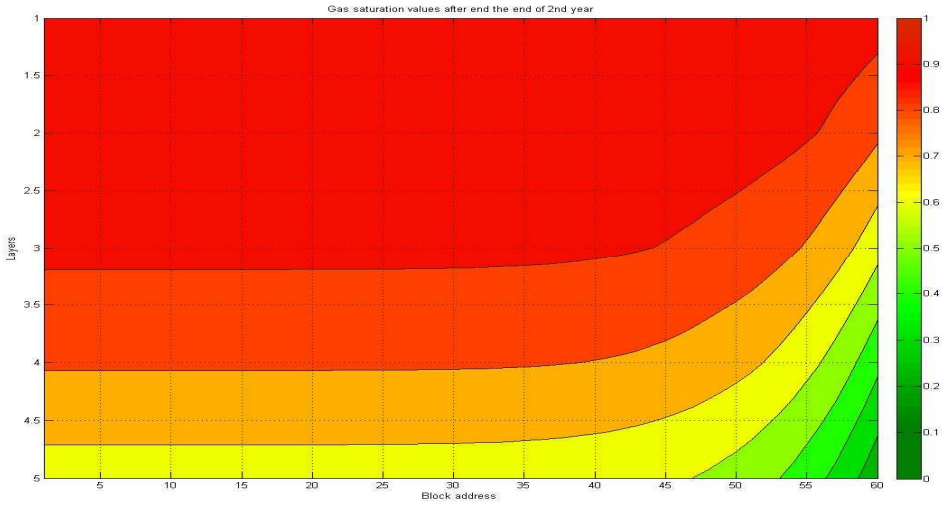

Figure **5-27**: Gas saturation values predicted by the numerical model at the end of 2nd year for case study no.2.

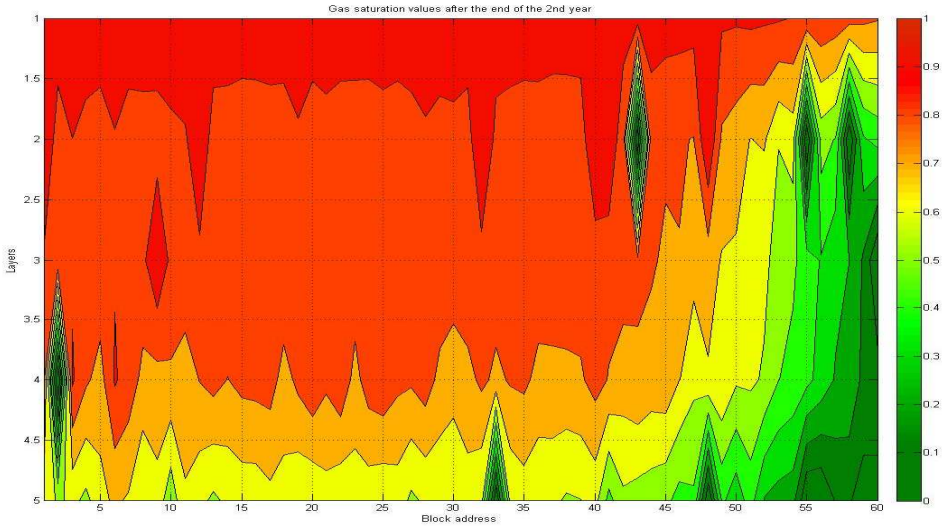

Figure **5-28**: Gas saturation values predicted by the expert system at the end of 2nd year for case study no.2.

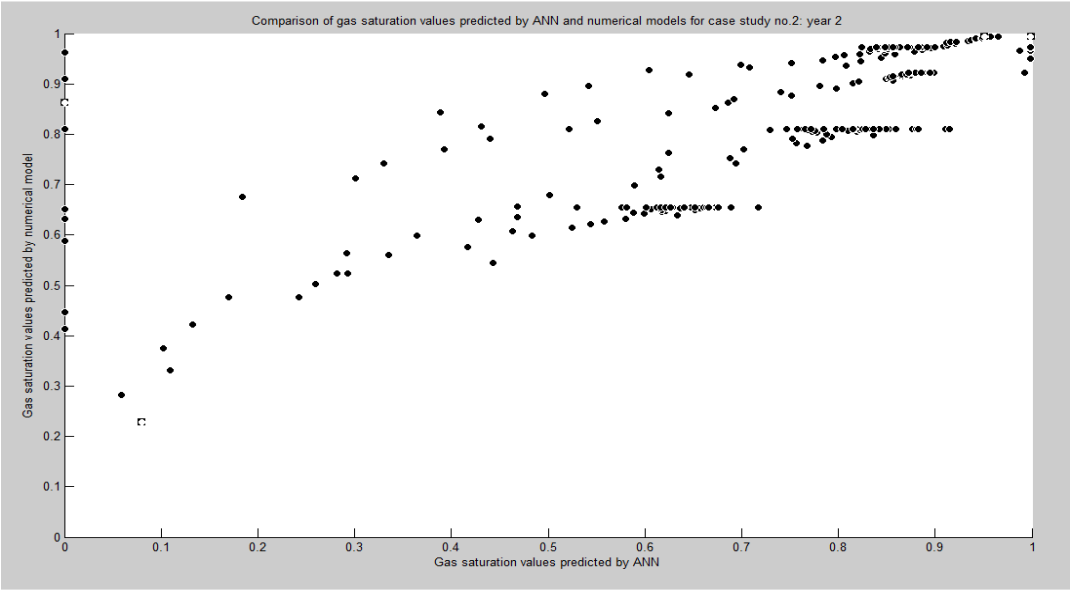

Figure **5-29**: Comparison of gas saturation values predicted by the expert system and the numerical model after the end of 2nd year for case study no.2.

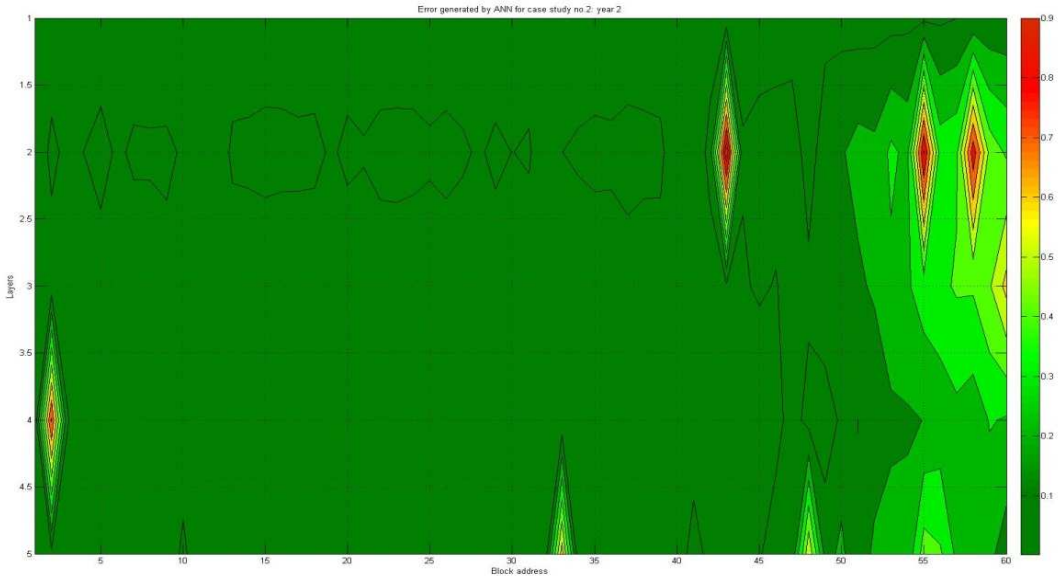

Figure **5-30**: Error plot for case study no.2 at the end of 2nd year.

Figure 5-31 shows the gas saturation values predicted by the numerical model for case study no.2 after the end of 3rd year of production. The average gas saturation value for the first three layers and region closer to the wellbore is still about 0.9. A similar result is predicted by the expert system as shown in Figure 5-32. The expert system predicts the average gas saturation for the 1st and 2nd layer to be around 0.9 and for the 3rd layer it is 0.8. There are a significantly high number of outliers in each layer but much further away from the wellbore. Figure 5-33 shows the comparison of the gas saturation values predicted by the numerical model and the expert system. Most of the data points fall on the unit slope line passing through the origin which indicates a very good match and the regression correlation coefficient obtained is also above 90% in spite of the presence of certain outliers. Figure 5-34 shows the error plot for the entire area of interest. The error produced is close to 0.1 for the region closer to the wellbore but the error increases significantly closer to the boundaries. This is confirmed by observing lighter shades of green color near the boundary which indicates higher amount of error.

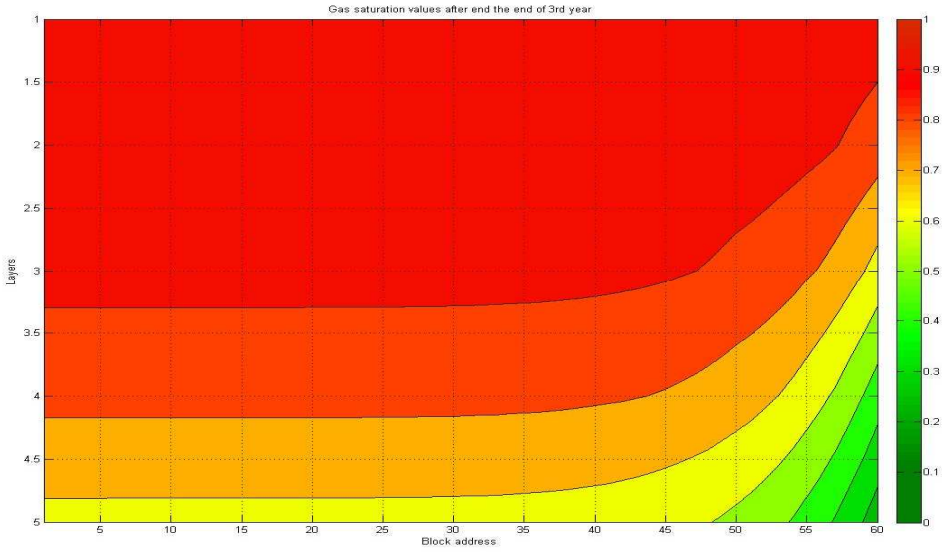

Figure **5-31**: Gas saturation values predicted by the numerical model at the end of 3rd year for case study no.2.

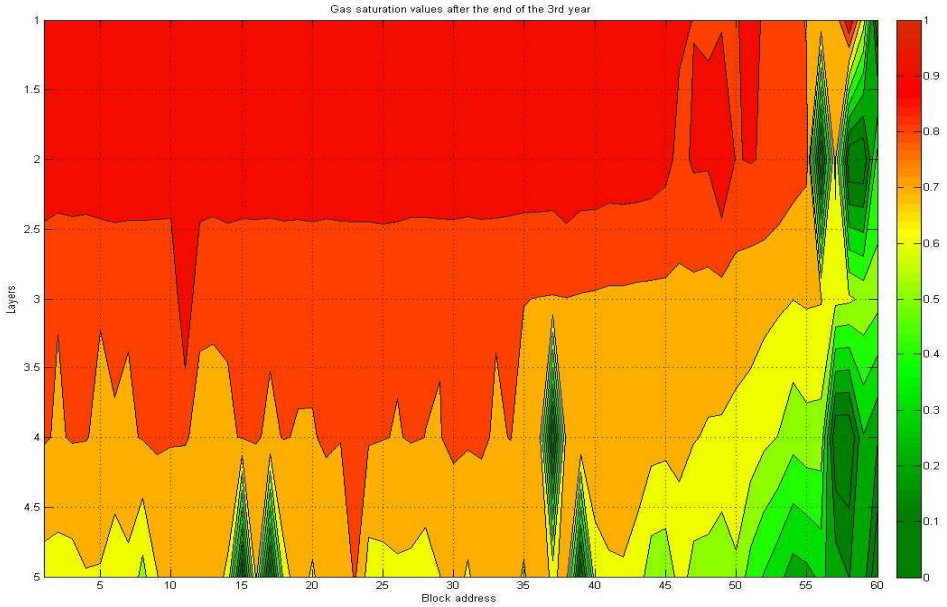

Figure **5-32**: Gas saturation values predicted by the expert system at the end of 3rd year for case study no.2.

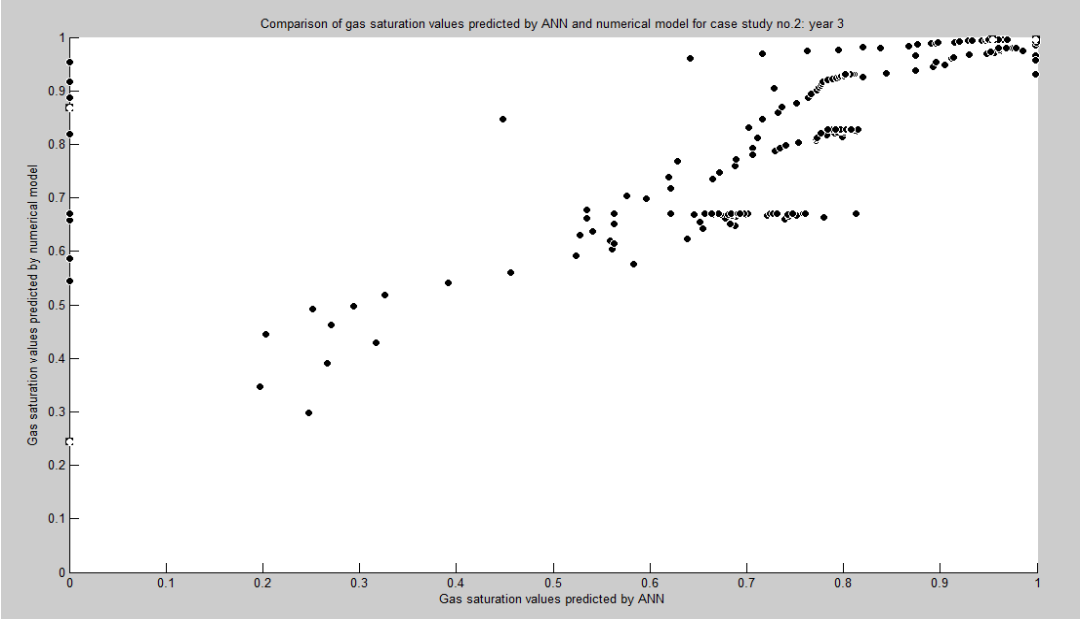

Figure **5-33**: Comparison of gas saturation values predicted by the expert system and the numerical model for the end of 3rd year for case study no.2.

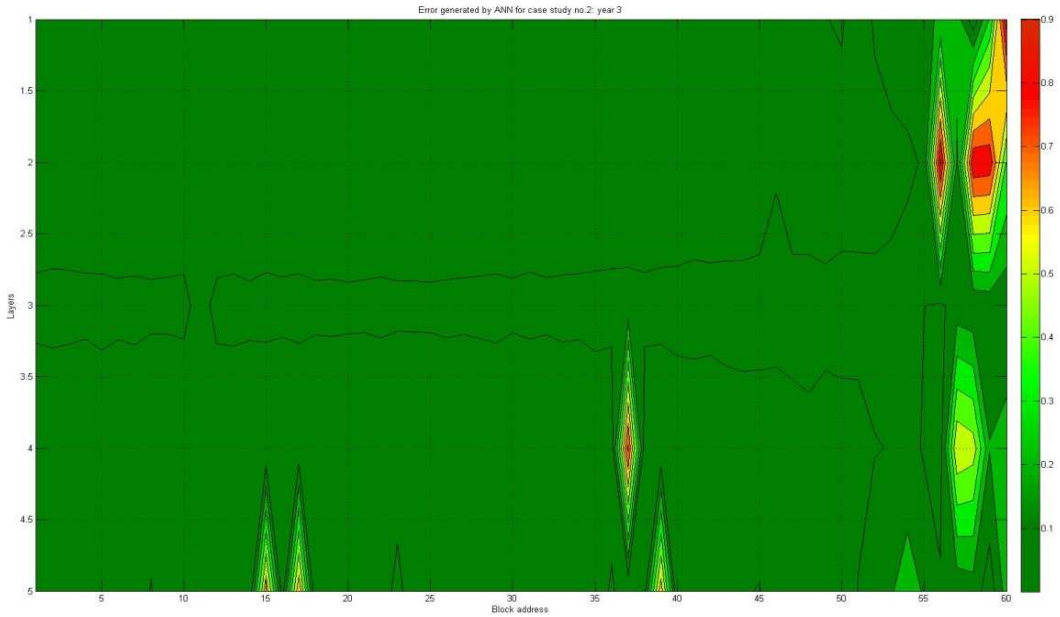

Figure **5-34**: Error plot for case study no.2 at the end of 3rd year.

Figure 5-35 shows the gas saturation values predicted by the numerical model for case study no.2 after the end of 4th year. Figure 5-36 shows the result generated using ANN. The plot shows that the expert system underestimates the gas saturation value by 10% in the 1st layer and 2nd layer. The error is slightly higher in the 3rd layer and finally the gas saturation values predicted in the 4th and the 5th layer are overestimated by a large difference. Results predicted by the expert system shows a sharp increase in deviation from the numerical model near the block number 40 from the wellbore. Figure 5-37 shows the comparison of the results generated using the numerical model and the artificial neural network. The plot shows that the expert system produces result with reasonable accuracy, however, for higher gas saturation values the error increases. This happened when the error near the boundaries was significantly higher in the 1st and 2nd layer and the gas saturation in this region was also high. Figure 5-38 shows the error plot and confirms the fact that the error in the 1st and the 2nd layer is significantly higher.

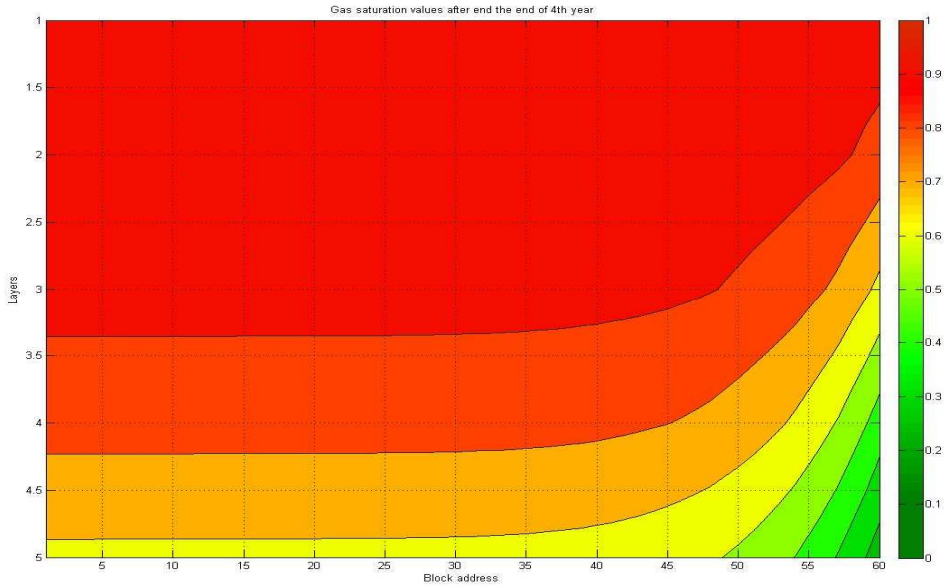

Figure **5-35**: Gas saturation values predicted by the numerical model at the end of 4th year for case study no.2.

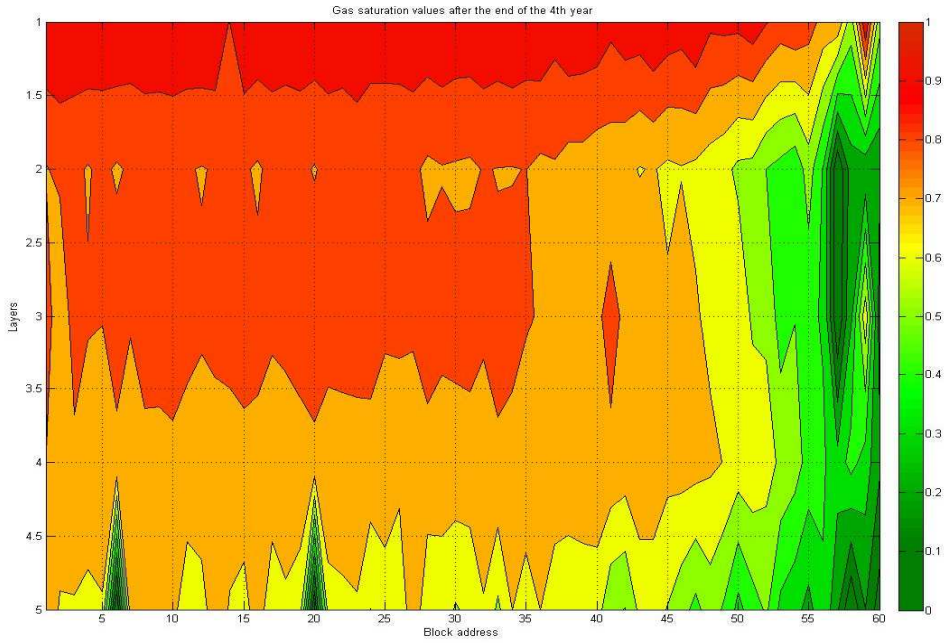

Figure **5-36**: Gas saturation values predicted by the expert system at the end of 4th year for case study no.2.

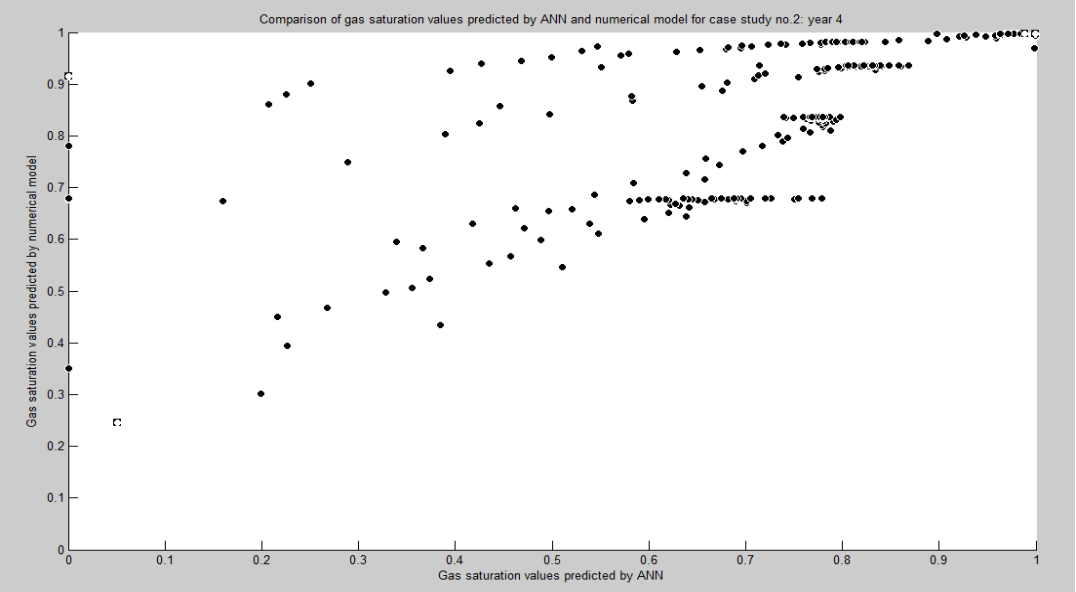

Figure **5-37**: Comparison of gas saturation values predicted by the expert system and the numerical model after the end of 4th year for case study no.2.

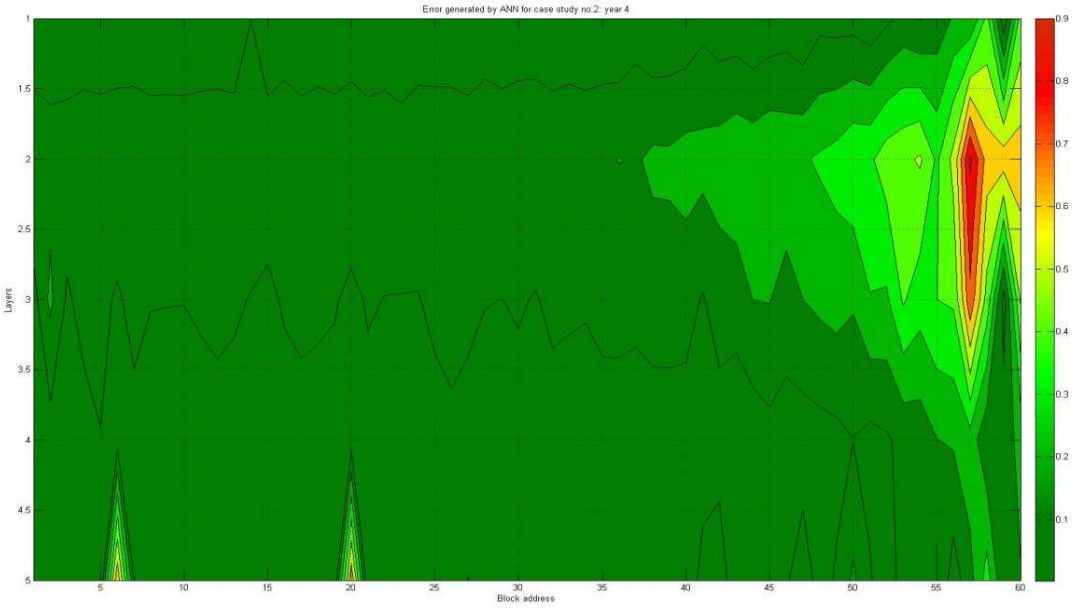

Figure **5-38**: Error plot for case study no.2 at the end of 4th year.

Figure 5-39 shows gas saturation values predicted by the numerical model after the end of 5th year. The plot shows that the gas cone extent has increased significantly both in the vertical and in the horizontal directions. Figure 5-40 shows the result generated using ANN. Figure 5-42 shows that error is most significant in the 3rd layer. The error between the numerical model and the expert system in the 3rd layer is between 0.2 and 0.3. The error plot also confirms that the error near the boundaries of the area of interest is higher. Figure 5-41 compares the gas saturation values predicted using the numerical model and expert system. The regression correlation coefficient is around 70% and is low due to error in the 3rd layer and layers lower than that.

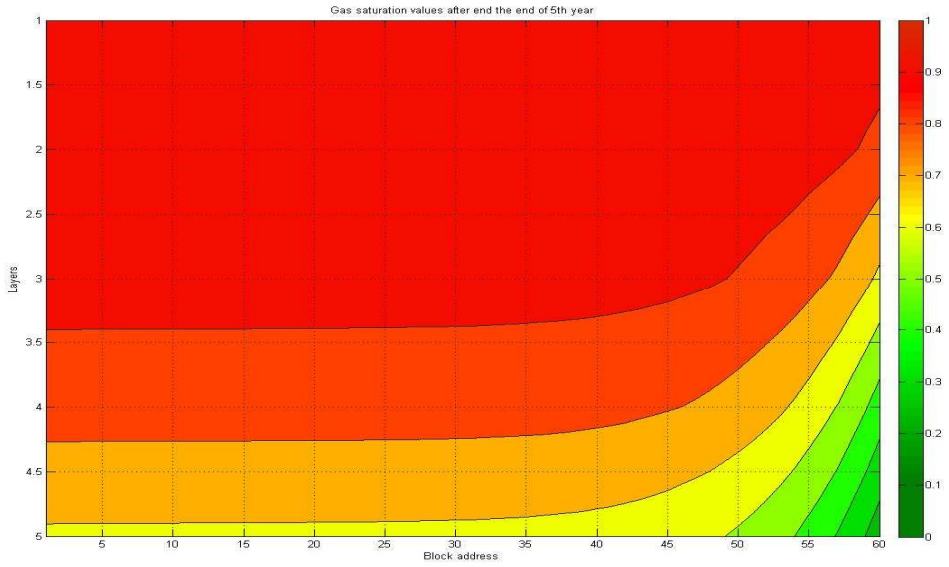

Figure **5-39**: Gas saturation values predicted by the numerical model at the end of 5th year for case study no.2.

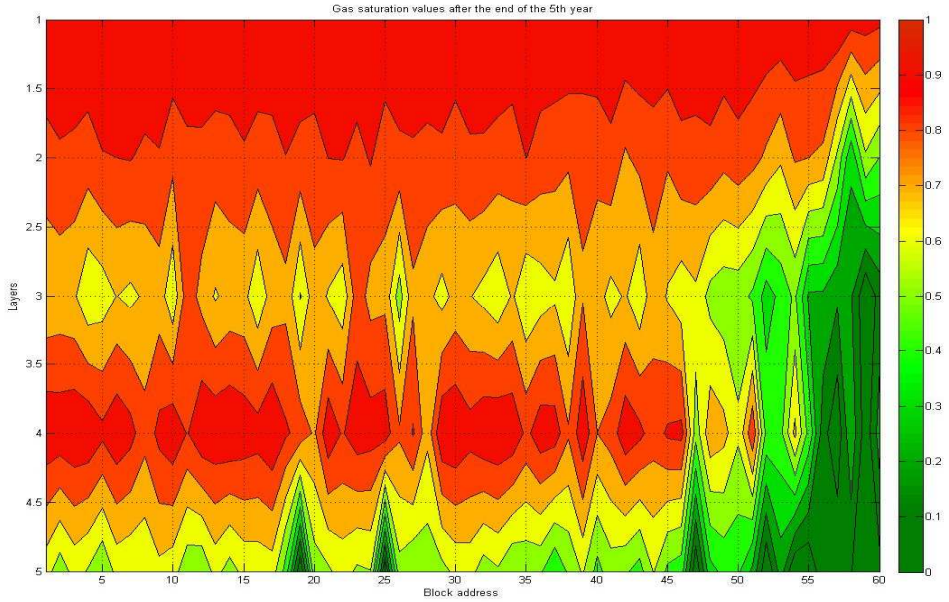

Figure **5-40**: Gas saturation values predicted by the expert system at the end of 5th year for case study no.2.

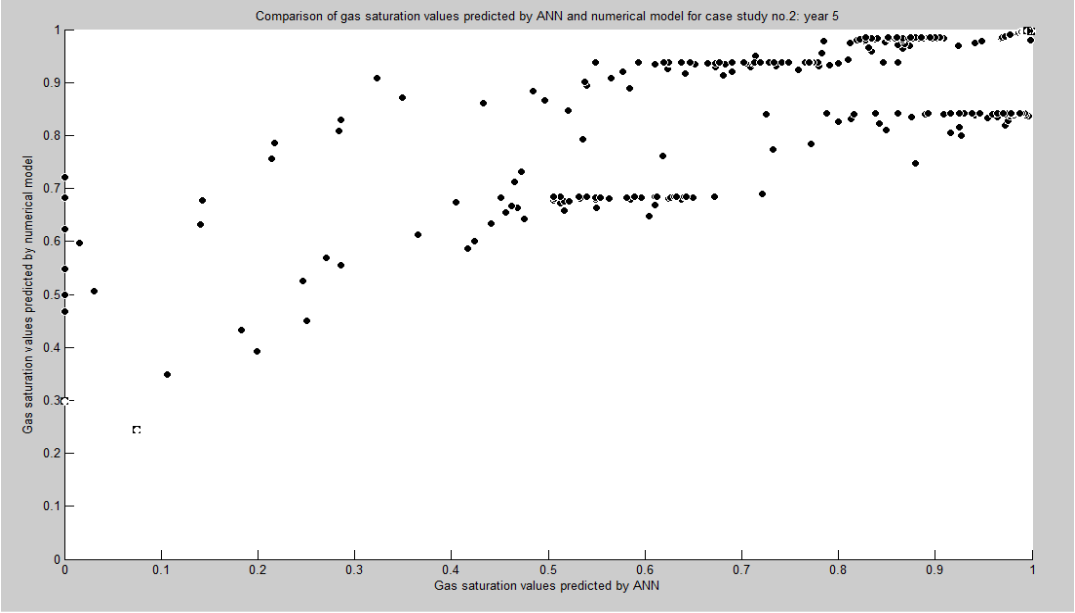

Figure **5-41**: Comparison of gas saturation values predicted by the expert system and the numerical model after the end of 5th year for case study no.2.

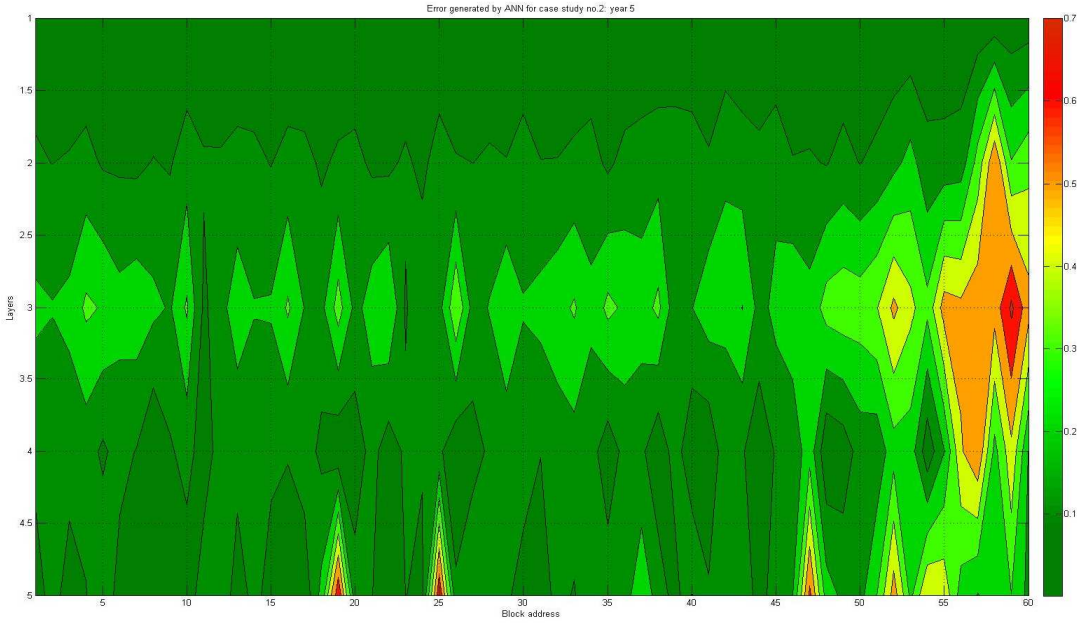

Figure **5-42**: Error plot for case study no.2 at the end of 5th year.

5.3.3Results and discussion for case study no.3

Table 5-4 shows the input values used for case study no.3 used to test neural networks. The vertical and horizontal permeability values are highest in this case study and the production rate is also much higher at 1000 bbls/ day. As a result of these, the gas coning problem will be most severe for this reservoir.

Table **5-4**: Input used for case study no.3 used to test the neural networks.

Sr. No.	Input	value
1.	Horizontal permeability (md)	100
2.	Vertical permeability anisotropy (fraction)	0.25
3.	Porosity (fraction)	0.25
4.	Production rate (bbls/ day)	1000
5.	Oil density (API)	51
6.	Gas gravity (fraction)	1
7.	Reservoir Pressure (psi)	4500
8.	Gas cap height (feet)	50
9.	Oil bearing zone thickness (in feet)	60

Figure 5-43 shows the result generated using the numerical model for case study no.3 after the end of 1st year. The curvature of the gas cone curve is much higher and this is because the vertical permeability is highest in this case study as compared to the other case studies. Also, as expected, the gas cone is developing much more aggressively in this case as the production rate, the vertical and the horizontal permeability values are kept high. The average gas saturation value in the 1st and the 2nd layer is about 0.9. Figure 5-44 shows the gas saturation values predicted by the expert system and shows the result is in good agreement with the numerical model. The regression correlation coefficient is more than 90% with very small number of outliers. The expert system slightly underestimates the gas saturation value in the 1st and the 2nd layer but the error is still less than 10%. Figure 5-46 shows the error plot for the domain of interest. As seen from the plot, the error increases as the distance from the wellbore increases. There are very few outliers in each of the layers and these are mostly located toward the boundaries of the domain of interest. Figure 5-45 shows the comparison of the gas saturation values generated by the numerical model and the expert system. The plot confirms that the values generated by the expert system are in reasonable agreement with the results generated by the numerical model.

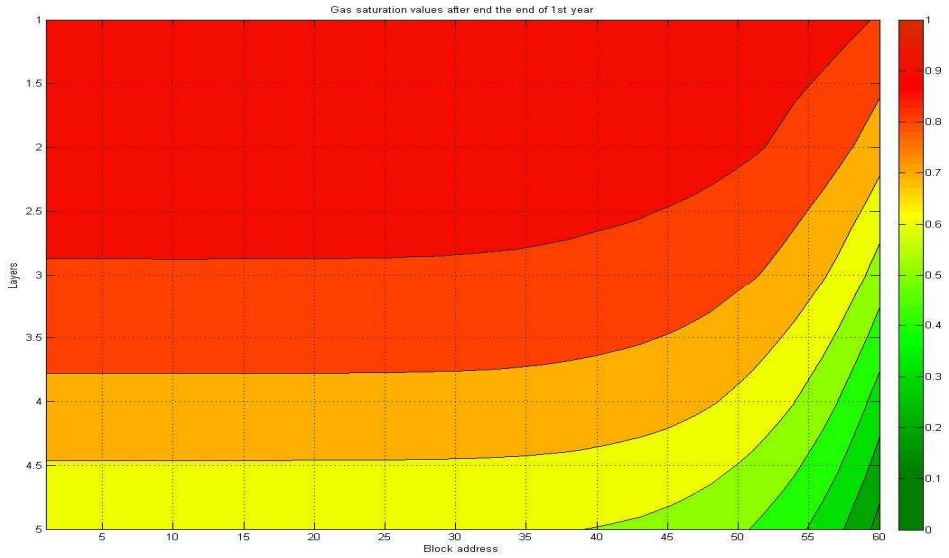

Figure **5-43**: Gas saturation values predicted by the numerical model at the end of 1st year for case study no.3.

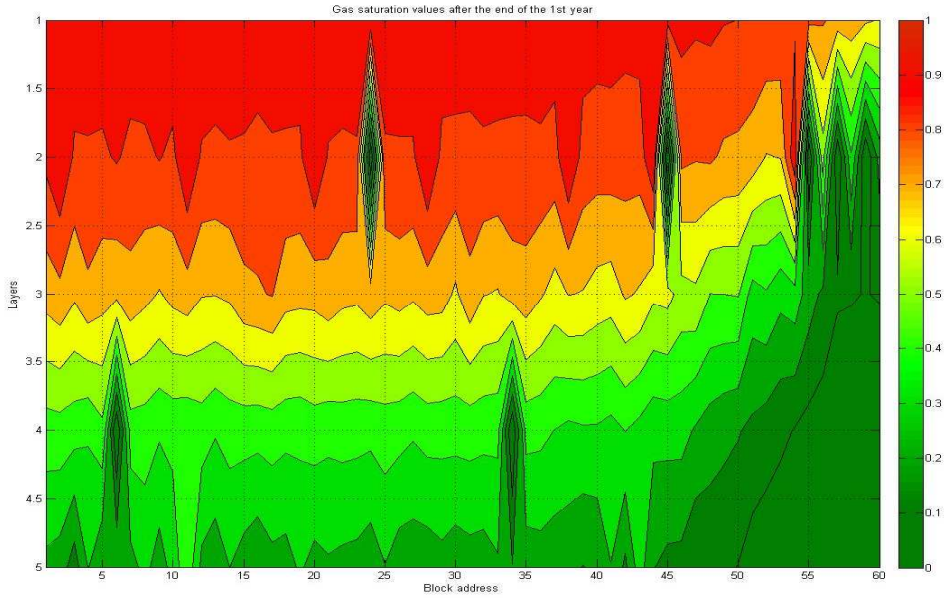

Figure **5-44**: Gas saturation values predicted by the expert system at the end of 1st year for case study no.3.

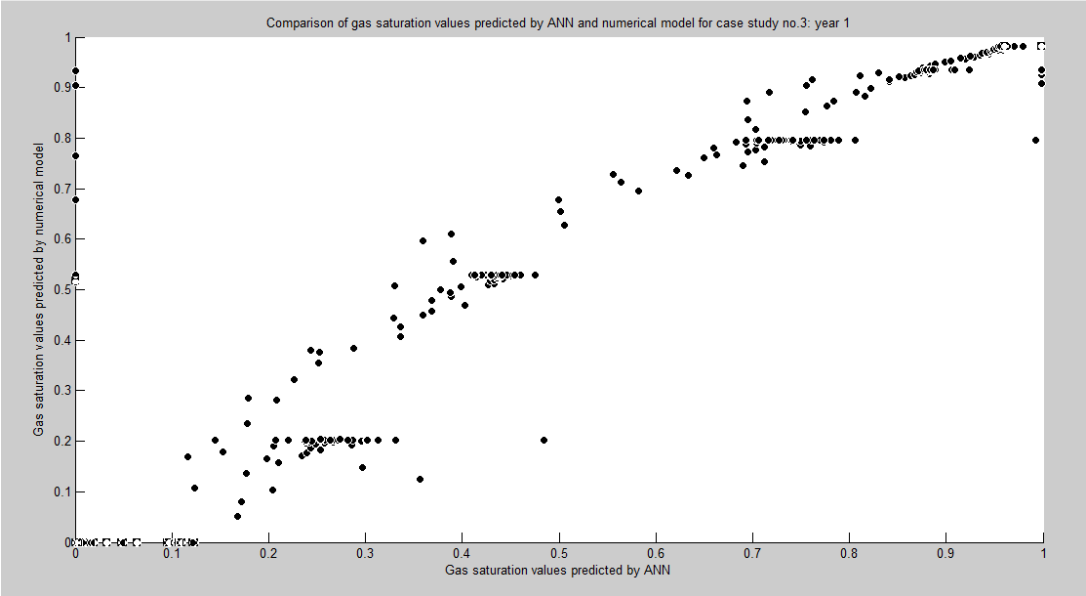

Figure **5-45**: Comparison of gas saturation values predicted by the expert system and the numerical model after the end of 1st year for case study no.3.

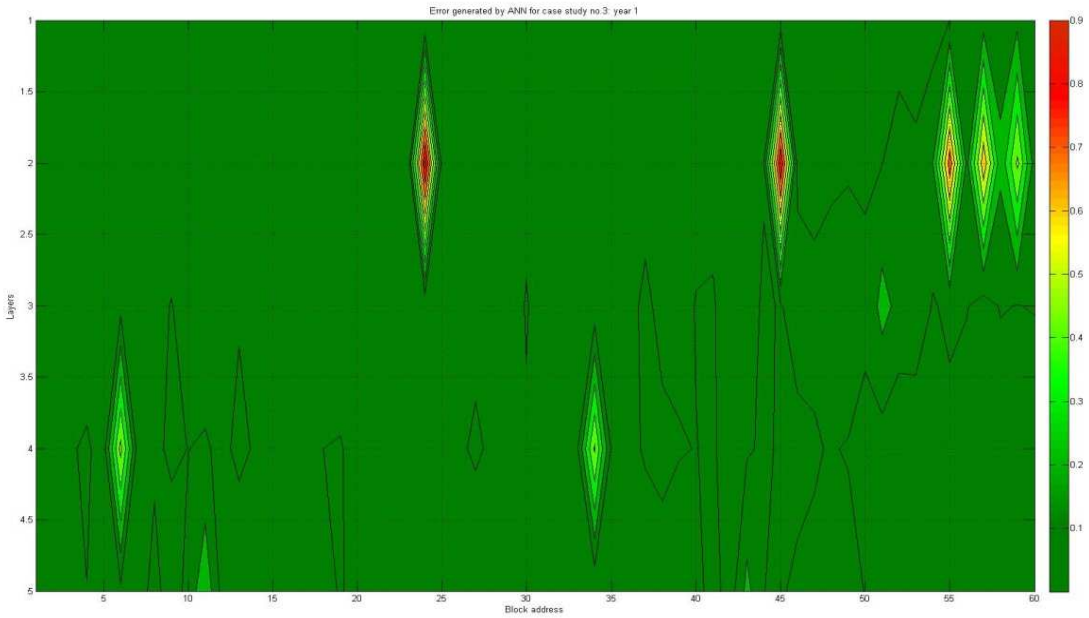

Figure **5-46**: Error plot for case study no.3 at the end of 1st year.

Figure 5-47 shows the gas saturation plot generated using the numerical model for case study no.3 after the end of 2nd year. The gas cone formation rate is high and the gas cone is encroaching more aggressively in the vertical and in the horizontal directions. The average gas saturation value in the 1st and the 2nd layer has slightly increased and is about 0.95. Figure 5-48 shows the gas saturation values predicted by the expert system and shows that the result is in good agreement with the numerical model. The gas saturation value predicted by the expert system in the 2nd layer is slightly underestimated but the error is less than 10%. Figure 5-50 shows the error plot for the domain of interest. The plot indicates that error increases as the distance from the wellbore increases as seen in earlier case studies. Most of the outliers present in the networks are away from the wellbore and can be excluded from the consideration. Figure 5-49 shows the comparison of the gas saturation values generated by the numerical model and the expert system. Lower gas saturation values deviate significantly from the regression line hence indicating that the expert system overestimated these values. The error plot as shown in Figure 5-50 also confirms that the expert system is less accurate in predicting lower gas saturation values, these lower gas saturation values are usually present in the lower layers where the error produced by the expert system is usually higher. The regression correlation coefficient obtained in this case is close to 80%.

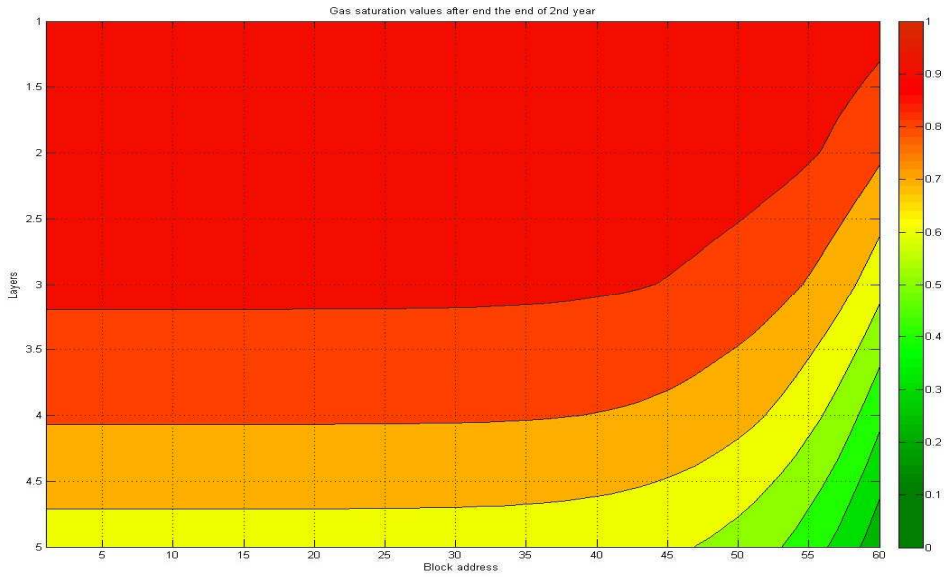

Figure **5-47**: Gas saturation values predicted by the numerical model at the end of 2nd year for case study no.3.

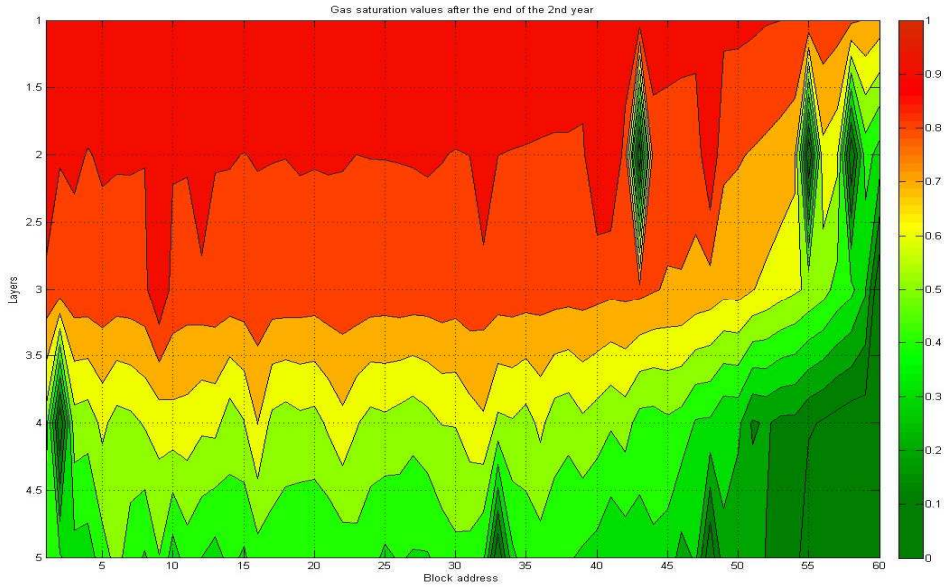

Figure **5-48**: Gas saturation values predicted by the expert system at the end of 2nd year for case study no.3.

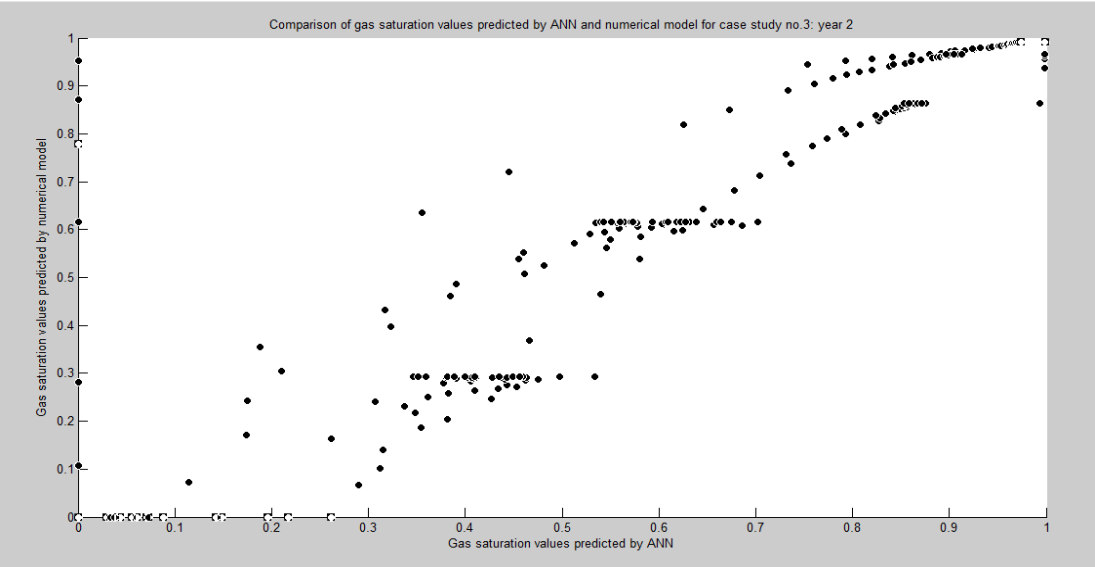

Figure **5-49**: Comparison of gas saturation values predicted by the expert system and the numerical model for the end of 2nd year for case study no.3.

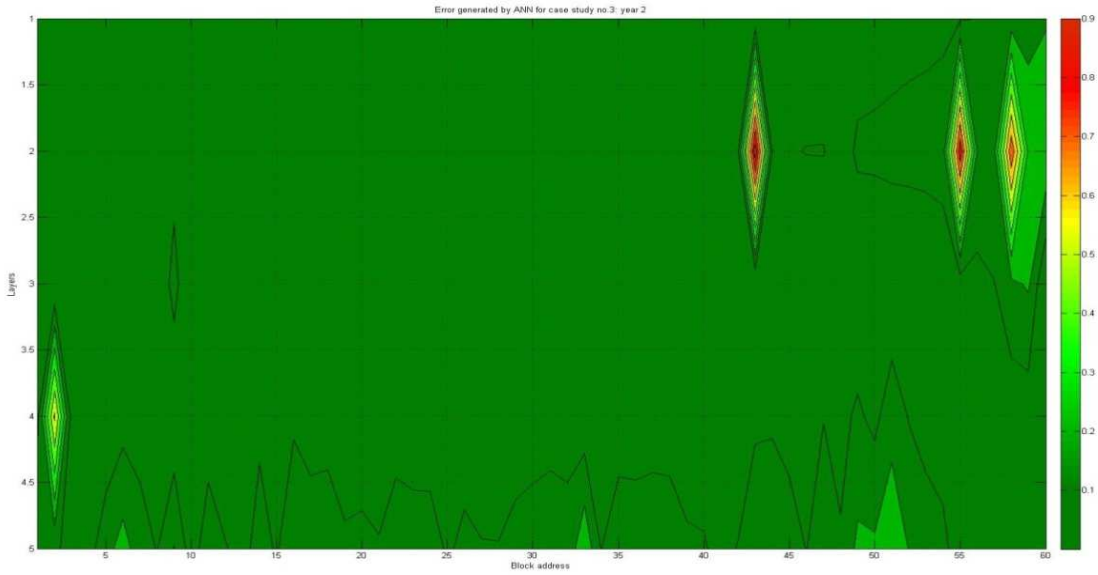

Figure **5-50**: Error plot for case study no.3 at the end of 2nd year.

Gas saturation values predicted by the numerical model are shown in Figure 5-51. The average gas saturation value in the 1st and the 2nd layer has further increased and is close to1 indicating that gas cone has significantly advanced in the downward direction. Figure 5-52 shows that the gas saturation values predicted by the expert system are in good agreement with the numerical model. The error produced by the expert system for the 1st layer and 2nd layer is close to 10%. Figure 5-54 shows the error plot for the domain of interest. The plot shows that error increases as the distance from the wellbore increases. There are very fewer outliers in the first three layers than compared to the 4th and the 5th layer and hence the accuracy is higher in the first three layers. Most of them are present near the boundaries of the domain of interest. Figure 5-53 shows the comparison of the gas saturation values generated by the numerical model and the expert system. The plot show that the expert system is less accurate in predicting lower gas saturation values which are usually present in the lower layers. The regression correlation coefficient obtained is however close to 85%.

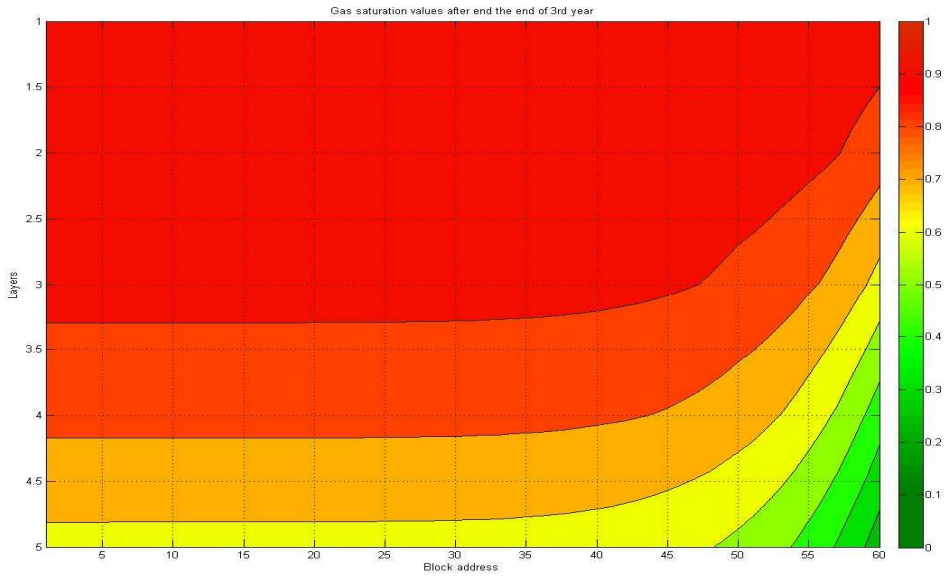

Figure **5-51**: Gas saturation values predicted by the numerical model at the end of 3rd year for case study no.3.

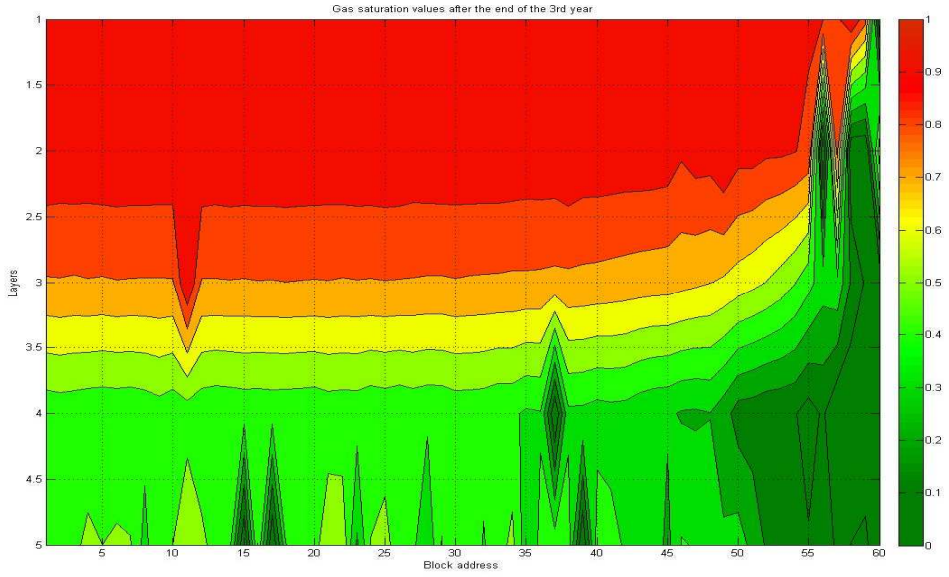

Figure **5-52**: Gas saturation values predicted by the expert system at the end of 3rd year for case study no.3.

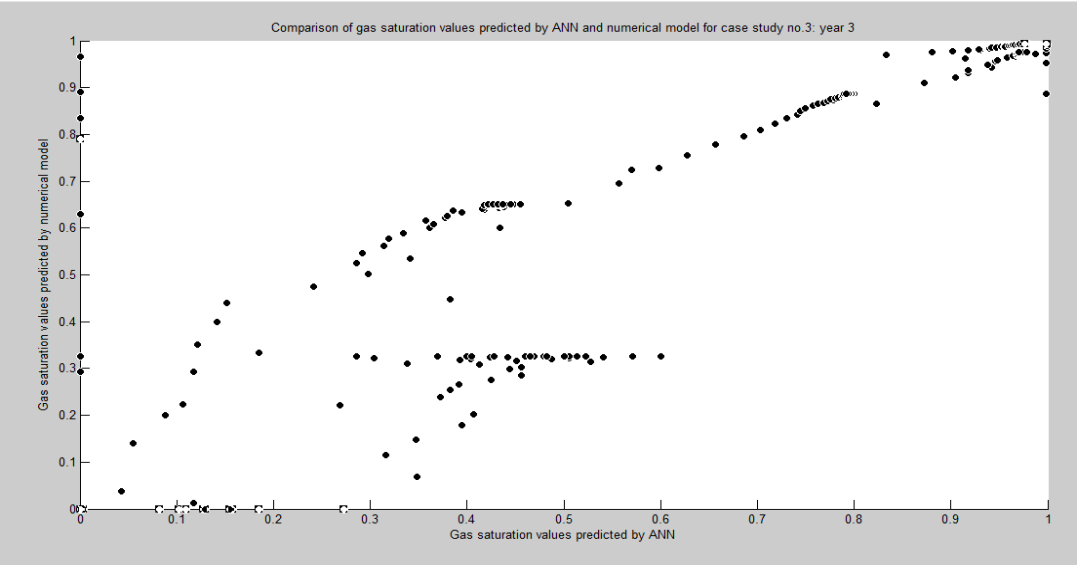

Figure **5-53**: Comparison of gas saturation values predicted by the expert system and the numerical model for the end of 3rd year for case study no.3.

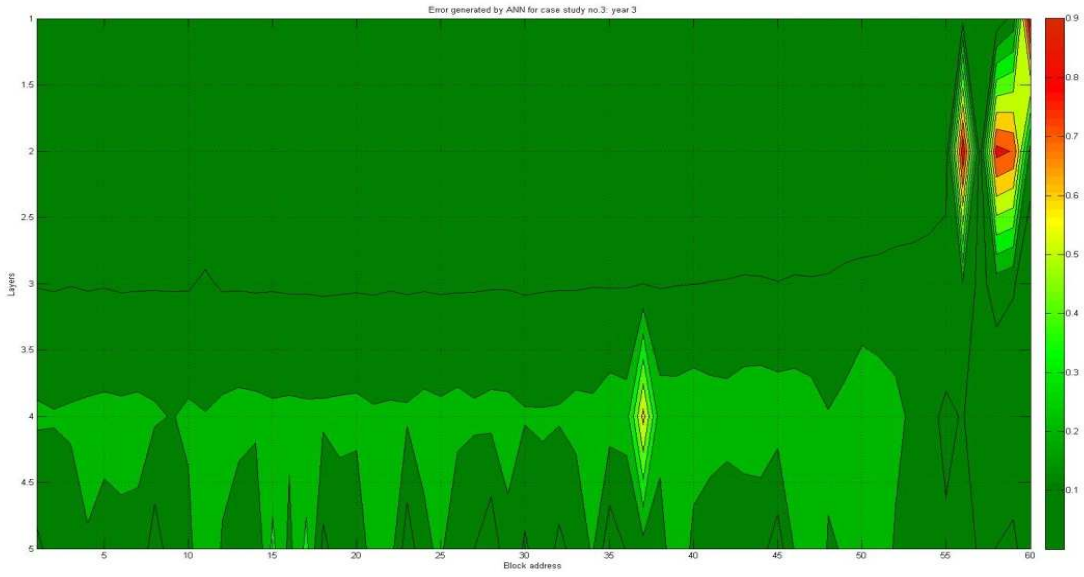

Figure **5-54**: Error plot for case study no.3 at the end of 3rd year.

Figure 5-55 shows the gas saturation plot generated using the numerical model for case study no.3 after the end of 4thyear. The average gas saturation value in the 1st and the 2nd layer is now almost1. Figure 5-56 shows that the error produced by the expert system varies between 0 and 0.15 for most part of the domain of interest. The gas saturation values predicted by the expert system hence are in good agreement with the numerical model. Figure 5-57 shows a comparison of the gas saturation values predicted using the expert system and the numerical model and confirms that the match is satisfactory. Very few points deviate from the regression line which indicates a high regression correlation coefficient value. Figure 5-58 shows the error plot for the domain of interest. The region near the boundary of the area of interest indicates a larger deviation from the numerical model and it is in the range of 0 to 0.5. The plot also shows that error is higher for lower layers. Most of the outliers present are located in the lower layers and this can be confirmed in tandem with Figure 5-57.

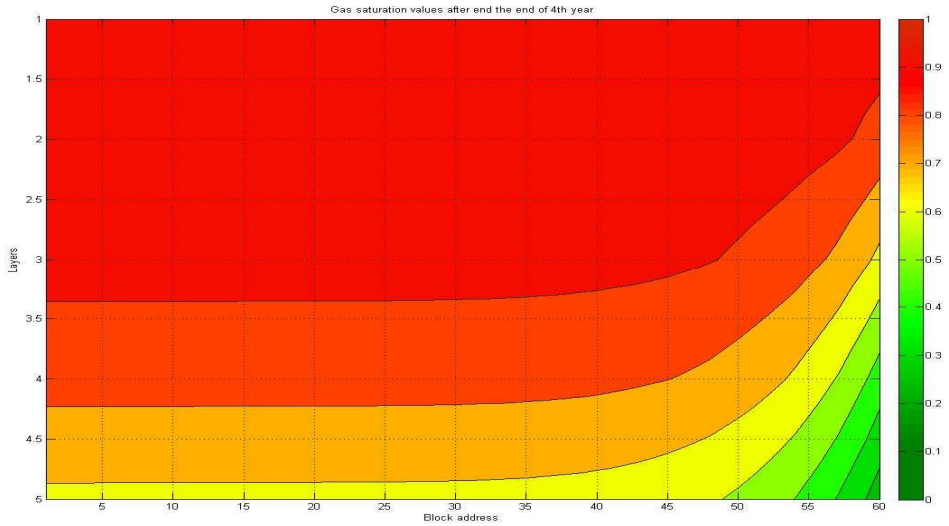

Figure **5-55**: Gas saturation values predicted by the numerical model at the end of 4th year for case study no.3.

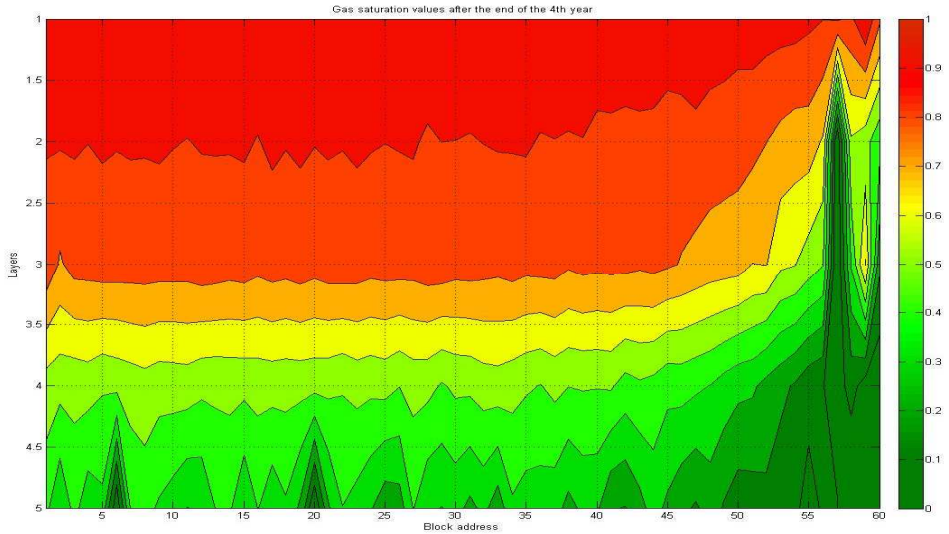

Figure **5-56**: Gas saturation values predicted by the expert system at the end of 4th year for case study no.3.

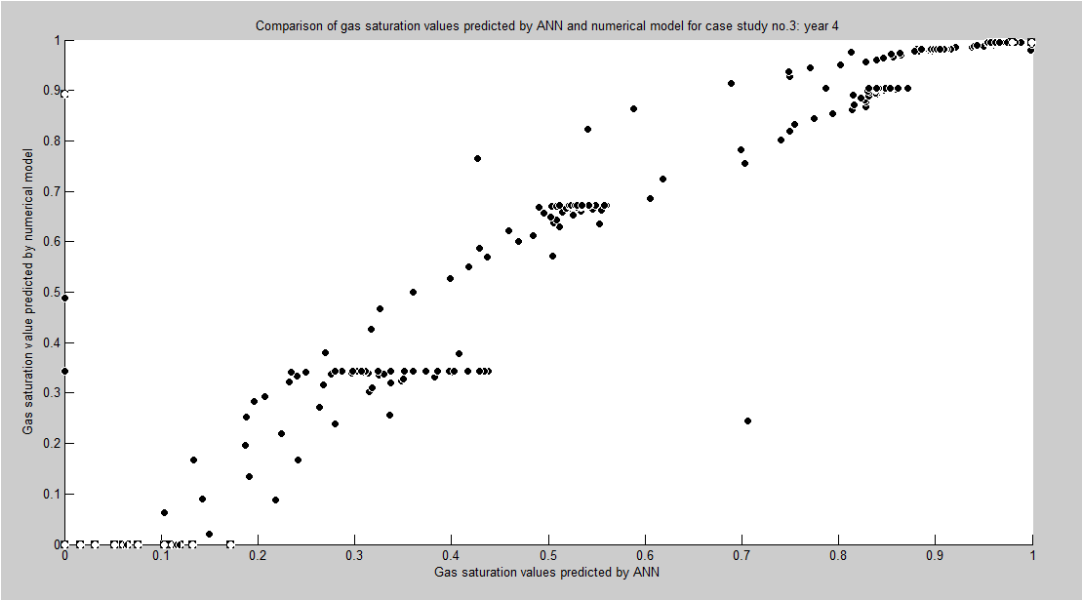

Figure **5-57**: Comparison of gas saturation values predicted by the expert system and the numerical model for the end of 4th year for case study no.3.

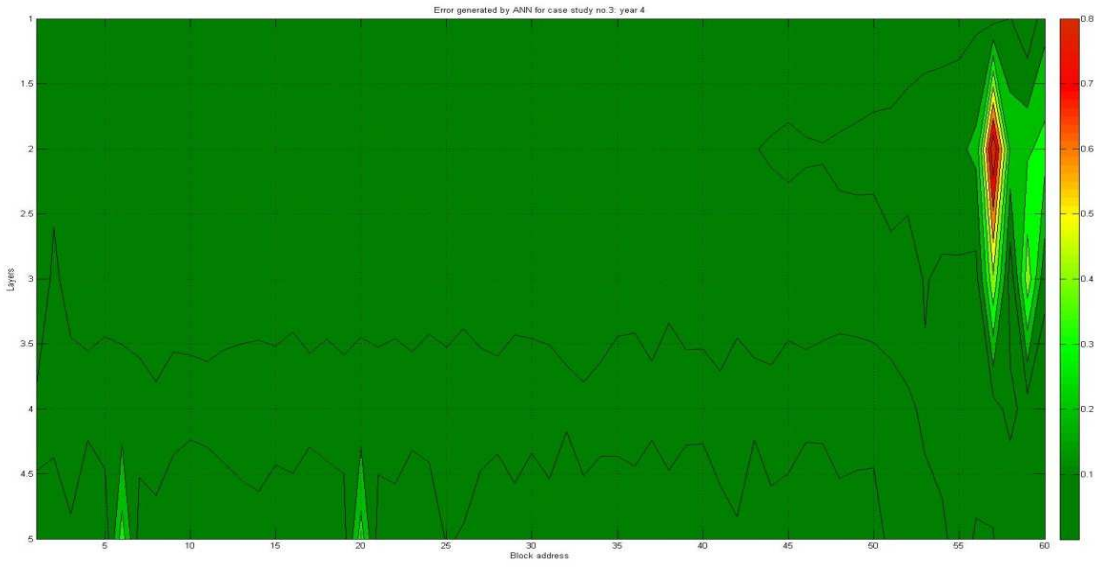

Figure **5-58**: Error plot for case study no.1 at the end of 4th year.

Figure 5-59 shows the gas saturation plot generated using the numerical model for case study no.3 after the end of 5thyear. The average gas saturation value in the 5th layer after the end of first year was close to 0.2 whereas after the end of 5th year, the average has increased to 0.4. This confirms that when the vertical permeability is significantly high as in this case, the gas cone formation rate is also much higher in the vertical direction. Figure 5-62 shows the error plot for the domain of interest. The plot indicates that error is much higher for lower layers and also the error increases as the distance from the wellbore increases. The gas saturation curve predicted by the expert system in the lower layers is severely distorted due to presence of the many outliers present in that region and therefore the error produced in this region is also significantly high. This lowers the regression correlation coefficient significantly which is only about 70% in this case. Figure 5-61 shows the comparison of the gas saturation values generated by the numerical model and the expert system. The plot also suggests that expert system predicts lower gas saturation values with lesser degree of accuracy.

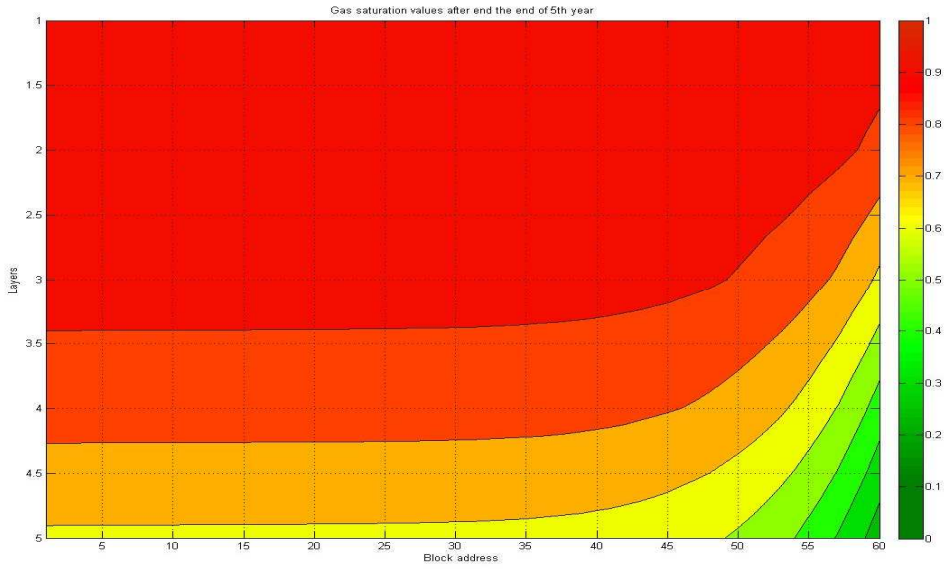

Figure **5-59**: Gas saturation values predicted by the numerical model at the end of 5th year for case study no.3.

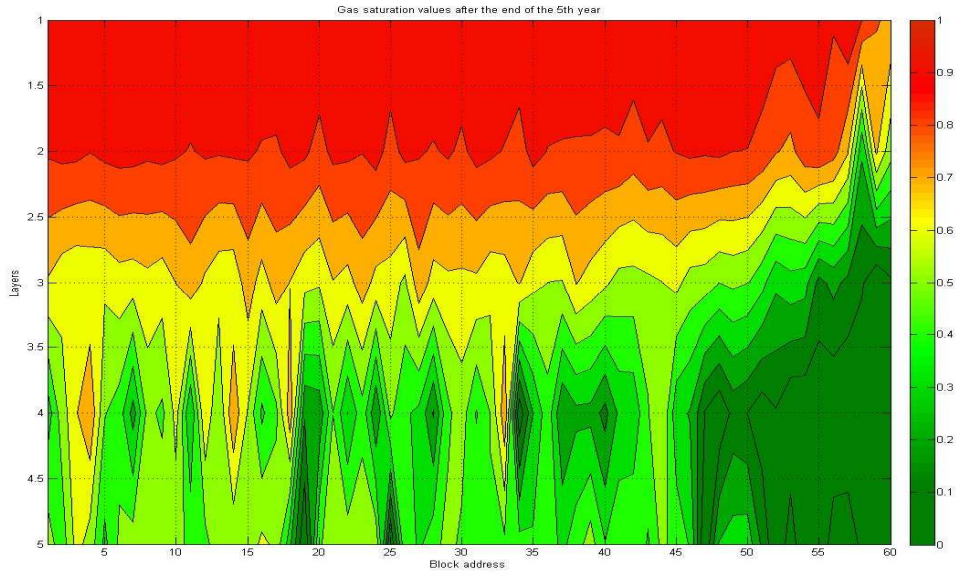

Figure **5-60**: Gas saturation values predicted by the expert system at the end of 5th year for case study no.3.

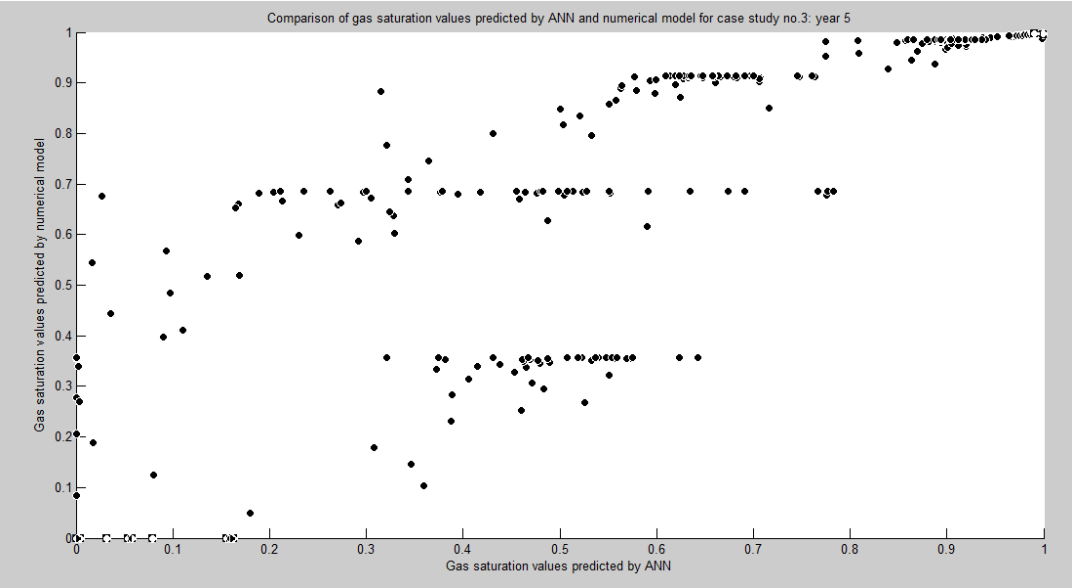

Figure **5-61**: Comparison of gas saturation values predicted by expert system and the numerical model for the end of 5th year for case study no.3.

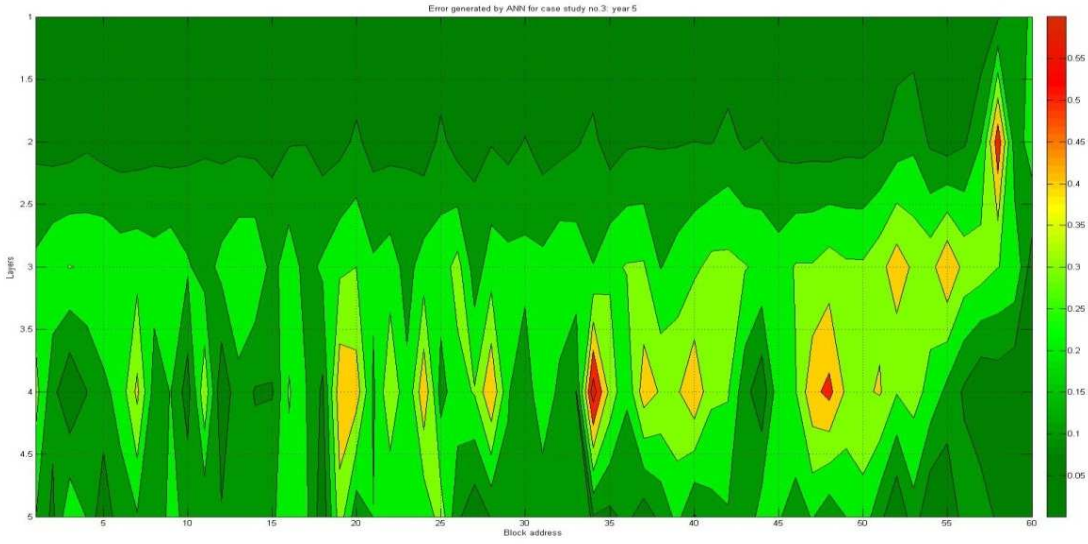

Figure **5-62**: Error plot for case study no.3 at the end of 5th year.

Chapter 6

CONCLUSIONS AND RECOMMENDATIONS

Artificial neural networks were trained to investigate the impact of reservoir properties and well production on gas cone formation rate. A commercial simulator was used to generate training data for the networks. The reservoir considered was anisotropic and homogenous and black oil model was used for simulation. The well was centrally located and perforated only in the oil bearing zone and a radial cylindrical grid system was constructed for the analysis.

The following conclusions are drawn from this study:

- Artificial neural networks were developed for the upper half of oil bearing zones using feed-forward back propagation algorithm with two hidden layers.
- The error given by ANN increases as one proceeds from the 1st layer to the 5th layer.
- ANNs developed in this study were trained using following strategies
    1. Appropriate number of layers and neurons were chosen to train the networks.
        a. Too few neurons will give erroneous results
        b. Too many neurons and layers will over-train the network and also increase the computational time required.
    2. The results generated from ANN were compared with numerical models generated using a commercial black oil simulator.

a. Levenberg-Marquardt training algorithm generated better results however the computational time required was more.

- Scaled conjugate gradient training algorithm was used to predict gas saturation values for lower layers of the domain of interest.
- The study confirms the fact that higher vertical permeability increases gas cone formation rate and this was successfully predicted by ANN.
- Higher production rate also increases gas cone growth rate and this was confirmed by ANN.
- The study suggests that higher porosity retards the gas cone formation rate. The simulation runs and the ANN trained both confirm the same observation.
- Higher horizontal permeability as expected will directly extend the base of the gas cone in the horizontal plane and this was confirmed from the simulation runs and results generated from ANN.
- The study suggests oil density is not as influential as other parameters such as reservoir permeability and production rate.
- Results from numerical models and ANN indicate that gas gravity in the gas cap region also does not significantly influence gas cone growth rate.
- Reservoirs with larger gas cap thickness will show slightly lower gas saturation values in the gas cone as compared to reservoirs with smaller gas cap thickness.

Following recommendations are made for further development and applicability of this project:

- Residual, critical and connate gas and oil saturations all were kept as 0. These can be incorporated so that reservoirs with varying residual, critical and connate gas and oil saturations can also be considered.
- Relative permeability values at connate and irreducible gas and oil saturations were kept as 1. These can be included as inputs so that reservoirs with varying relative permeability values can also be considered for analysis.
- The perforation length and the oil column thickness were kept equal. Varying perforation length can be included as input.

Bibliography

Cartsen Peterson, B. S. (1997). "Artificial Neural Networks". In D. W. Patterson, *Artificial Neural Networks: theory and application.*

Chaney P.E., N. M.: "How to perforate your well to prevent water and gas coning". *Oil and Gas Journal,1956*.

Chierici G.L, C. G.: "A systematic study of gas and water coning by potentiometric models". *Journal of Petroleum technology (JPT), 1*964.

D.G. Hatzignatiou, F. Mohamed.. "Water and Gas coning in Horizontal and Vertical Wells". *Petroleum Society of CIM and AOSTRA, paper No. 94-26,* 1994.

Gurney, K.: Neural networks for perceptual processing: from simulation tools to theories. In G. D. Colin R. Tosh, *Modelling Perception with artificial neural networks.* CAMBRIDGE, ISBN 978-0-521-76395-0, 2010.

Meyer H. L, Garder A.O.: "Mechanics of two immiscible fluids in porous media", *Journal of Applied Physics,Vol. 25, No.11, pp.1400ff,* 1954.

R. Recham, P. S.: "Super-Critical Rate based on Economic Recovery in Water and Gas coning by using vertical and horizontal well performance", *Society of Petroleum engineers, SPE 71820,* 2001.

Appendix A

SAMPLE CMG FILE USED

```
load INPUT.mat

for i=1:size(INPUT,2)

   temp = ['check' num2str(i) '.dat'];
   fid = fopen(temp)

fprintf(fid,'RESULTS SIMULATOR IMEX 200900\n\n');

fprintf(fid,'INUNIT FIELD');
fprintf(fid,'WSRF WELL 1');
fprintf(fid,'WSRF GRID TIME');
fprintf(fid,'WSRF SECTOR TIME');
fprintf(fid,'OUTSRF WELL LAYER NONE');
fprintf(fid,'OUTSRF RES ALL')
fprintf(fid,'OUTSRF GRID SO SG SW PRES OILPOT BPP SSPRES WINFLUX');
fprintf(fid,'WPRN GRID 0');
fprintf(fid,'OUTPRN GRID NONE');
fprintf(fid,'OUTPRN RES NONE');
fprintf(fid,'**$  Distance units: ft');
fprintf(fid,'RESULTS XOFFSET          0.0000');
fprintf(fid,'RESULTS YOFFSET          0.0000');
fprintf(fid,'RESULTS ROTATION          0.0000  **$  (DEGREES)');
fprintf(fid,'RESULTS AXES-DIRECTIONS 1.0 -1.0 1.0');
fprintf(fid,'**$
**********************************************************************
***');
fprintf(fid,'**$ Definition of fundamental cylindrical grid');
fprintf(fid,'**$
**********************************************************************
***');
fprintf(fid,'GRID RADIAL 100 1 20 *RW          1');
fprintf(fid,'KDIR DOWN');
fprintf(fid,'       DI IVAR       0.0889043      0.0968082       0.105415       0.114787');
fprintf(fid,'       0.124992       0.136104       0.148204        0.16138       0.175728');
fprintf(fid,'       0.191351       0.208363       0.226887       0.247058       0.269023');
fprintf(fid,'       0.29294       0.318983       0.347342       0.378223       0.411848');
fprintf(fid,'       0.448463       0.488334       0.531749       0.579023       0.630501');
fprintf(fid,'       0.686555       0.747593       0.814057        0.88643       0.965238');
fprintf(fid,'        1.05105        1.14449        1.24624        1.35704        1.47769');
```

```
fprintf(fid,'       1.60906       1.75211       1.90788        2.0775       2.2622');
fprintf(fid,'       2.46332       2.68232       2.92079       3.18046       3.46322');
fprintf(fid,'       3.77111       4.10638       4.47145       4.86899       5.30186');
fprintf(fid,'       5.77322       6.28648       6.84538       7.45396       8.11665');
fprintf(fid,'       8.83825       9.62401        10.4796       11.4113       12.4258');
fprintf(fid,'       13.5305       14.7335       16.0433       17.4696       19.0228');
fprintf(fid,'        20.714       22.5555       24.5608       26.7444       29.1221');
fprintf(fid,'       31.7111       34.5304       37.6003       40.9431       44.5831');
fprintf(fid,'       48.5468       52.8628       57.5625       62.6801       68.2526');
fprintf(fid,'       74.3205        80.928       88.1228       95.9573       104.488');
fprintf(fid,'       113.778       123.893       134.908       146.902       159.962');
fprintf(fid,'       174.183       189.669       206.531       224.893       244.886');
fprintf(fid,'       266.658       290.365        316.18       344.289       374.898');
fprintf(fid,'       408.228');
fprintf(fid,'DJ JVAR            360');
fprintf(fid,'DK ALL');
fprintf(fid,' 2000*5');
fprintf(fid,'DTOP');
fprintf(fid,' 100*6000');
fprintf(fid,'**$ Property: NULL Blocks  Max: 1  Min: 1');
fprintf(fid,'**$  0 = null block, 1 = active block');
fprintf(fid,'NULL CON           1');
fprintf(fid,'**$ Property: Porosity  Max: 0.1  Min: 0.1
fprintf(fid,'POR CON          %f\n',INPUT(i,4));
fprintf(fid,'**$ Property: Permeability I (md)   Max: 60  Min: 60
%% whereever you have to change a paramter
fprintf(fid,'PERMI CON          %f\n',INPUT(i,1));

fprintf(fid,'**$ Property: Permeability J (md)   Max: 60  Min: 60
fprintf(fid,'PERMJ CON          %f\n',INPUT(i,1));
fprintf(fid,'**$ Property: Permeability K (md)   Max: 0.12  Min: 0.12
fprintf(fid,'PERMK CON        %f\n',INPUT(i,1).*INPUT(i,2));
fprintf(fid,'**$ Property: Pinchout Array  Max: 1  Min: 1');
fprintf(fid,'**$  0 = pinched block, 1 = active block');
fprintf(fid,'PINCHOUTARRAY CON           1');
fprintf(fid,'CPOR 0.000001');
fprintf(fid,'MODEL BLACKOIL ');
fprintf(fid,'TRES 150');
fprintf(fid,'PVT EG 1');

fprintf(fid,'**$        p          Rs       Bo       Egvisovisg           co');
fprintf(fid,'      14.696      6.58228   1.04307   4.81846   2.62488  0.0104053       3e-005');
fprintf(fid,'      109.464       28.336   1.05343   36.7207   2.28521  0.0105455       3e-005');
fprintf(fid,'      204.233      53.7884   1.06585   70.1558   1.99606   0.010738       3e-005');
```

```
fprintf(fid,'     299.001     81.5486   1.07972   105.268   1.76323  0.0109717       3e-
005');
fprintf(fid,'      393.77     111.043   1.09481   142.216   1.57601   0.011246       3e-005');
fprintf(fid,'     488.538     141.947   1.11097   181.168   1.42385  0.0115634       3e-
005');
fprintf(fid,'     583.307     174.046    1.1281   222.301   1.29849  0.0119282       3e-005');
fprintf(fid,'     678.075     207.189   1.14614    265.79   1.19379   0.012346       3e-005');
fprintf(fid,'     772.844     241.261   1.16502   311.793   1.10524   0.012824       3e-005');
fprintf(fid,'     867.612     276.174   1.18469   360.426   1.02948  0.0133701       3e-
005');
fprintf(fid,'     962.381     311.856   1.20513   411.729  0.963972   0.013993       3e-
005');
fprintf(fid,'     1057.15     348.246   1.22628   465.621  0.906813  0.0147013       3e-
005');
fprintf(fid,'     1151.92     385.296   1.24814   521.849  0.856518  0.0155024       3e-
005');
fprintf(fid,'     1246.69     422.962   1.27065   579.961   0.81193  0.0164011       3e-
005');
fprintf(fid,'     1341.45     461.207   1.29382   639.303  0.772134  0.0173982       3e-
005');
fprintf(fid,'     1436.22         500    1.3176   699.073    0.7364  0.0184895       3e-005');
fprintf(fid,'     2208.98     833.746   1.53265   1119.23  0.540983  0.0293122  2.18218e-
005');
fprintf(fid,'     2981.73     1192.47   1.78056   1372.07  0.433753  0.0395795  1.47867e-
005');
fprintf(fid,'     3754.49  1622.345219    2.0567    1527.5  0.365551  0.0479455  1.09686e-
005');
fprintf(fid,'     4527.24  2125.574987    2.3579   1635.64  0.318079  0.0549495   8.6072e-
006');
fprintf(fid,'        5300   2695.49065   2.68183   1717.98  0.282972   0.061053  7.01844e-
006');
fprintf(fid,'BWI 1.01944');
fprintf(fid,'CVW 0.000001');
fprintf(fid,'CW 3.1589e-006');
fprintf(fid,'DENSITY OIL %f\n',INPUT(i,6));
fprintf(fid,'DENSITY WATER 61.6381');
fprintf(fid,'REFPW 14.696');
fprintf(fid,'VWI 0.47184');
fprintf(fid,'GRAVITY GAS %f\n',INPUT(i,7));
fprintf(fid,'**$ Property: PVT Type  Max: 1  Min: 1');
fprintf(fid,'PTYPE CON           1');
fprintf(fid,'ROCKFLUID');
fprintf(fid,'RPT 1');
fprintf(fid,'SWT');
fprintf(fid,'**$        Swkrwkrow');
```

```
fprintf(fid,'          0          0          1');
fprintf(fid,'      0.0625  0.00390625    0.878906');
fprintf(fid,'       0.125    0.015625    0.765625');
fprintf(fid,'      0.1875   0.0351563    0.660156');
fprintf(fid,'        0.25      0.0625      0.5625');
fprintf(fid,'      0.3125   0.0976563    0.472656');
fprintf(fid,'       0.375    0.140625    0.390625');
fprintf(fid,'      0.4375    0.191406    0.316406');
fprintf(fid,'         0.5        0.25        0.25');
fprintf(fid,'      0.5625    0.316406    0.191406');
fprintf(fid,'       0.625    0.390625    0.140625');
fprintf(fid,'      0.6875    0.472656   0.0976563');
fprintf(fid,'        0.75      0.5625      0.0625');
fprintf(fid,'      0.8125    0.660156   0.0351563');
fprintf(fid,'       0.875    0.765625    0.015625');
fprintf(fid,'      0.9375    0.878906  0.00390625');
fprintf(fid,'          1          1          0')
fprintf(fid,'SLT');
fprintf(fid,'**$       Slkrgkrog');
fprintf(fid,'          0          1          0');
fprintf(fid,'      0.0625    0.878906  0.00390625');
fprintf(fid,'       0.125    0.765625    0.015625');
fprintf(fid,'      0.1875    0.660156   0.0351563')
fprintf(fid,'        0.25      0.5625      0.0625');
fprintf(fid,'      0.3125    0.472656   0.0976563');
fprintf(fid,'       0.375    0.390625    0.140625');
fprintf(fid,'      0.4375    0.316406    0.191406');
fprintf(fid,'         0.5        0.25        0.25');
fprintf(fid,'      0.5625    0.191406    0.316406');
fprintf(fid,'       0.625    0.140625    0.390625');
fprintf(fid,'      0.6875   0.0976563    0.472656');
fprintf(fid,'        0.75      0.0625      0.5625');
fprintf(fid,'      0.8125   0.0351563    0.660156');
fprintf(fid,'       0.875    0.015625    0.765625');
fprintf(fid,'      0.9375  0.00390625    0.878906')
fprintf(fid,'          1          0          1');
fprintf(fid,'INITIAL');
fprintf(fid,'VERTICAL DEPTH_AVE WATER_OIL_GAS EQUIL');

fprintf(fid,'REFDEPTH 6050')
fprintf(fid,'REFPRES %f\n',INPUT(i,8));
fprintf(fid,'DWOC 9000');
fprintf(fid,'DGOC 6050
fprintf(fid,'**$ Property: Bubble Point Pressure (psi)   Max: 1436.22  Min: 1436.22');
fprintf(fid,'PB CON      1436.22');
```

```
fprintf(fid,'NUMERICAL');
fprintf(fid,'RUN');
fprintf(fid,'DATE 2010 1 1');

fprintf(fid,'**$');
fprintf(fid,'WELL  'Well-1");
fprintf(fid,'PRODUCER 'Well-1");
fprintf(fid,'OPERATE  MAX  STO  %f\n',INPUT(i,5)  CONT);
fprintf(fid,'**$          rad  geofacwfrac  skin');
fprintf(fid,'GEOMETRY  K  0.25  0.37  1.  0.');
fprintf(fid,'PERF  GEOA  'Well-1");
fprintf(fid,'**$ UBA     ff  Status  Connection');
fprintf(fid,'    1 1 1   1.  CLOSED  FLOW-TO  'SURFACE'  REFLAYER');
fprintf(fid,'    1 1 2   1.  CLOSED  FLOW-TO  1');
fprintf(fid,'    1 1 3   1.  CLOSED  FLOW-TO  2');
fprintf(fid,'    1 1 4   1.  CLOSED  FLOW-TO  3');
fprintf(fid,'    1 1 5   1.  CLOSED  FLOW-TO  4');
fprintf(fid,'    1 1 6   1.  CLOSED  FLOW-TO  5');
fprintf(fid,'    1 1 7   1.  CLOSED  FLOW-TO  6');
fprintf(fid,'    1 1 8   1.  CLOSED  FLOW-TO  7');
fprintf(fid,'    1 1 9   1.  CLOSED  FLOW-TO  8');
fprintf(fid,'    1 1 10  1.  CLOSED  FLOW-TO  9');
fprintf(fid,'    1 1 11  1.  OPEN    FLOW-TO  10');
fprintf(fid,'    1 1 12  1.  OPEN    FLOW-TO  11');
fprintf(fid,'    1 1 13  1.  OPEN    FLOW-TO  12');
fprintf(fid,'    1 1 14  1.  OPEN    FLOW-TO  13');
fprintf(fid,'    1 1 15  1.  OPEN    FLOW-TO  14');
fprintf(fid,'    1 1 16  1.  OPEN    FLOW-TO  15');
fprintf(fid,'    1 1 17  1.  OPEN    FLOW-TO  16');
fprintf(fid,'    1 1 18  1.  OPEN    FLOW-TO  17');
fprintf(fid,'    1 1 19  1.  OPEN    FLOW-TO  18');
fprintf(fid,'    1 1 20  1.  OPEN    FLOW-TO  19');
fprintf(fid,'DATE 2010 2  1.00000');
fprintf(fid,'DATE 2010 3  1.00000');
fprintf(fid,'DATE 2010 4  1.00000');
fprintf(fid,'DATE 2010 5  1.00000');
fprintf(fid,'DATE 2010 6  1.00000');
fprintf(fid,'DATE 2010 7  1.00000');
fprintf(fid,'DATE 2010 8  1.00000');
fprintf(fid,'DATE 2010 9  1.00000');
fprintf(fid,'DATE 2010 10  1.00000');
fprintf(fid,'DATE 2010 11  1.00000');
fprintf(fid,'DATE 2010 12  1.00000');
fprintf(fid,'WSRF GRID TNEXT');
fprintf(fid,'DATE 2011 1  1.00000');
```

```
fprintf(fid,'DATE 2011 2  1.00000');
fprintf(fid,'DATE 2011 3  1.00000');
fprintf(fid,'DATE 2011 4  1.00000');
fprintf(fid,'DATE 2011 5  1.00000');
fprintf(fid,'DATE 2011 6  1.00000');
fprintf(fid,'DATE 2011 7  1.00000');
fprintf(fid,'DATE 2011 8  1.00000');
fprintf(fid,'DATE 2011 9  1.00000');
fprintf(fid,'DATE 2011 10  1.00000');
fprintf(fid,'DATE 2011 11  1.00000');
fprintf(fid,'DATE 2011 12  1.00000');
fprintf(fid,'WSRF GRID TNEXT');
fprintf(fid,'DATE 2012 1  1.00000');
fprintf(fid,'DATE 2012 2  1.00000');
fprintf(fid,'DATE 2012 3  1.00000');
fprintf(fid,'DATE 2012 4  1.00000');
fprintf(fid,'DATE 2012 5  1.00000');
fprintf(fid,'DATE 2012 6  1.00000');
fprintf(fid,'DATE 2012 7  1.00000');
fprintf(fid,'DATE 2012 8  1.00000');
fprintf(fid,'DATE 2012 9  1.00000');
fprintf(fid,'DATE 2012 10  1.00000');
fprintf(fid,'DATE 2012 11  1.00000');
fprintf(fid,'DATE 2012 12  1.00000');
fprintf(fid,'WSRF GRID TNEXT');
fprintf(fid,'DATE 2013 1  1.00000');
fprintf(fid,'DATE 2013 2  1.00000');
fprintf(fid,'DATE 2013 3  1.00000');
fprintf(fid,'DATE 2013 4  1.00000');
fprintf(fid,'DATE 2013 5  1.00000');
fprintf(fid,'DATE 2013 6  1.00000');
fprintf(fid,'DATE 2013 7  1.00000');
fprintf(fid,'DATE 2013 8  1.00000');
fprintf(fid,'DATE 2013 9  1.00000');
fprintf(fid,'DATE 2013 10  1.00000');
fprintf(fid,'DATE 2013 11  1.00000');
fprintf(fid,'DATE 2013 12  1.00000');
fprintf(fid,'WSRF GRID TNEXT');
fprintf(fid,'DATE 2014 1  1.00000');
fprintf(fid,'DATE 2014 2  1.00000');
fprintf(fid,'DATE 2014 3  1.00000');
fprintf(fid,'DATE 2014 4  1.00000');
fprintf(fid,'DATE 2014 5  1.00000');
fprintf(fid,'DATE 2014 6  1.00000');
fprintf(fid,'DATE 2014 7  1.00000');
```

```
fprintf(fid,'DATE 2014 8  1.00000');
fprintf(fid,'DATE 2014 9  1.00000');
fprintf(fid,'DATE 2014 10  1.00000');
fprintf(fid,'DATE 2014 11  1.00000');
fprintf(fid,'DATE 2014 12  1.00000');
fprintf(fid,'WSRF GRID TNEXT');
fprintf(fid,'DATE 2015 1  1.00000');
fprintf(fid,'DATE 2015 2  1.00000');
fprintf(fid,'DATE 2015 3  1.00000');
fprintf(fid,'DATE 2015 4  1.00000');
fprintf(fid,'DATE 2015 5  1.00000');
fprintf(fid,'DATE 2015 6  1.00000');
fprintf(fid,'DATE 2015 7  1.00000');
fprintf(fid,'DATE 2015 8  1.00000');
fprintf(fid,'DATE 2015 9  1.00000');
fprintf(fid,'DATE 2015 10  1.00000');
fprintf(fid,'DATE 2015 11  1.00000');
fprintf(fid,'DATE 2015 12  1.00000');

STOP
```

Appendix B

NEURAL NETWORK TOOL GRAPHIC USER INTERFACE

Figure B-1 shows the graphic user interface for neural network manager, this allows the user to define the inputs, targets and also create a new network. This interface also allows the user to import and export networks and errors.

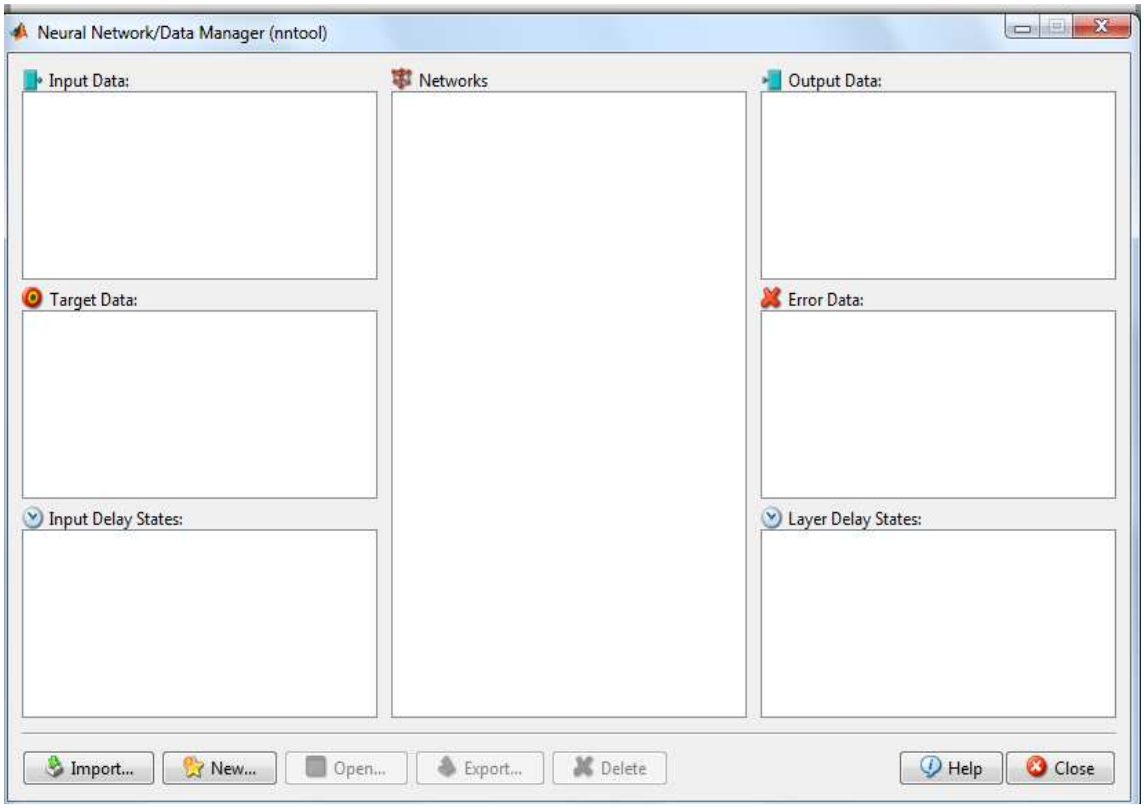

Figure **B-1**: Neural network data manager.

Figure B-2 shows the options to choose the inputs, initial layer states and the training set for training the networks.

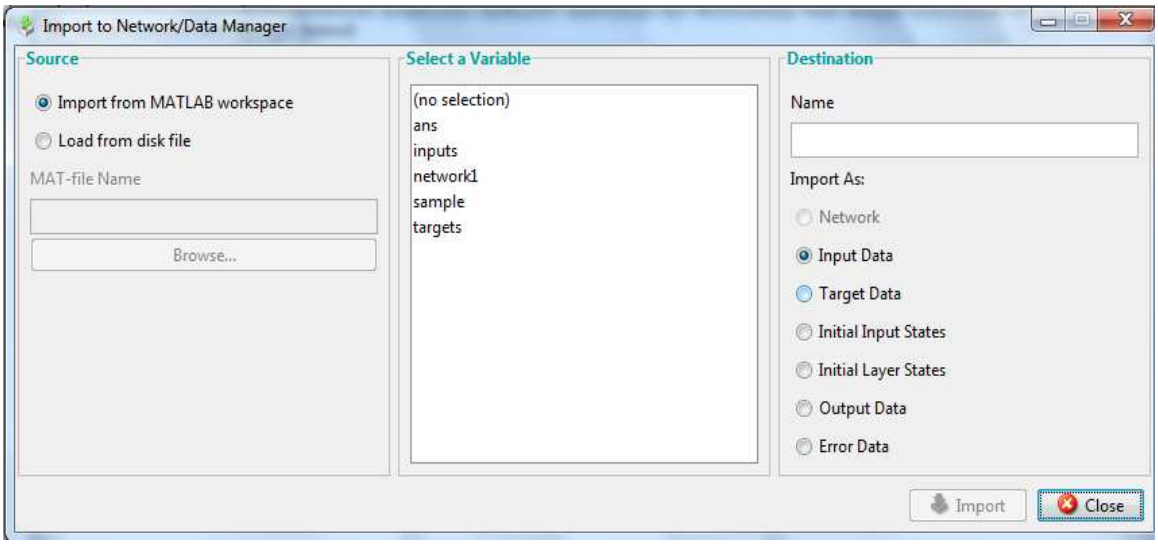

Figure **B-2**: Selection of inputs, targets and networks.

Figure B-3 shows the options provided by the graphic user interface to create new neural networks. The user can decide the training algorithm to be used, the number of hidden layers, the number of neurons for each hidden layer and the transfer function for each hidden layer.

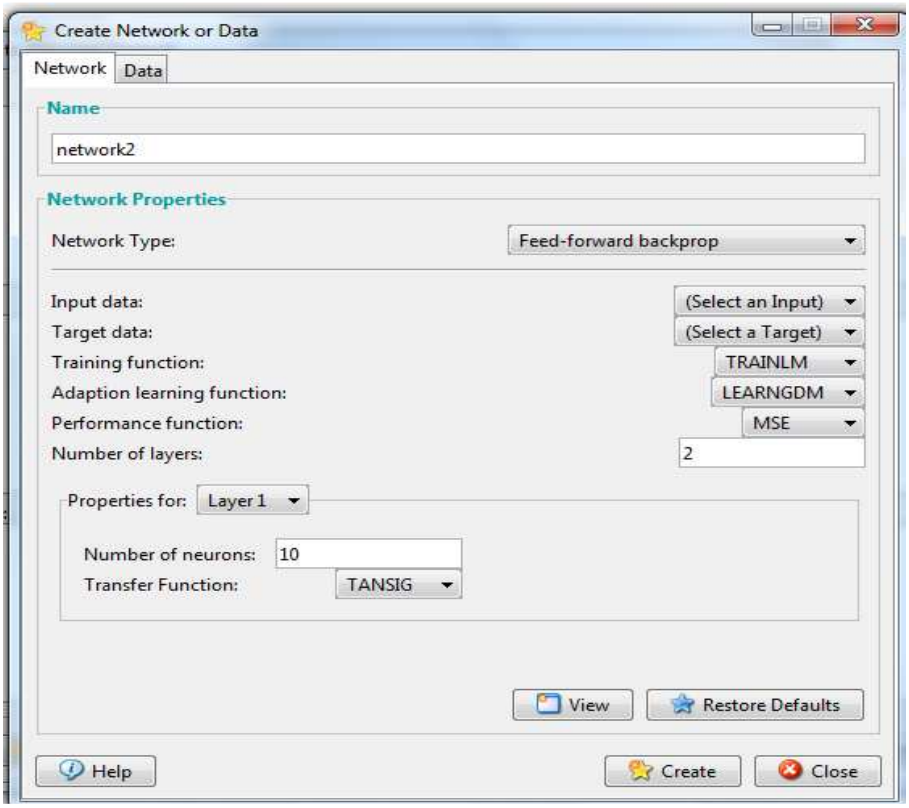

Figure **B-3**: Selection of network type and properties of networks.

Figure B-4 shows the options provided to the user to view the structure of the network created and also start the training of the network.

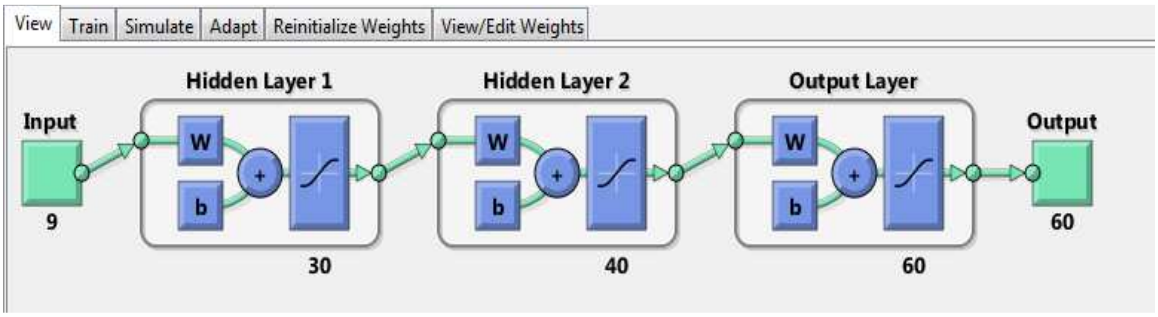

Figure **B-4**: Options provided to users to view and train the network.

Appendix C

MATLAB GENERATED PLOTS FOR TRAINING THE ARTIFICIAL NEURAL NETWORKS

Figure C-1 shows the plots used to assess the training of the neural networks. A high regression correlation coefficient suggests stronger relationship between the input and the output. 60% of the training set is used to train the network, 20% is used to validate the results and 20% is used to test the trained networks. Training set is used to adjust the weights of the networks and testing set is used to test the networks once they have been trained. Validation set is used to make sure the weights are updated to increase the accuracy of the networks and avoid over-fitting of the weights. This set is used to validate that any increase in accuracy of the network actually increases accuracy over the data set that has been not been exposed to the network before.

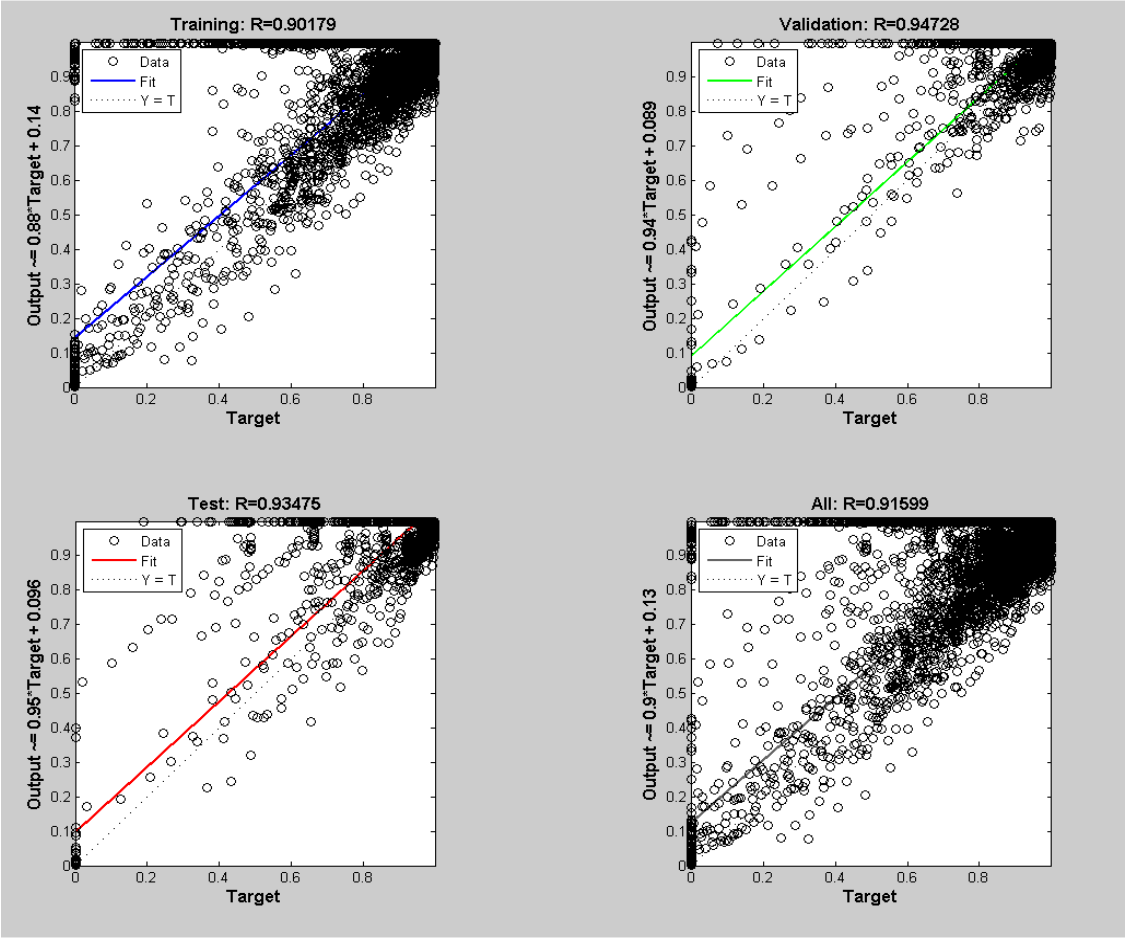

Figure **C-1**: Regression correlation plots for trained neural networks.

Figure C-2 shows the mean square error (MSE) plot versus number of epochs for training, testing and validation set. The MSE should be as small as possible so that the artificial neural networks are able to predict the output with higher accuracy.

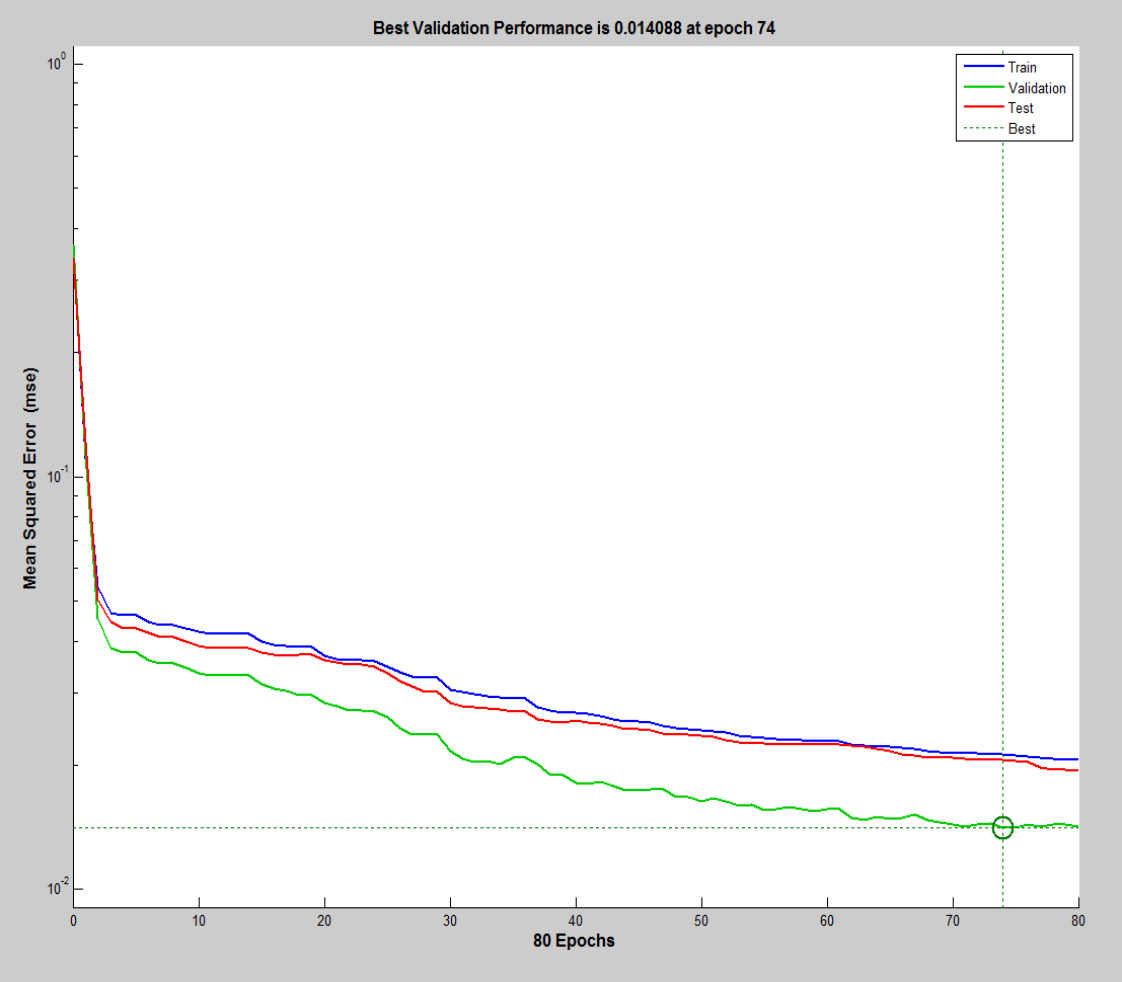

Figure **C-2**: Mean square error (MSE) versus epoch for training, testing and validation set.

Figure C-3 shows the plot of gradient versus epoch. Smaller gradient indicates stronger tendency of neural networks to converge to a solution. The plot also includes the number of validation checks of the weights of the neural networks versus epochs.

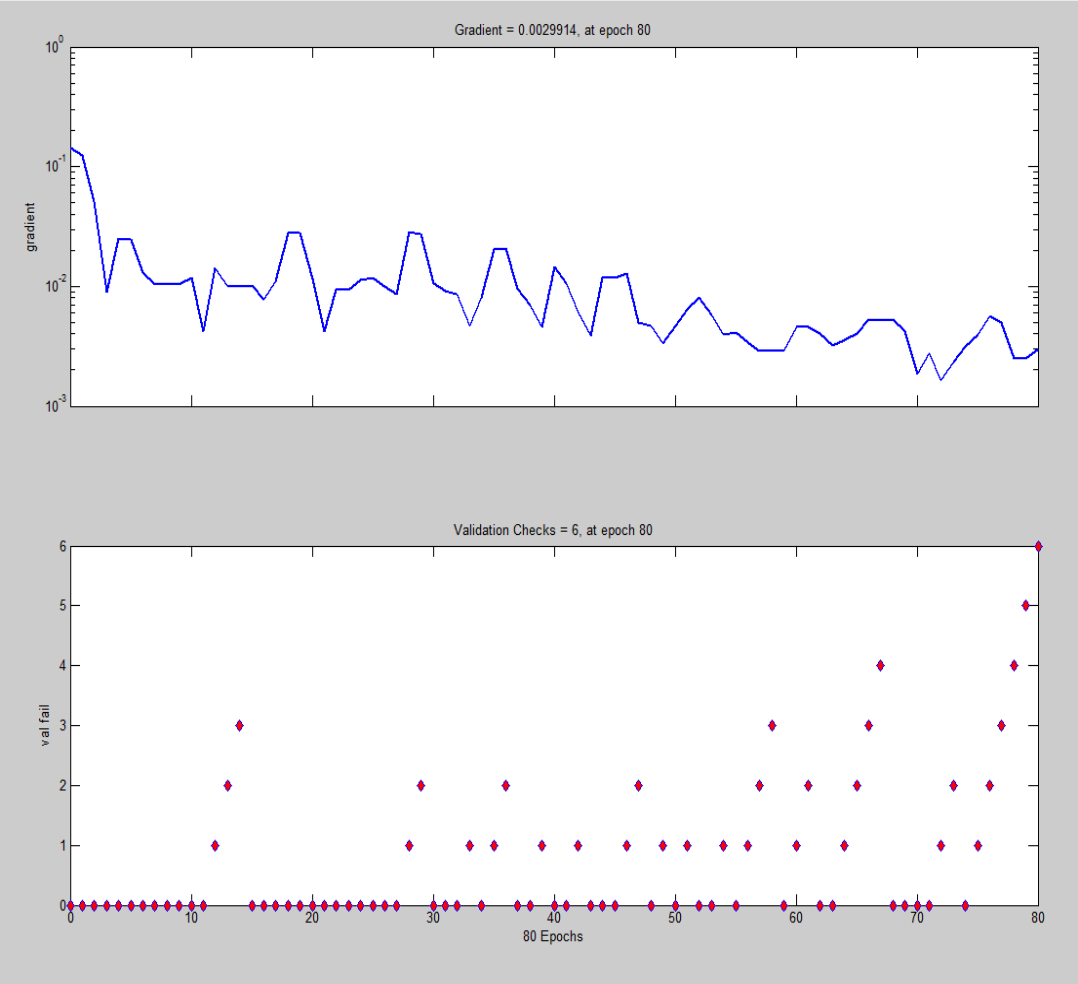

Figure **C-3**: Plot of gradient and validation check versus epochs.

Appendix D

MATLAB PROGRAMS USED

```
% Program used to extract data from all of the neural networks trained

load layer1_1.mat
network1(para);
test = network1(para);
test = test';
target1 = [test];
clear test;
clear network1;
clear network2;
clear network3;
clear network4;

load layer2_1.mat
network1(para);
test = network1(para);
test = test';
target1 = [target1;test];
clear test;
clear network1;
clear network2;
clear network3;
clear network4;

load layer3_1.mat
network1(para);
test = network1(para);
test = test';
target1 = [target1;test];
clear test;
clear network1;
clear network2;
clear network3;
clear network4;


load layer4_1.mat;
network1(para);
test = network1(para);
```

```
test = test';
target1 = [target1;test];
clear test;
clear network1;
clear network2;
clear network3;
clear network4;


load layer5_1.mat;
network1(para);
test = network1(para);
test = test';
target1 = [target1;test];
clear test;
clear network1;
clear network2;
clear network3;
clear network4;

load layer1_2.mat;
network1(para);
test = network1(para);
test = test';
target2 = [test];
clear test;
clear network1;
clear network2;
clear network3;
clear network4;

load layer2_2.mat;
network1(para);
test = network1(para);
test = test';
target2 = [target2;test];
clear test;
clear network1;
clear network2;
clear network3;
clear network4;

load layer3_2.mat;
network1(para);
test = network1(para);
```

```
test = test';
target2 = [target2;test];
clear test;
clear network1;
clear network2;
clear network3;
clear network4;

load layer4_2.mat;
network1(para);
test = network1(para);
test = test';
target2 = [target2;test];
clear test;
clear network2;
clear network1;
clear network3;
clear network4;

load layer5_2.mat;
network1(para);
test = network1(para);
test = test';
target2 = [target2;test];
clear test;
clear network1;
clear network2;
clear network3;
clear network4;

load layer1_3.mat
network1(para);
test = network1(para);
test = test';
target3 = [test];
clear test;
clear network1;
clear network2;
clear network3;
clear network4;

load layer2_3.mat;
network1(para);
test = network1(para);
test = test';
```

```
target3 = [target3;test];
clear test;
clear network1;
clear network2;
clear network3;
clear network4;

load layer3_3.mat;
network1(para);
test = network1(para);
test = test';
target3 = [target3;test];
clear test;
clear network1;
clear network2;
clear network3;
clear network4;

load layer4_3.mat;
network1(para);
test = network1(para);
test = test';
target3 = [target3;test];
clear test;
clear network1;
clear network2;
clear network3;
clear network4;

load layer5_3.mat;
network1(para);
test = network1(para);
test = test';
target3 = [target3;test];
clear test;
clear network1;
clear network2;
clear network3;
clear network4;

load layer1_4.mat;
network1(para);
test = network1(para);
test = test';
target4 = [test];
```

```
clear test;
clear network1;
clear network2;
clear network3;
clear network4;

load layer2_4.mat;
network1(para);
test = network1(para);
test = test';
target4 = [target4;test];
clear test;
clear network1;
clear network2;
clear network3;
clear network4;

load layer3_4.mat;
network1(para);
test = network1(para);
test = test';
target4 = [target4;test];
clear test;
clear network1;
clear network2;
clear network3;
clear network4;

load layer4_4.mat;
network1(para);
test = network1(para);
test = test';
target4 = [target4;test];
clear test;
clear network1;
clear network2;
clear network3;
clear network4;

load layer5_4.mat;
network1(para);
test = network1(para);
test = test';
target4 = [target4;test];
clear test;
```

```
clear network1;
clear network2;
clear network3;
clear network4;

load layer1_5.mat;
network1(para);
test = network1(para);
test = test';
target5 = [test];
clear test;
clear network1;
clear network2;
clear network3;
clear network4;

load layer2_5.mat;
network1(para);
test = network1(para);
test = test';
target5 = [target5;test];
clear test;
clear network1;
clear network2;
clear network3;
clear network4;

load layer3_5.mat;
network1(para);
test = network1(para);
test = test';
target5 = [target5;test];
clear test;
clear network1;
clear network2;
clear network3;
clear network4;

load layer4_5.mat;
network1(para);
test = network1(para);
test = test';
target5 = [target5;test];
clear test;
clear network1;
```

```
clear network2;
clear network3;
clear network4;

load layer5_5.mat;
network1(para);
test = network1(para);
test = test';
target5 = [target5;test];
clear network1;
clear network2;
clear network3;
clear network4;


% Program used to generate gas saturation plot from the output
figure (1);
[C,h]= contourf(x,y,data,'DisplayName','Y,plot,x');
%clabel (C,h);
title(['Error generated by ANN for case study no.3: year 1']);
xlabel('Block address');
ylabel('Layers');
% set(gca,'YDir','reverse'); %this will reverse the y-axis
colorbar;
colormap( [0 0.498039215803146 0;0 0.498039215803146 0;0
0.498039215803146 0;0 0.498039215803146 0;0 0.498039215803146 0;0
0.498039215803146 0;0 0.498039215803146 0;0 0.498039215803146 0;0
0.529411792755127 0;0 0.560784339904785 0;0 0.592156887054443 0;0
0.623529434204102 0;0 0.65490198135376 0;0 0.686274528503418 0;0
0.717647075653076 0;0 0.749019622802734 0;0 0.780392169952393 0;0
0.811764717102051 0;0 0.843137264251709 0;0 0.874509811401367 0;0
0.905882358551025 0;0 0.937254905700684 0;0 0.968627452850342 0;0 1
0;0.062745101749897 1 0;0.125490203499794 1 0;0.18823529779911 1
0;0.250980406999588 1 0;0.313725501298904 1 0;0.376470595598221 1
0;0.439215689897537 1 0;0.501960813999176 1 0;0.560784339904785 1
0;0.623529434204102 1 0;0.686274528503418 1 0;0.749019622802734 1
0;0.811764717102051 1 0;0.874509811401367 1 0;0.937254905700684 1 0;1 1 0;1
0.937254905700684 0;1 0.874509811401367 0;1 0.811764717102051 0;1
0.749019622802734 0;1 0.686274528503418 0;1 0.623529434204102 0;1
0.560784339904785 0;1 0.501960813999176 0;1 0.439215689897537 0;1
0.376470595598221 0;1 0.313725501298904 0;1 0.250980406999588 0;1
0.18823529779911 0;1 0.125490203499794 0;1 0.062745101749897 0;1 0
0;0.980392158031464 0.0235294122248888 0;0.960784316062927
0.0470588244497776 0;0.941176474094391 0.0666666701436043
0;0.925490200519562 0.0862745121121407 0;0.905882358551025 0.105882354080677
```

```
0;0.886274516582489 0.125490203499794 0;0.866666674613953 0.14509804546833
0;0.847058832645416 0.160784319043159 0]);
        grid on


        %set(gcf, 'Position', get(0,'Screensize')); % Maximize figure.
```